UCRL-10321

University of California

Ernest O. Lawrence Radiation Laboratory

HYPERFINE STRUCTURES AND NUCLEAR MOMENTS OF Lu^{176m}, Br^{80}, Br^{80m}, AND I^{132}

Berkeley, California

DISCLAIMER

Research and Development

UCRL-10321
UC-34 Physics
TID-4500 (18th Ed.)

UNIVERSITY OF CALIFORNIA

Lawrence Radiation Laboratory
Berkeley, California

Contract No. W-7405-eng-48

HYPERFINE STRUCTURES AND NUCLEAR MOMENTS OF Lu^{176m}, Br^{80}, Br^{80m}, AND I^{132}

Matthew B. White

(Thesis)

September, 1962

Printed in USA. Price $2.75. Available from the
Office of Technical Services
U. S. Department of Commerce
Washington 25, D.C.

HYPERFINE STRUCTURES AND NUCLEAR MOMENTS OF Lu^{176m}, Br^{80}, Br^{80m} AND I^{132}

Table of Contents

Table of Contents, Cont.

HYPERFINE STRUCTURES AND NUCLEAR MOMENTS OF Lu^{176m}, Br^{80}, Br^{80m} AND I^{132}

Matthew B. White

(Thesis)

Lawrence Radiation Laboratory
University of California
Berkeley, California

ABSTRACT

The method of Atomic-beam Radiofrequency Spectroscopy has been used to determine some nuclear and atomic properties of Lu^{176m}, Br^{80}, Br^{80m}, and I^{132}. Hyperfine structure measurements were made to determine the magnetic dipole interaction constants, a, and the electric quadrupole interaction constants, b, of all these isotopes. Also the nuclear spin, I, and the electronic g_J factor were measured for Lu^{176m}. The following results were obtained

for Lu^{176m}

$^2D_{3/2}$ Atomic State:	$^2D_{5/2}$ Atomic State:
I = 1	I = 1
a = 97.195 ± .008 mc/sec	a = 77.6 ± 4.8 mc/sec
b = -635.19 ± .01 mc/sec	b = -782.3 ± 9.6 mc/sec
g_J = -.79931 ± .00005	g_J = -1.2001 ± .0006

for Br^{80}

I = 1*
|a| = 323.9 ± .4 mc/sec
|b| = 227.62 ± .10 mc/sec
b/a < 0

for Br^{80m}

I = 5*
a = 166.05 ± .02 mc/sec
b = -874.9 ± .2 mc/sec

for I^{132}

I = 4*
|a| = 567.6 ± 2.6 mc/sec
|b| = 128.2 ± 20.6 mc/sec
b/a > 0

* The spins of the halogen isotopes were not determined during the experiments reported here but are included for completeness.

From the above hyperfine interaction constants the following values of the nuclear magnetic dipole moments, μ_I, and electric quadrupole moments, Q, were calculated. Both corrected (for diamagnetic shielding) and uncorrected values of μ_I are given but, because of the large uncertainties associated with core polarization correction factors, only uncorrected values of Q are presented.

For Lu^{176m}

μ_I(uncorr.) = 0.3160 ± .0014 n.m.
μ_I(corr.) = 0.3186 ± .0014 n.m.
Q = 2.40 ± .05 barns

For Br^{80}

$|\mu_I(\text{uncorr.})|$ = 0.4905 ± .0006 n.m.
$|\mu_I(\text{corr.})|$ = 0.5138 ± .0006 n.m.
|Q| = 0.182 ± .008 barns
$Q/\mu_I > 0$

For I^{132}

$|\mu_I(\text{uncorr.})|$ = 3.06 ± .02 n.m.
$|\mu_I(\text{corr.})|$ = 3.08 ± .02 n.m.
|Q| = 0.075 ± .015 barns
$Q/\mu_I < 0$

For Br^{80m}

μ_I(uncorr.) = 1.2573 ± .0006 n.m.
μ_I(corr.) = 1.3170 ± .0006 n.m.
Q = 0.70 ± .03 barns

INTRODUCTION

The experiments reported in this paper were undertaken as part of a general program, being carried on at the Lawrence Radiation Laboratory, to measure the atomic and nuclear properties of as many rare-earth and halogen isotopes as is possible using the atomic-beam magnetic resonance method.

The rare-earth region of the Periodic Table is especially interesting both with regard to electronic and nuclear structure. The electronic structure of the elements in this region is characterized by filling of the 4f electron shell and configurations of the types $6s^2 5d\ 4f^n$ or $6s^2 4f^{n+1}$ (with n = 1 - 14) are expected to occur. For many rare-earth elements, little or no work has been done, by methods other than atomic-beam spectroscopy, to determine the exact nature of these configurations. Measurements of electronic g_J factors and hyperfine structure separations by this method, however, have yielded much valuable information. Furthermore the J values associated with low lying atomic energy levels can also often be determined using this method and sometimes even the relative populations of these levels can be inferred. Thus detailed information concerning fine structure ordering and spacing has been obtained in some cases.

The nuclear structures of the rare-earths are of particular interest because of the large electric quadrupole moments exhibited by some of these nuclides. These large moments indicate that collective aspects of the nuclear system are important and hence nuclear moment and spin data obtained for elements in this region constitute a good test for the Collective Model of the nucleus. In particular its ability to predict the spin and nuclear moments of Lu^{176m} is a very stringent test since this nuclide is a metastable isomeric state of a highly deformed odd-odd nucleus.

The halogen isotopes, on the other hand, have very simple electronic structures (single hole outside closed shells) and thus their electronic properties should be accurately describable by existing atomic theory. The degree to which this is true acts as a test of the theory and so measurements of these properties lead to a better general understanding of atomic systems.

From the standpoint of nuclear physics the halogen isotopes lie

in an atomic mass region where collective aspects of the nuclear system would not be expected to dominate. Hence the Shell Model of the nucleus would seem applicable. Nuclear data for Br^{80} and Br^{80m} are particularly well suited for a test of this model's ability to account for the existence of nuclear isomerism in odd-odd nuclei as well as for the parities of such nuclei. Furthermore there is some evidence of collective nuclear effects in the Br isotopes so that interesting questions regarding the relative applicability of the two above mentioned nuclear models can be answered by studying these data.

This paper concerns itself primarily with the nuclear aspects of atomic-beam measurements. That is, the main experimental objective is considered to be the obtaining of nuclear spin and moment values with sufficient accuracy to allow the predictions of existing nuclear models to be tested. The atomic data necessary for carrying out the experiments reported are known quite accurately and no attempt was made (except incidentally in the case of Lu) to improve these data.

The paper is divided into two main parts. The first part is made up of Section I - III and concerns the theory necessary for carrying out the experiments and analyzing the results. Section I presents a systematic (though necessarily brief) development of those aspects of the theory of hyperfine structure that are needed. Section II is concerned with the general theoretical basis of the atomic-beam method, while Section III contains a description of the nuclear models mentioned above and equations, based on these models, are given for the calculation of nuclear moments.

The second main part of the paper, which comprises Sections IV-VII, concerns the actual experimental measurements. Section IV discusses the atomic-beam apparatus used, while Sections V, VI, and VII discuss, in more or less detail, the experimental techniques and results for the Lu^{176m}, $Br^{80,80m}$, and I^{132} experiments, respectively. Each of these latter Sections also include discussions of the methods used to calculate the nuclear moments from the hyperfine structure data as well as an analysis of the results on the basis of nuclear models.

Notation:

In the writing of a paper which encompasses an appreciable range of subject matter, one is usually faced with the problem of adopting a clear, consistent notation. In the cases of atomic and

nuclear physics, however, much of the notation has become quite well standardized so that little confusion should result as long as this standard notation is adhered to. Therefore, in what follows, definitions of quantities occurring in various equations have been made, in text, only when it was felt that the notation used to specify them is not sufficiently standard to make their definitions obvious. The values of all physical constants used below were taken from Reference 60 and the notation used there has, for the most part, been adopted for use in this paper.

I. THEORY OF HYPERFINE STRUCTURE

A. A Resume of the Theory of Atomic Spectra

The theory of atomic spectra, as it is usually developed, starts by hypothesizing that the following Hamiltonian is approximately valid for an atom in field free space

$$\mathcal{H} = \sum_{i=1}^{Z} \left[\frac{\vec{p}_i^{\,2}}{2m} - \frac{Ze^2}{r_i} + \sum_{j>i} \frac{e^2}{r_{ij}} + \zeta(r_i)\, \vec{l}_i \cdot \vec{s}_i \right] + \mathcal{H}_{hfs} \qquad (1)$$

where the summation extends over all electrons in the atom. Since the Schrodinger's Equation resulting from this Hamiltonian is in general inseparable and too complicated to be solved directly, the normally adopted procedure is to write Eq. (1) as a part, $\mathcal{H}_o$, which leads to a Schrodinger's Equation that can be solved directly plus a series of terms which can be treated as perturbations. The effects of these perturbations are then considered in order of decreasing importance by first order perturbation theory. Therefore we have

$$\mathcal{H} = \mathcal{H}_o + \mathcal{H}_t + \mathcal{H}_{fs} + \mathcal{H}_{hfs}$$

where

$$\mathcal{H}_o = \sum_i \left[\frac{\vec{p}_i^{\,2}}{2m} + U(r_i) \right]$$

$$\mathcal{H}_t = \sum_i \left[\sum_{j>i} \frac{e^2}{r_{ij}} - \frac{Ze^2}{r_i} - U(r_i) \right] \qquad (2)$$

$$\mathcal{H}_{fs} = \sum_i \zeta(r_i)\, \vec{l}_i \cdot \vec{s}_i$$

Here $U(r_i)$ is a spherically symmetric approximation to the actual potential produced at the position of the i^{th} electron by the nucleus and the other Z-1 electrons.

Once a value of $U(r_i)$ has been decided upon the Schrodinger's Equation $\mathcal{H}_o \psi = E \psi$ can be solved by separation of variables and solutions obtained in the form of products of individual electron wave functions. These highly degenerate product wave functions, after antisymmetrization to assure conformance with the Pauli Principle, serve as a zero order approximation for application of the perturbation theory.

The "configuration" of an atomic electron system is specified

by giving the principle quantum number, n, and orbital angular momentum quantum number, ℓ , of all electrons in the system. The ground state (lowest lying) configuration is determined by filling, in order of increasing energy, all available single electron energy levels in a manner consistent with the Pauli Principle. When the perturbation terms of Eq. (2) are considered, the usual procedure is to assume that the actually occurring ground state atomic wave function can be expressed as a linear combination of product wave functions arising from the ground state configuration only. In some cases, due to the perturbation term $\mathcal{H}_t$, this procedure is not justified and product wave functions arising from higher configurations must be included. (This appears to be true, for example, in the case of Lu). In this case "configuration interaction" is said to be present and must be accounted for by the theory.

Inclusion of the first (and usually most important) perturbation, $\mathcal{H}_t$, in the Hamiltonian leads to the so-called "terms" of optical spectroscopy. Since the operator corresponding to the square of the total electronic orbital angular momentum $\vec{L}^2 = \left\{ \sum_{i=1}^{Z} \vec{\ell}_i \right\}^2$ and the corresponding operator involving the electronic spin angular momentum $\vec{S}^2 = \left[\sum_{i=1}^{Z} \vec{s}_i \right]^2$ commute with $\mathcal{H} = \mathcal{H}_o + \mathcal{H}_t$, this Hamiltonian has no matrix elements between different eigenfunctions of these operators. Therefore the angular momentum q.n.'s L and S can be used to specify the different energy eigenvalues of this Hamiltonian and in general a different energy is associated with each value of L and S. This leads to a reduction in the degeneracy of the electron wave function corresponding to a given configuration and a $(2L + 1)(2S + 1)$ fold degenerate energy "term" appears for each distinct value of L and S.

Adding now the $\mathcal{H}_{fs}$ perturbation, we find that although this operator commutes with the total electronic angular momentum operator $\vec{J}^2 = (\vec{L} + \vec{S})^2$ it does not commute with either $\vec{L}^2$ or $\vec{S}^2$ separately, so that strictly speaking eigenvalues of these operators can no longer be used to specify the eigenfunctions of $\mathcal{H}$. However for most atoms $\mathcal{H}_t \gg \mathcal{H}_{fs}$ so that L and S can be retained as "good q.n.'s" and the effect of $\mathcal{H}_{fs}$ treated by first order perturbation theory. In this approximation each $(2L + 1)(2S + 1)$ fold degenerate term is split into $2L + 1$ or $2S + 1$ (whichever is smaller) separate "fine structure levels." These levels, which are $2J + 1$ fold degenerate, are characterized by different values of J and furthermore by distinct values of L and S if the inequality given above is well satisfied. [pure L-S coupling] .

If this is not the case, J is still a good q.n. but L and S are not, since the effect of $\mathcal{H}_{fs}$ must be treated by higher order perturbation theory which leads to wave functions that are mixtures of different $\vec{L}^2$ and $\vec{S}^2$ eigenfunctions. We are then said to have a departure from L-S coupling and if this situation is carried to the extreme [$\mathcal{H}_{fs} \gg \mathcal{H}_t$] we are said to be dealing with J-J coupling. For all of the elements considered in this paper there seems to be little or no departure from pure L-S coupling.

Finally we need to introduce the $\mathcal{H}_{hfs}$ perturbation. This term arises from the magnetic and non-coulomb electrostatic interactions between the nucleus and the atomic system. It has the effect of splitting each 2J + 1 fold degenerate fine structure level into either 2J + 1 or 2I + 1 (whichever is smaller) "hyperfine structure" levels. Here I is the spin (angular momentum in units of $\hbar$) of the nucleus. These levels are characterized by the q.n. F of the total angular momentum operator $\vec{F}^2 = (\vec{I} + \vec{J})^2$ and are 2F + 1 fold degenerate. If $\mathcal{H}_{hfs} \ll \mathcal{H}_{fs}$, as is usually the case, first order perturbation theory can be used to determine the degree of splitting and I and J as well as F can be considered as good q.n.'s. If this is not the case second or higher order perturbation theory must be resorted to and in general J can no longer be considered as a good q.n. For all the elements considered in this paper the hyperfine level separation/fine structure separation $\ll 1$, which is equivalent to the above condition, so that J (as well as L and S) can always be considered as a good q.n. A diagram is given in Fig. 1 which illustrates the various energy splittings discussed above.

Since atomic-beam radio frequency spectroscopy concerns transitions among h.f.s. levels, $\mathcal{H}_{hfs}$ is the perturbation term of Eq. (2) with which we will be most concerned in this paper. Therefore further discussion will be limited, almost exclusively, to it.

B. Atomic Hyperfine Structure in Field Free Space

In order to determine the explicit form of $\mathcal{H}_{hfs}$ we must consider classically the general electrostatic (magnetic) interaction between an electronic charge (current) distribution characterized by the charge density ρ_e (current density $\vec{j}_e$) and a nuclear charge (current) distribution characterized by the charge density ρ_n (current density $\vec{j}_n$). In treating these interactions we will assume that the nuclear and electronic charge

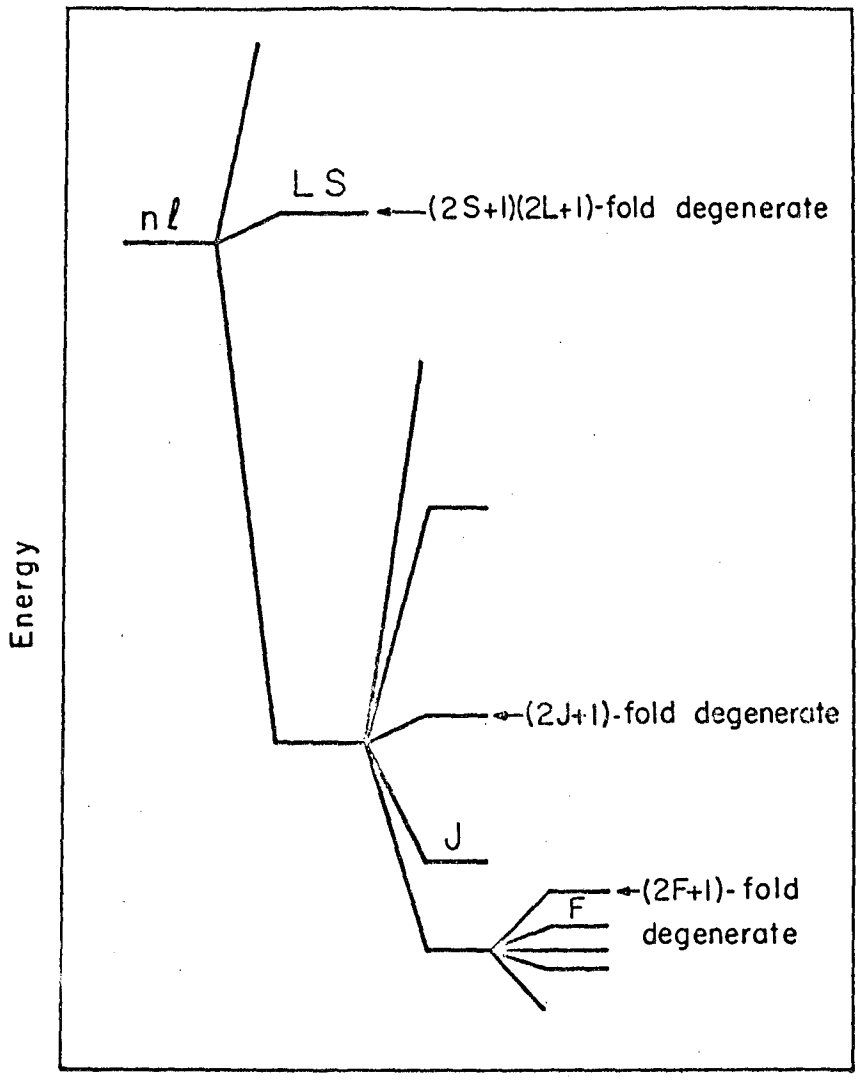

Fig. 1. Diagram illustrating degeneracies in atomic energy levels.

(current) distributions do not overlap and that consequently the magnitude of the vector $\vec{r}_n$, which denotes the position of some point within the nuclear volume (with respect to the center of the nucleus), is always less than the magnitude of the vector $\vec{r}_e$, which designates the position of some point within the electronic charge distribution (see Fig. 2). Ignoring possible overlap is equivalent in the final analysis, to neglecting consideration of the hyperfine anomaly. This is justified, to a good degree of approximation, for atoms without unpaired s electrons and so would not be expected to matter, to the reported degrees of accuracy, for the measurements considered in this paper. Under this assumption the general electrostatic interaction can be written[1]

$$\mathcal{H}_{\text{elect}} = \int_{\tau_e}\int_{\tau_n} \frac{\rho_e \rho_n}{r} \, d\tau_e \, d\tau_n \tag{3}$$

where $r = |\vec{r}_e - \vec{r}_n|$ is the distance between a volume element $d\tau_n$ within the nucleus and a volume element $d\tau_e$ within the electron charge distribution (see Fig. 2). For the general magnetic interaction we have[1]

$$\mathcal{H}_{\text{mag.}} = \frac{-1}{c} \int_{d\tau_n} \vec{j}_n \cdot \vec{A}_e \, d\tau_n \tag{4}$$

where $\vec{A}_e$ is the vector potential produced at the nucleus by the electron current distribution. However, if we restrict ourselves to a nonrelativistic treatment and note that we are dealing with stationary nuclear and electronic current distributions, Eq. (4) can be written[1]

$$\mathcal{H}_{\text{mag.}} = \int_{\tau_e}\int_{\tau_n} \frac{(-\vec{\nabla}_n \cdot \vec{m}_n)(-\vec{\nabla}_e \cdot \vec{m}_e)}{r} \, d\tau_e \, d\tau_n \tag{5}$$

where by definition

$$\begin{aligned} \vec{j}_n &= c\,\vec{\nabla}_n \times \vec{m}_n \\ \vec{j}_e &= c\,\vec{\nabla}_e \times \vec{m}_e \end{aligned} \tag{6}$$

Eq. (5) is identical to Eq. (3) if the following substitutions are made

$$\begin{aligned} \rho_n &\rightarrow -\vec{\nabla}_n \cdot \vec{m}_n \\ \rho_e &\rightarrow -\vec{\nabla}_e \cdot \vec{m}_e \end{aligned} \tag{7}$$

It should be noted in passing that ρ_n and ρ_e are scaler function of their

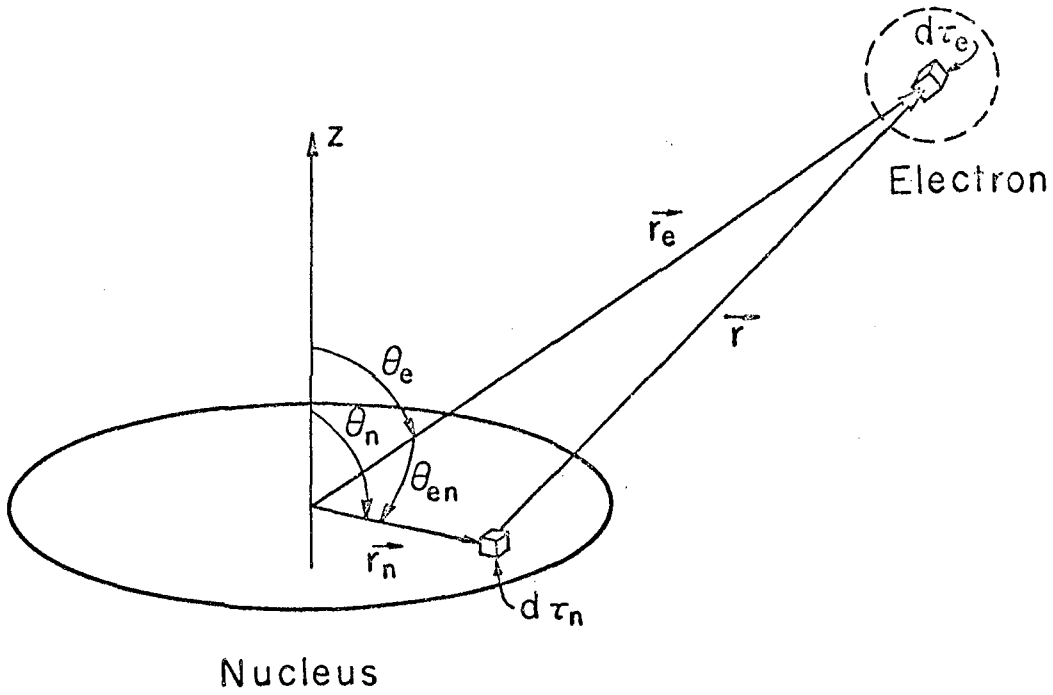

Fig. 2.

respective co-ordinates, that is $\rho(\vec{-r}) = +\rho(\vec{r})$. On the other hand, $(-\vec{\nabla}\cdot\vec{m})$ is a pseudoscaler since $-[\vec{\nabla}(\vec{-r})\cdot\vec{m}(\vec{-r})] = +\vec{\nabla}(\vec{r})\cdot\vec{m}(\vec{r})$. (See Eq. (6).) The similarity of Eqs. (5) and (3) enable us to apply expressions, derived for the case of electrostatic interactions, directly to the case of magnetic interactions by making the substitutions indicated in Eq. (7).

Returning then to Eq. (3) we expand this expression in terms of spherical Legendre polynomials in the usual way to obtain

$$\mathcal{H}_{elect} = \sum_k \int\int_{\tau_e\tau_n} \frac{\rho_e\rho_n}{r_e} \left(\frac{r_n}{r_e}\right)^k P_k(\cos\theta_{en})\, d\tau_n\, d\tau_e$$

where θ_{en} is the angle between r_e and r_n as indicated in Fig. 2. Expanding $P_k(\cos\theta_{en})$ using the Spherical Harmonic Addition Theorem, this equation can be expressed in the following form

$$\mathcal{H}_{elect} = \sum_k \sum_{q=-k}^{k} (-1)^q Q_q^{(k)} F_{-q}^{(k)} = \sum_k \tilde{F}_k \cdot \tilde{Q}_k = \sum_k \mathcal{H}_{elect}^{(k)} \qquad (8)$$

where

$$Q_q^{(k)} = \sqrt{\frac{4\pi}{2k+1}} \int_{\tau_n} \rho_n\, r_n^k\, Y_q^k(\cos\theta_n, \phi_n) d\tau_n$$

$$F_q^{(k)} = \sqrt{\frac{4\pi}{2k+1}} \int_{\tau_e} \rho_e r_e^{-(k+1)}\, Y_q^k(\cos\theta_e, \phi_e)\, d\tau_e. \qquad (9)$$

Hence we now have the general electrostatic interaction energy expressed as the sum of scaler products of the two (2k + 1 component) tensors $\tilde{F}_k$ and $\tilde{Q}_k$, one of which involves the nuclear coordinates only while the other involves the electronic coordinates. Equation (8) is said to constitute a "multipole expansion" of the interaction energy and $\mathcal{H}_{elect}^{(k)}$ is called the electrostatic k-pole interaction energy. By making the substitutions of Eq. (7) a similar multipole expansion of the magnetic interaction energy is obtained and $\mathcal{H}_{mag}^{k}$ is called the magnetic k-pole interaction energy.

Although the sum over k in Eq. (8) for the classical case, extends to infinity it will be shown below that only the first few terms need be considered in the quantum mechanical case. Furthermore the magnitude of the terms in Eq. (8) decrease rapidly as k increases so that unless extremely accurate results are required, all terms higher than k = 2 can be dropped (for example[1] $\mathcal{H}_{mag}^{(3)} / \mathcal{H}_{mag}^{(1)} \cong 10^{-5}$). Therefore,

due to the limited accuracy of the experiments reported in this paper, only multipole interaction terms up to k = 2 will be considered here. Furthermore if it is assumed that the charge and current densities of the nucleus are symmetric with respect to reflection through the origin (this is equivalent quantum mechanically to assuming that the nuclear ground state wave function possesses a definite parity) then, since ρ_n is a scaler and Y_q^k has the parity of k, for the electric case all $Q_q^{(k)}$ for k odd will vanish. On the other hand, since $-\vec{\nabla}_n \cdot \vec{m}_n$ is a pseudoscaler, for the magnetic case all $Q_q^{(k)}$ with k even will vanish. Hence it will only be necessary to consider the k = 1 (dipole) mangetic interaction energy and the k = 2 (quadrupole) electrostatic interaction energy.

Before proceeding to the quantum mechanical treatment it is instructive, at this point, to investigate the physical meanings of some tensor components that will be used later. Looking up the explicit forms of the spherical harmonics[2] we get, using Eq.(9)

$$Q_0^{(0)} = \int_{\tau_n} \rho_n d\tau_n \qquad F_0^{(0)} = \int_{\tau_e} \frac{\rho_e d\tau_e}{r_e} \qquad \text{electric case}$$

$$Q_0^{(1)} = -\int_{\tau_n} r_n \cos\theta_n (\vec{\nabla}_n \cdot \vec{m}_n) d\tau_n = -1/2c \int_{\tau_n} \left[(\vec{r}_n \times \vec{j}_n) d\tau_n \right]_z = -\left[\vec{\mu}_I \right]_z$$

magnetic case

$$F_0^{(1)} = -\int_{\tau_e} \frac{(\vec{\nabla}_e \cdot \vec{m}_e)\cos\theta_e}{r_e^2} d\tau_e = 1/c \int \left[\frac{\vec{j}_e x (-\vec{r}_e)}{r_e^3} d\tau_e \right]_z = \left[\vec{H}(0) \right]_z$$

magnetic case

$$Q_0^{(2)} = 1/2 \int_{\tau_e} \rho_n r_n^2 (2\cos^2\theta_n - \sin^2\theta_n) d\tau_n = 1/2 \int_{\tau_n} \rho_n (3Z_n^2 - r_n^2) d\tau_n = Q_n/2$$

electric case

$$F_0^{(2)} = 1/2 \int_{\tau_e} \frac{\rho_e}{r_e^3} (3\cos^2\theta_e - 1) d\tau_e = 1/2 \frac{\partial^2 V(0)}{\partial Z_e^2} \qquad \text{electric case}$$

Hence, classically, for the electric cases above

$Q_0^{(0)}$ = total charge on the nucleus Z_e

$F_0^{(0)}$ = coulomb potential at the nucleus due to the electrons

$Q_0^{(2)}$ = 1/2 times the classically defined electric quadrupole moment of the nucleus.

$F_0^{(2)}$ = -1/2 times the Z component of the gradient of the Z component of the electric field produced at the nucleus by the electron charge distribution,

and for the magnetic case

$Q_0^{(1)}$ = minus the Z component of the classically defined nuclear magnetic moment.

$F_0^{(1)}$ = Z component of the magnetic field produced at the nucleus by the electron current distribution.

Since the electric monopole interaction energy corresponds, according to the above, to the usual central coulomb interaction of Eq. (1) it is not considered as part of $\mathcal{H}_{hfs}$.

Derivation of the Hyperfine Structure Hamiltonian

According to the discussion at the beginning of this section, the hyperfine structure energy splitting can be obtained, to first order, by taking the diagonal matrix elements of $\mathcal{H}_{hfs} = \mathcal{H}_{elec} + \mathcal{H}_{mag}$ in a representation specified by the q.m.'s L,S,J,I, and F. These matrix elements consist of sums of matrix elements each of which corresponds to a particular k-pole electric or magnetic interaction. That is

$$< IJF|\mathcal{H}_{hfs}|IJF> = \sum_k < IJF|\tilde{\vec{F}}_k \cdot \tilde{\vec{Q}}_k|IJF>_{mag} + \sum_k < IJF|\tilde{\vec{F}}_k \cdot \tilde{\vec{Q}}_k|IJF>_{elec} \cdots \quad (10)$$

The most simple and straightforward way to evaluate these matrix elements of tensor scaler products is by introducing the idea of an irreducible spherical tensor operator.

An irreducible tensor operator[3] of rank k is defined as an operator with 2k + 1 components, $T_\mu^{(k)}$, which transform among themselves, upon rotation of the coordinate system, in the same way as the 2k + 1 degenerate eigenfunction of an angular momentum operator characterized by the eigenvalue k(k+1). From this definition the following important theorem can be proved[3] for the matrix element of $T_\mu^{(k)}$

$$< N'j'm'|T_\mu^{(k)}|N\ j\ m> = a^{jk}_{j'm\mu}\ _{m',m+\mu} < N'j'\|T^{(k)}\|Nj> \quad (11)$$

where $a^{jk}_{j'm\mu}$ is a Wigner vector coupling coefficient[3] relating eigenfunctions of the form $|jmk\mu>$ to eigenfunctions of the form $|jkj'm'>$. This coefficient vanishes unless j,k and j' satisfy the "triangular condition," that is

unless a closed triangle can be formed with sides proportional to j, k and j'. The above expression is known as the Wigner-Eckhart Theorem and is useful in explicitly exhibiting the spatial (m and m') dependence of the matrix elements of tensor operators. The double barred or "reduced" matrix element on the right is independent of μ, m and m'. All the dependence on these q.n.'s is contained in the Wigner coefficient.

If $\tilde{T}^{(k)}(1)$ is a tensor operator which involves the coordinates of some system no. 1 with characteristic angular momentum j_1, and $\tilde{T}^{(k)}(2)$ is a tensor operator which involves the coordinates of another independent system no. 2 with characteristic angular momentum j_2, then Eq. (11) and the above definition of $T^{(k)}_{\mu}$ can be used to derive the following expression for the matrix elements of the scalar product of these tensors in a representation characterized by angular momentum $j = j_1 + j_2$. (See Ref. 3.)

$$\langle j'm'j_1'j_2' | \tilde{T}^{(k)}(1) \cdot \tilde{T}^{(k)}(2) | j\ m\ j_1j_2\rangle = \delta_{m'm}\,\delta_{j'j}\,(-1)^{j_1'+j_2-j}\,W(j_1j_2j_1'j_2';\ jk)$$

$$\times \left[(2j_1'+1)(2j_2'+1)\right]^{1/2}\langle j_1' \| T^{(k)}(1) \| j_1\rangle$$

$$\langle j_2' \| T^{(k)}(2) \| j_2\rangle \qquad (12)$$

Here W is a Racah Coefficient related to the coupling of three angular momentum vectors (see Ref. 3). From its definition the above Racah Coefficient vanishes unless the following angular momentum triads satisfy the "triangular condition;" (j_1j_2j),$(j\ j_2'\ j_1')$,$(j_2j_2'k)$, and (j_1kj_1').

Finally, again using the definition of $T^{(k)}_{\mu}$ and Eq. (11), the following equation for the matrix elements of $T^{(k)}_{\mu}(1)$ in the $|j_1j_2j\ m\rangle$ representation can be derived,

$$\langle j'm'j_1'j_2' | T^{(k)}_{\mu}(1) | j\ m\ j_1j_2\rangle = a^{jk}_{j'm\mu}\ \delta_{m',m+\mu}\langle j'j_1'j_2' \| T^{(k)}(1) \| j\ j_1j_2\rangle \qquad (13)$$

where

$$\langle j'j_1'j_2' \| T^{(k)}(1) \| j\ j_1j_2\rangle = \delta_{j_2'j_2}(-1)^{j_2+k-j_1-j}\left[(2j'+1)(2j+1)\right]^{1/2}$$

$$W(j_1jj'_1\ j';\ j_2k)\ \langle j_1' \| T^{(k)}(1) \| j_1\rangle \qquad (14)$$

Using Eqs. (11) and (12) we are now ready to evaluate the matrix elements indicated in Eq. (10). First it is noted that since the $Q^{(k)}_{\mu}$ and

$F_{\mu}^{(k)}$ tensor components of Eq. (9) are proportional to the spherical harmonics which themselves can serve as angular momentum eigenfunctions, the $\tilde{Q}^{(k)}$ and $\tilde{\tilde{F}}^{(k)}$ tensors certainly qualify as irreducible tensor operators. Furthermore $\tilde{Q}^{(k)}$ involves only coordinates of the nuclear system which has a characteristic angular momentum I while $\tilde{F}^{k}$ involves only coordinates of the electronic system which has a characteristic angular momentum J. Hence the conditions for application of Eq. (12) are satisfied. If we identify the electronic system with system no. 1 and the nuclear system with system no. 2, the diagonal matrix elements of the magnetic dipole and electric quadrupole interaction energies are given by Eq. (12) to be

$$\langle IJF | \mathcal{H}^{(1)}_{mag} | IJF \rangle = \frac{K}{2IJ} \frac{(2J)!(2I)! \langle J \| F^{(1)}_{mag} \| J \rangle \langle I \| Q^{(1)}_{mag} \| I \rangle}{\left[(2J-1)! (2J+2)! (2I-1)! (2I+2)! \right]^{1/2}} \tag{15}$$

$$\langle IJF | \mathcal{H}^{2}_{elect} | IJF \rangle = \frac{6\left[K(K+1) - 4/3\, I(I+1)J(J+1) \right] (2J)!(2I)! \langle J \| F^{(2)}_{elect} \| J \rangle}{2I(2I-1)2J(2J-1) \left[(2I-2)!(2J+3)! (2I-2)! \right]}$$

$$\frac{\langle I \| Q^{(2)}_{elect} \| I \rangle}{(2I+3)!\,]^{1/2}}$$

where

$$K = F(F+1) - I(I+1) - J(J+1) .$$

To obtain explicit expressions for the reduced matrix elements of Eq. (15) we use Eq. (11). Taking the simplest case of $j' = j = m = m'$ and $\mu = 0$ Eq. (11) gives

$$\langle jj | T^{(k)}_{o} | jj \rangle = a^{jk}_{jjo} \langle j \| T^{(k)} \| j \rangle \tag{16}$$

where the Wigner Coefficient is now given by

$$a^{jk}_{jjo} = \frac{(2j)!}{\left[(2j-k)! (2j+k+1)! \right]^{1/2}} \tag{17}$$

substituting these expressions into Eq. (15), first letting $j = J$, $\tilde{T}^{k} = \tilde{F}^{k}$

and then $j = I$, $\tilde{T}^k = \tilde{Q}^k$ we get

$$< IJF | \mathcal{H}^{(1)}_{mag} | IJF > = \frac{K}{2IJ} < II | Q^{(1)}_o | II > <JJ | F^{(1)}_o | JJ >$$

$$<IJF | \mathcal{H}^{(2)}_{elect} | IJF > = \frac{6[K(K+1)-4/3I(I+1)J(J+1)]}{2I(2I-1)\ 2J(2J-1)} < II | Q^{(2)}_o | II >$$

$$< JJ | F^{(2)}_o | JJ > \qquad (18)$$

A general statement can be made about the series of Eq. (10) by examination of Eq. (12). Identifying J with j_1, j_1' and I with j_2, j_2', the triangular conditions given above for W shows that the only non-vanishing terms of Eq. (10) are those for which $2I \leq k$ and $2J \leq k$. Hence, as implied above, the series terminates at $k = 2I$ or $2J$ (whichever is smaller).

Finally, noting the (classical) physical interpretations given above for the tensor components which appear in Eq. (18), we have for the energy of the hyperfine level specified by F

$$W_o(IJF) = - \frac{K}{2IJ} < II | (\vec{\mu}_I)_z | II > <JJ | H_z(0) | JJ>$$

$$+ \frac{6[K(K+1)-4/3I(I+1)J(J+1)]}{8I(2I-1)\ 2J(2J-1)} < II | Q_n | II> < JJ | \frac{\partial^2 V(0)}{\partial Z_e^2} | JJ>$$

where $(\mu_I)_z$, $H_z(0)$, Q_n, and $\frac{\partial^2 V(0)}{\partial Z_e^2}$ are now considered as quantum mechanical operators. This expression can be rewritten in the more usual form

$$W^o(IJF) = \frac{aK}{2} + b/4 \quad \frac{3K(K+1)-4I(I+1)J(J+1)}{2I(2I-1)\ J(2J-1)} \qquad (19)$$

where

$$a = \frac{-< II | (\vec{\mu}_I)_z | II> <JJ | H_z(0) | JJ>}{IJ} = \frac{-\mu_I <JJ | H_z(0) | JJ >}{IJ} \qquad (20)$$

$$b = e< II | \sum_{i=1}^{Z} (3Z_i^2 - r_i^2) | II > <JJ | \frac{\partial^2 V(0)}{\partial Z_1^2} | JJ > = eQ< JJ | \frac{\partial^2 V(0)}{\partial Z_2} | JJ > \qquad (21)$$

To obtain this expression for b the formula for $Q^{(2)}_o$ has been taken over to the quantum mechanical case by substituting $\rho_n = \sum_{i=1}^{Z} e\, \delta(\vec{r}-\vec{r}_i)$,

where $\vec{r}_i$ is the position vector of the i^{th} proton in the nucleus and the sum runs over all protons. Eqs. (20) can be considered as defining equations for the magnetic dipole interaction constant "a" and the nuclear magnetic dipole moment "μ_I". Similarly Eqs. (21) serve to define the electric quadrupole interaction constant "b" as well as the nuclear electric quadrupole moment "Q".

Since $\vec{I} \cdot \vec{J} = \frac{\vec{F}^2 - \vec{I}^2 - \vec{J}^2}{2}$ this operator is diagonal in the $|IJFm_F>$ representation with eigenvalues given by K/2. Furthermore, according to Eqs. (12) and (8) and the discussion following Eq. (8), $\mathcal{H}_{hfs}$ has no non-zero off-diagonal matrix elements in this representation. Hence as long as matrix elements are taken in the $|IJFm_F>$ representation and I and J are considered to be good q.n.'s, $\mathcal{H}_{hfs}$ (including only up to quadrupole interactions) can be written in the following form

$$\mathcal{H}_{hfs} = a\, \vec{I} \cdot \vec{J} + b\, \frac{3(\vec{I} \cdot \vec{J})^2 + 3/2\, \vec{I} \cdot \vec{J} - I(I+1)J(J+1)}{2I(2I-1)\, J(2J-1)} \qquad (22)$$

This Hamiltonian is usually expressed in units of mc/sec for atomic-beam work.

Since, using the atomic-beam method, the "a" and "b" interaction constants defined by Eqs. (20) and (21) are usually what is measured, it is necessary, in order to extract the desired nuclear moment values, to evaluate the electronic matrix elements appearing in these equations. Although quite difficult to do in general, this has been done by several authors[4] for the special case where; a) There is a single, non-s, valance electron (hole) outside of closed spherically symmetric electron shells. b) The radial part of the electron wave function is separable from the angular part. c) The atom exhibits pure L-S coupling.

If all three of these conditions are satisfied the following expressions are obtained for "a" and "b"

$$a = \frac{\mu_o^2}{h \times 10^6}\, \frac{\mu_I}{I}\, \frac{m}{M}\, \frac{2L(L+1)}{J(J+1)}\, F(J,Z_i) < r^{-3} > \qquad (23)$$

$$b = -\frac{e^2 Q}{h \times 10^6}\, \frac{2J-1}{2J+2}\, R(L,J,Z_i) < r^{-3} > \qquad (24)$$

The $F(J,Z_i)$ and $R(L,J,Z_i)$ which appear in these equations are relativistic correction factors which have been worked out by Casimer[4].

They are both near unity and arise because of our restriction to a non-relativistic treatment.

Solving the ratio of Eqs. (23) and (24) for Q we get

$$Q = -4 \frac{m}{M} \frac{\mu_I}{I} \frac{\mu_o^2}{e^2} F/R \frac{L(L+1)}{J(2J-1)} b/a \quad . \qquad (25)$$

Although, if μ_I is known, Q can be obtained directly in terms of measured quantities from this equation, μ_I cannot be obtained directly from Eq. (23) because of the $< r^{-3} >$ term. There are, however, two ways in which the value of μ_I can be obtained from the measured value of "a". The first, and most accurate, way (since it does not depend on any specialized assumptions regarding electronic structure) is to use known nuclear data for another isotope of the element in question. If an expression like Eq. (20) is written for two isotopes of the same element x and y, the electronic matrix element of Eq. (20) cancels from the ratio of these expressions and we are left with

$$\frac{a(x)}{a(y)} = \frac{\mu_I(x)\ I(y)}{\mu_I(y)\ I(x)}$$

hence

$$\mu_I(x) = \mu_I(y) \frac{a(x)}{a(y)} \frac{I(x)}{I(y)} \quad . \qquad (26)$$

So if the "a" and "μ_I" of one isotope are known the μ_I of the other can be determined from its "a" value. Eq. (26) is only valid under the assumption that the hyperfine anomaly between isotopes x and y can be ignored.

The other way of using Eq. (23) to determine μ_I is to use an expression for the fine structure separation, δ , which also depends on $< r^{-3} >$ to eliminate this term from Eq. (23). This expression for δ , which is derived under essentially the same assumptions as given above for the derivation of Eqs. (23) and (24), is[4]

$$\delta = \frac{\mu_o^2}{hc} Z_i (2L + 1) H(L,Z_i) < r^{-3} > \text{(in units of cm}^{-1}\text{)}. \qquad (27)$$

Here $H(L,Z_i)$ is another relativistic correction factor given by Casimer. Solving this Equation for $< r^{-3} >$ and substituting into Eq. (23) leads to the following result for μ_I

$$\mu_I = I \frac{M}{m} \frac{a \times 10^6}{c} Z_i \frac{J(J+1)(2L+1)}{2L(L+1)} H/F \text{ (in units of } \mu_n). \quad (28)$$

The accuracy attainable using this equation is usually limited by the uncertainty in the value of Z_i. This parameter, which corresponds to the charge seen by the valance electron when it is inside the electron core, can be estimated from optical spectroscopy data but is usually known to only about 4 or 5% accuracy.

In addition to the relativistic correction factors already mentioned, the value of μ_I obtained from Eq. (28) must be further corrected for "diamagnetic shielding" and the value of Q from Eq. (25) corrected for "core polarization" effects. The Diamagnetic Shielding Effect occurs because, upon application of an external magnetic field H, the circulating electrons of an atom classically change their orbital frequencies in such a way as to oppose (by Lenz' Law) the applied field. Hence a field $H(0) = -\sigma H$ is superimposed, at the position of the nucleus, on the applied field and therefore makes μ_I (through its interaction with the total field) appear smaller than it actually is. The Core Polarization or Sternheimer Effect, on the other hand, arises because of the distortion of the, assumed spherically symmetric, closed electron shells by the nuclear quadrupole moment. In some cases this makes Q appear smaller than it really is (shielding) while in other cases the reverse is true (anti-shielding).

The factor, K, by which the μ_I of Eq. (28) must be multiplied to account for diamagnetic shielding has been tabulated, for various atoms, by Kopfermann.[5] This correction amounts to from .003% for the lightest elements to about 1% for the heaviest and is known to about 5%. The Sternheimer Correction Factor, C, usually ranges in value from about 1% to 20% for atoms and is only very inaccurately known[6]. K and C, along with the necessary Relativistic Correction Factors, are given in Appendix B for all atoms considered in this paper. In presenting the final calculated μ_I and Q values, both corrected and uncorrected μ_I values are given but, due to the large uncertainties in C, only uncorrected Q's are given.

Configuration Interaction:

If an atom exhibits "configuration interaction," that is, if the actual ground state wave function is not derived from a single electron configuration, then Eqs. (23) and (24) are invalidated because in general

conditions a) and b) assumed in their derivation are violated. Therefore Eqs. (25) and (28) cannot be used to calculate Q and μ_I respectively. Schwartz[7], however, has shown how the effect of configuration interaction can be taken into account for the special case where a configuration of the type $s\, s''\ell$ is mixed with the $s^2\ell$ ground state configuration of a single valance electron.

If we assume L-S coupling, the wave function for either the $J'' = \ell + 1/2$ or $J'' = \ell - 1/2$ component of the fine structure doublet can be written for atoms having the above type of configuration mixing as

$$\psi_J = \alpha_o \,|\, s^2(S=0)\ ^2L_J > + \alpha_1 |\, s\ s'(S=1)^2L_J > + \alpha_2 |\, ss'(S=0)^2L_J > . \tag{29}$$

This follows because $\mathcal{H}_{fs}$, which is responsible for configuration interactions of this type, can only mix wave functions having the same S, L, and J. In Eq. (29), $|\, s^2(S=0)^2L_J >$ signifies the usual ^2L_J wave function if no mixing of the $ss'\ell$ configuration were present, $|\, ss'\ (S=1)^2L_J >$ is the wave function resulting when the spins of the s and s' electrons combine to give S = 1 which then combines with the ℓ electron spin to give S = 1/2, while $|\, ss'\ (S=0)^2L_J >$ is the wave function for the case where the s and s' electron spins first combine to give S = 0.

Now the magnetic field operator $H_z(0)$ can be written

$$H_z(0) = H_z^{\ell}(0) + H_z^{s}(0)$$

where $H_z^{\ell}(0)$ operates on the coordinates of the ℓ electron only and $H_z^{s}(0)$ operates on the coordinates of the s and s' electrons only. Making this substitution and using ψ_J from Eq. (29), Eq. (20) gives

$$a(J) = -\ \frac{\mu_I}{IJ} < JJ |\, H_z^{\ell}(0) \,|\, JJ > - \frac{\mu_I}{IJ}\ \Delta_{JJ} . \tag{30}$$

The first term on the right is just $a_o(J)$, the contribution to a(J) from the ℓ electron only, while Δ_{JJ} is a sum of matrix elements involving various terms of Eq. (24). All these matrix elements are of the form

$$\Delta_{JJ} \approx < S\ 1/2,\ 1/2\ \ell\ ,\ JJ |\, H_z^{s}(0) \,|\, S'\ 1/2,\ 1/2\ \ell\ ,\ JJ >$$

so the wave functions involved only differ in the way in which the spins

of the s, s', and ℓ electrons couple to give S = 1/2. Putting j' = j = m' = m = J, $j_1 = j_1' = 1/2$, $j_2 = j_2' = L$, and $T^{(k)}_{\mu}(1) = H^{s}_{z}(0)$ in Eqs. (13) and (14) then gives

$$\Delta_{JJ} = \frac{(2J)!}{[(2J-1)!(2J+2)!]^{1/2}} \; W(1/2\ J1/2J;\ L1)(2J+1)(-1)^{L+1/2-J} \times \text{sum of terms not involving J or L.} \tag{31}$$

Writing Eq. (30) for both the J' and J" fine structure states we get

$$\begin{aligned} a(J') &= a_o(J') + \delta(J') \\ a(J'') &= a_o(J'') + \delta(J'') \end{aligned} \tag{32}$$

where from Eq. (31)

$$\frac{\delta(J')}{\delta(J'')} = \frac{J''\,\Delta_{J'J'}}{J'\Delta_{J''J''}} = -1 \quad . \tag{33}$$

Furthermore, since $a_o(J)$ is due to the ℓ electron only, Eqs. (23) and (28) are applicable if $a_o(J)$ is used instead of the total measured a(J). Hence Eq. (23) gives

$$\frac{a_o(J')}{a_o(J'')} = \frac{F'}{F''}\;\frac{J''(J''+1)}{J'(J'+1)} \quad . \tag{34}$$

If the magnetic dipole interaction constants a(J') and a(J") are measured for both fine structure states of an atom exhibiting configuration mixing of the type considered, Eqs. (32), (33) and (34) afford a method of determining a_o and hence μ_I using Eq. (28). This follows since these four independent equations can be solved for the four unknown $a_o(J')$, $a_o(J'')$, $\delta(J')$, and $\delta(J'')$. For example, if $a_o(J')/a_o(J'') \equiv s$ and $a(J')/a(J'') \equiv r$ then solving these equations for $\delta(J')$ yields

$$\delta(J') = \frac{r-s}{1+s}\; a(J'') \tag{35}$$

which in conjunction with Eq. (32) gives $a^o(J')$.

No analysis, similar to the above, has been carried out to correct the "b" value of Eq. (24) for configuration mixing. However since (according to Eq. (21)) b depends on the gradient of the electric field at the nucleus, raising one s electron to a higher s state would not be expected

to influence this interaction constant nearly as much as "a". This is because the charge distribution of an s electron is spherically symmetric and so does not influence $\frac{\partial E_z}{\partial z}$ directly. On the other hand the unpairing of s electron spins can have a very large effect on the value of "a".

C. Hyperfine Structure with an Applied Magnetic Field

Postponing the consideration of hyperfine structure temporarily we consider first the effect that introducing a magnetic field has on the fine structure levels. Since each electron in a given atom has a magnetic dipole moment associated with both its orbital motion and spin (of magnitudes $-\mu_o \vec{\ell}$ and $-2\,\mu_o \vec{s}$ respectively*) upon application of a magnetic field H in the z direction we must add to the Hamiltonian of Eq. (1) a term

$$\mathcal{H}_m^{fs} = \frac{\mu_o H}{h} \sum_i \left[\ell_z(i) + 2\, s_z(i) \right] \quad \text{(expressed in mc/sec)} .$$

Or, in terms of the total $\vec{S}$ and $\vec{L}$ operators

$$\mathcal{H}_m^{fs} = \frac{\mu_o H}{h} \left[L_z + 2S_z \right] . \qquad (36)$$

Now although L_z and S_z commute with $\vec{S}^2$ and $\vec{L}^2$ these operators do not commute with $\vec{J}^2$. Therefore, strictly speaking, J is no longer a good q.n. after Eq. (36) is added to the Hamiltonian. However, if we restrict ourselves to magnetic fields of sufficiently small magnitude that $\mathcal{H}_m^{fs} \ll \mathcal{H}_{fs}$, J can be retained as a good q.n. and first order perturbation theory used. Assuming pure L-S coupling, so that L and S as well as J can be used to designate eigenstates of the total Hamiltonian, the matrix elements diagonal in L, S, and J of $\mathcal{H}_m^{fs}$ are[8]

$$\langle SLJm_J | \mathcal{H}_m^{fs} | SLJm_J' \rangle = \frac{\mu_o H m_J}{h} \delta_{m_J m_J'} \left[\frac{J(J+1)+L(L+1)-S(S+1)}{2J(J+1)} + 2\, \frac{J(J+1)+S(S+1)-L(L+1)}{2J(J+1)} \right] .$$

It is customary to write this expression as

$$\langle SLJm_J | \mathcal{H}_m^{fs} | SLJm_J \rangle = W_H^{fs}(m_J) = -g_J \frac{\mu_o H}{h} m_J = -\vec{\mu}_{elect} \cdot \vec{H} \qquad (37)$$

where

---

* Actually the "g factor" associated with electron spin is not exactly equal to 2 but equals instead[1]

$$g_s = 2(1.001146 \pm 0.000012)$$

$$g_J = - \frac{J(J+1)+L(L+1)-S(S+1)}{2J(J+1)} - 2 \frac{J(J+1)+S(S+1)-L(L+1)}{2J(J+1)} \qquad (38)$$

g_J is called the electronic Lande g factor. According to Eq. (37), upon application of a weak magnetic field each degenerate fine structure level is split into 2J + 1 equally spaced levels, the spacing being proportional to g_J and the applied field (Linear Zeeman Effect for fine structure levels). It is obvious from its derivation that Eq. (38) holds only for the special case of L-S coupling. In fact the degree to which this equation is valid is usually taken as a measure of the purity of L-S coupling in any given case. Furthermore Eqs. (37) and (38) hold only for "weak" fields, that is for fields such that

$$g_J \frac{\mu_o H}{h} \ll \mathcal{H}_{fs} \qquad (39)$$

For the worse case considered in this paper, this leads to the "weak" field criterion that $H \ll 10^7$ gauss.

If Eq. (39) is satisfied (as is certainly the case for the fields of $H < 1000$ gauss used during the course of the experiments reported in this paper) Eq. (37) shows that for matrix elements diagonal in L, S, and J, $\mathcal{H}_m^{fs}$ can be written as

$$\mathcal{H}_m^{fs} = -g_J \frac{\mu_o H}{h} J_z \ . \qquad (40)$$

Considering now the nucleus to be part of the total quantum mechanical system, we must include a term in the Hamiltonian

$$\mathcal{H}_m^{hfs} = - \frac{\vec{\mu}_I \cdot \vec{H}}{h} = \frac{-g_I' \mu_o \vec{I} \cdot \vec{H}}{h} = - \frac{g'_I \mu_o H}{h} I_z \text{ (in units of mc/sec)} \qquad (41)$$

to account for the interaction of the nuclear magnetic dipole moment with the applied magnetic field. g_I' is called the nuclear g factor, the prime denotes that it is defined with respect to μ_o instead of in the usual way, with respect to μ_n. g_I' is related to the usual g_I by the expression

$$g_I' = \frac{\mu_n}{\mu_o} g_I = \frac{m}{M} g_I \ .$$

$g_I \vec{I}$ gives the nuclear magnetic dipole moment operator in units of μ_n

and $g_I I$ is equal to the μ_I defined by Eq. (20). Since $\mu_I \approx \mu_n$ while electronic magnetic moments are $\approx \mu_o$ (see Eq. (37)), $g'_I/g_J \approx \mu_n/\mu_o = 1/1836$.

If we restrict ourselves, as is usual in atomic-beam magnetic resonance experiments, to magnetic fields such that

$$g_J \frac{\mu_o H}{h} \approx \mathcal{H}_{hfs}$$

then Eq. (39) is well satisfied and both $\mathcal{H}^{fs}$ and $\mathcal{H}^{hfs}$ are of the same order as (or less than) $\mathcal{H}_{hfs}$ of Eq. (22). Hence, including these interaction energies as part of the hyperfine structure Hamiltonian we have finally

$$\mathcal{H}_{hfs} = a\vec{I}\cdot\vec{J} + b\frac{3(\vec{I}\cdot\vec{J})^2 + 3/2\,\vec{I}\cdot\vec{J} - I(I+1)\,J(J+1)}{2I(2I-1)\,J(2J-1)} - g_J\frac{\mu_o H}{h}J_z - g'_I\frac{\mu_o H}{h}I_z \quad . \tag{42}$$

It should be noted that this Hamiltonian holds only for matrix elements taken in the $|IJFm_F>$ representation as mentioned above, in connection with Eq. (22).

Now the last two terms of Eq. (42) do not commute with the $\vec{F}^2$ operator so that they will not be diagonal in the $|IJFm_F>$ representation and F will no longer be a good q.n. However if we restrict ourselves to values of H such that $g_J \frac{\mu_o H}{h} \ll \frac{aK}{2}$ [Linear Zeeman region for hfs levels] we can keep F as a good q.n. and use first order perturbation theory to get the energy splitting caused by H. Then[8]

$$<IJFm_F|\mathcal{H}_{hfs}|IJFm'_F> = W(IJFm_F) = \frac{aK}{2} + bQ_{op} - \frac{m_F\mu_o H}{h}\delta_{m_F m_F'}$$
$$\times\left[g_J\frac{F(F+1)+J(J+1)-I(I+1)}{2F(F+1)} + g'_I\frac{F(F+1)+I(I+1)-J(J+1)}{2F(F+1)}\right]$$

where the definition of Q_{op} is obvious from Eq. (19). This expression is usually written in the form

$$W(IJFm_F) = \frac{aK}{2} + bQ_{op} - g_F\frac{\mu_o H}{h}m_F \tag{43}$$

where

$$g_F = g_J\frac{F(F+1)+J(J+1)-I(I+1)}{2F(F+1)} + g_I\frac{F(F+1)+I(I+1)-J(J+1)}{2F(F+1)} \tag{44}$$

Hence each degenerate hyperfine structure level is split into 2F + 1 equally spaced components that are separated by

$$\nu\,(IJF) = g_F \frac{\mu_o H}{h} \quad \text{(in units of mc/sec)} . \tag{45}$$

As the magnetic field is increased the hyperfine structure "weak field" criterion given above becomes less and less well satisfied so that it is necessary to use perturbation theory of higher order than 1st to obtain the hyperfine energy splitting. Finally, at some value of field, the necessary order of perturbation theory becomes so high that the most practical way to determine the energy levels is to diagonalize the Hamiltonian of Eq. (42) directly in the $|IJFm_F>$ representation (intermediate field region for hyperfine structure). If the field is increased even further a point is reached where the first and second terms of Eq. (42) are small compared to the third (Paschen-Back region for hyperfine structure). Then I_z and J_z are the most important operators in this equation and $\mathcal{H}_{hfs}$, although far from diagonal in the $|IJFm_F>$ representation, is close to diagonal in the $|Im_I Jm_J>$ representation. It can be shown[9] that in the limit $g \frac{\mu_o H}{h} \gg a\, m_I m_J$ the eigenvalues of $\mathcal{H}_{hfs}$ are given by

$$W(Im_I Jm_J) = am_I m_J + b/4 \frac{\left[3m_J^2 - J(J+1)\right]\left[3m_I^2 - I(I+1)\right]}{J(2J-1)\, I(2I-1)} - g_J \frac{\mu_o H}{h} m_J - g'_I \frac{\mu_o H}{h} m_I . \tag{46}$$

Equation (46) holds under the assumption that the condition of Eq. (39) is still not violated.

Hence, considering the whole range of magnetic field, at low values of H the h.f.s. energy levels specified by different values of F are well separated in energy, each one being split up in 2F + 1 closely spaced magnetic sublevels (see Eq. (43)). As the field is increased these magnetic sublevels separate further and further until it is no longer possible to associate any given one of them with a particular value of F. However, since F_z commutes with all of the operators in Eq. (42), each magnetic sublevel does preserve its $m_F = m_I + m_J$ throughout the intermediate field region. Finally, as the field is further increased a value is reached where $g_J \mu_o H/h \gg a$. Then, according to Eq. (46), the hyperfine levels corresponding to different values of m_J are well separated in energy, and superimposed on each of these are 2I + 1 closely spaced levels

associated with different values of m_I.

A rough idea of the behaviour of the magnetic sublevels at intermediate fields can be obtained by noting that the magnetic q.n. $m_F = m_I + m_J$ is conserved throughout and that levels having the same value of m_F, which arise initially from zero field levels of different F, can never cross (m_F no-crossing rule). Using these rules and Eqs. (43) and (46) each magnetic sublevel can be unambiguously identified at any value of field and a schematic diagram (such as is given in Fig. 21) drawn showing the correspondence between the high field and low field magnetic sublevels.

II. THE ATOMIC BEAM METHOD

A. Introduction

Atomic-beam Radiofrequency Spectroscopy, like any other type of spectroscopy, has three main requirements. First an appropriate source of the material to be studied must be available. Second a means must be at hand to induce transitions between various energy states of the system under consideration. And third there must be some mechanism available for determining whether or not such transitions occur, under varying experimental conditions. The discussion below concerns itself with the way these requirements are met in the particular case of the atomic-beam method.

B. General Discussion of the Method

As its name implies, the material studied by the method under consideration must be converted, for investigation, to a beam of neutral, essentially non-interacting, atoms. This is usually done, in the case of metals, by heating the material to a high temperature in an appropriately designed oven containing a source slit. Atoms effusing from the slit at thermal velocities are then properly collimated to produce the beam. On the other hand for volitile non-metals, such as the halogens, more elaborate beam production methods utilizing leaks, accurate temperature control measures, and various types of molecular dissociators, often need be used. In general the techniques used to produce atomic-beams vary widely from case to case and even rather widely used methods usually must be specially adapted for application to each particular case.

In Atomic-beam Spectroscopy, as it is applied here, magnetic dipole transitions are induced between the hyperfine energy levels of isolated atomic systems. These systems are studied in the presence of a uniform magnetic field which can be varied in strength over a wide range. The transitions are induced by applying an oscillating magnetic field at R.F. frequencies corresponding to the energy differences between various eigenstates of $\mathcal{H}_{hfs}$ (see Eq. (42)).

The occurrence of such transitions is sensed by noting the resulting changes in the "effective magnetic moments," μ_{eff}, of the atoms. μ_{eff} is defined,[1] for an atomic system, as $-\partial W/\partial H$ where W is the total "spectroscopical" energy of the atom. From the general equation for the force on a conservative system, $\vec{F} = -\vec{\nabla} W$, it follows

that the force, in the z direction, exerted on an atom by an inhomogeneous magnetic field of magnitude H and gradient $\partial H/\partial z \ \hat{k}$ is given by $F_z = \mu_{eff} \partial H/\partial z$. In particular if H is of such a magnitude that the Paschen-Back region for hyperfine structure is reached then, from Eq.(46)

$$F_z \equiv g_J \mu_o \, dH/dz \, m_J \text{ and } \mu_{eff} \equiv g_J \mu_o \, m_J \quad . \tag{47}$$

The method used to detect changes in μ_{eff} (for a so-called "flop-in" configuration) is illustrated in Fig. 3, which gives a schematic diagram of an atomic-beam machine such as the one used during the experiments reported here. Atoms leaving the source at position O first pass between the pole tips of the A-magnet, where there is an inhomogeneous magnetic field (H_A) of sufficient strength to render Eq. (47) applicable and which has a gradient $(\partial H/\partial z)_A$ in the z direction. A collimator at the end of this magnet eliminates all atoms except those having initial trajectories similar to the one shown in the figure. The remaining atoms then pass between the pole tips of the C-magnet where a homogeneous magnetic field exists. Superimposed on this field is the weak oscillating field mentioned above and this may or may not cause atomic transitions leading to a change in the value of μ_{eff}.

After leaving the C field the atoms enter the B field region where H_B is also sufficiently strong to "Paschen-Back" the hyperfine levels and has a gradient, $(dH/dz)_B$, in the same direction as $(dH/dz)_A$. The magnitude of $(dH/dz)_B$ is adjusted so that if μ_{eff} of Eqs. (47) reverses sign in the C field region a trajectory such as (2) of Fig. 3 is followed by the atoms and they reach the detector D. On the other hand, if such a reversal of sign does not take place a path such as (1) is followed and the atoms are not focussed at D. Hence, by noting the number of atoms reaching the detector, the occurrence of atomic transitions can be sensed. It is important that all changes in magnetic field seen by the atoms as they pass down the apparatus are slow enough that their μ_{eff}'s adiabatically maintain/the same orientation with respect to the magnetic field in all regions, unless an R.F. induced transition takes place. For this reason the A, B, and C fields are all applied in the same direction and sufficient space is left between the various magnets to allow the fields gradually to fringe together.

The stop wire, indicated by S in the figure, is mounted on the centerline of the apparatus to eliminate high velocity and molecular

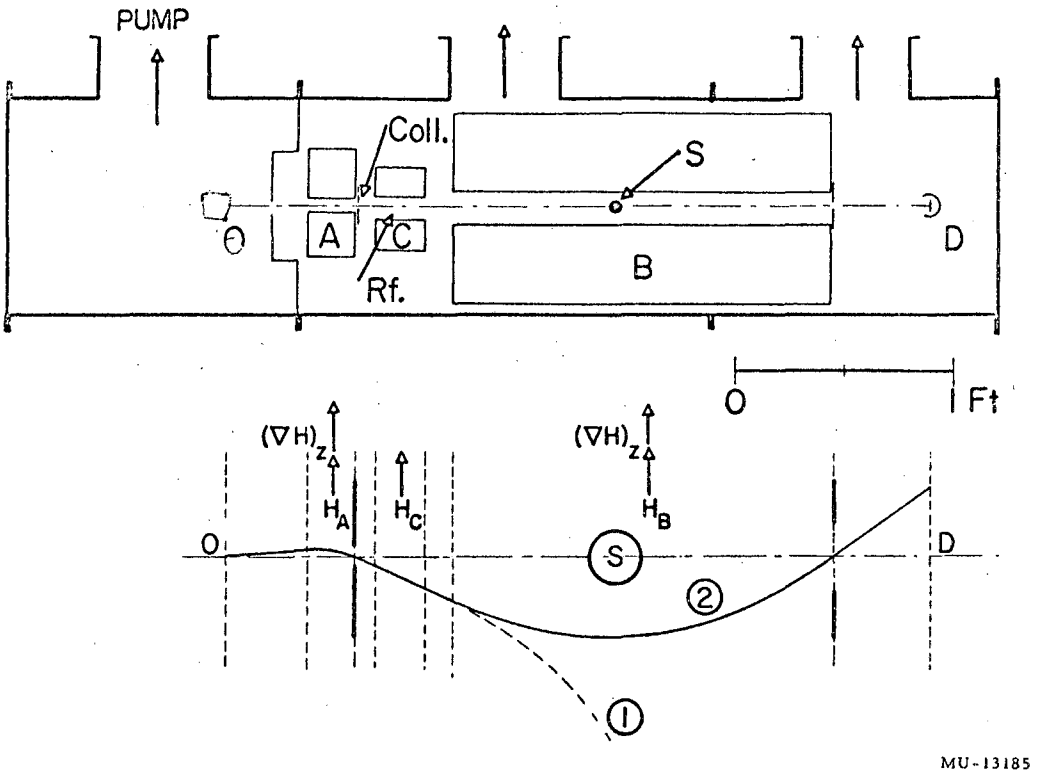

Fig. 3. Schematic diagram illustrating possible atom-beam trajectories.

components of the beam. These are not deflected enough, in the absence of transitions, to miss the detector and therefore, without the stop wire in position, would add to the "apparatus background." This background, which is caused by beam atoms which reach the detector without undergoing transitions, is held to a minimum by accurate allignment of the various slits and stops and by maintaining a low pressure ($\approx 10^{-6}$mm) throughout the whole system to eliminate gas scattering.

Although the flop-in configuration, as depicted in Fig. 3, has the advantage of yielding a low apparatus background over which even moderate number of atoms which have undergone transitions can be detected, it has the disadvantage that only those transitions which lead to a change of sign of m_J in the high field region can be detected. This restricts the number of "observable" transitions to only a small percentage of all possible hyperfine transitions. For a given I and J the transitions in the low and intermediate field regions which lead to a change in sign of m_J in the high field region can be determined, as described in Section I.C., by drawing an energy level diagram such as Fig. 21. The nature of these transitions depend, in general, on the ordering of the zero field hyperfine levels, that is on the relative values of the $W^o(I\ J\ F)$ of Eq. (19) for different values of F. (For example, see Fig. 21 a and b.)

As implied above the occurrence of transitions, using the flop-in configuration, is indicated by an increase in the relative number of beam atoms traversing the entire length of the apparatus. Hence the presence of these atoms at the detector position must be ascertainable for the atomic-beam method to be usable. This, in fact, constitutes one of the major problems encountered in beam work and has, in the past, severly limited the applicability of the method. The only methods of detection used during the course of the experiments reported here are "hot wire detection," which was used for the C field calibration isotope (K^{39}), and "radioactive detection," which was used for all the radioactive species studied. The former depends on the ability of a hot metallic wire with a high work function to capture electrons from free atoms with low ionization potentials, thus producing a detectable ion current. This method has been used successfully to detect most of the alkali metals as well as some of the halogens and is described in detail in Ref. 1. Radioactive detection, on the other hand, depends on the collection of radioactive beam atoms on some appropriate surface at the detector position. The collecting surface is removed from the apparatus, after a

given period of exposure to the beam, and the amount of radioactivity deposited on it measured by standard counting techniques. The measured activity is then proportional to the number of atoms reaching the detector during the period of exposure.

C. Inducing Transitions

The transition inducing R.F. magnetic field is supplied by driving alternating electric current through an appropriately designed R.F. loop (or "hairpin") which is usually placed in the middle of the C field and through which the atomic-beam passes (see Figs. 8 and 9). Determining the probability of a transition occurring when the frequency of this field is in the neighborhood of the Bohr Frequency, $\nu = \frac{W_1 - W_2}{h}$, is in general a quite complicated quantum mechanical problem and depends upon the value of the C field (H); the amplitude, direction, and spacial dependence of the R.F. field; the number of transitions having Bohr Frequencies near ν; and the velocity spectrum of the atomic-beam. This probability has been worked out by several authors for various special conditions (see Refs. 1, 10, 11, 12, 13) and although the results differ considerably in details they all indicate that for a single "Rabbi type" hairpin the transition probability should have a maximum at (or at least by symmetric about) the Bohr Frequency. This is born out in practice for reasonably designed R.F. loops (see, for example, the resonance curves exhibited in this paper). Furthermore in all cases there is some optimum R.F. field amplitude where the transition probability has its maximum value at resonance (that is at the Bohr Frequency) while at the same time the resonance width (that is the width of the transition probability curve as a function of frequency) is reasonably narrow. This width, although differing from case to case, can never be less than the "natural width" determined by the Heisenberg Uncertainty Principle ($\Delta\nu \gtrsim 1/\tau$ where τ is the time spent by the atoms in the R.F. region).

In actual experiments the optimum R.F. field amplitude is usually determined by trial and error since the detailed information needed for its calculation is not available. Furthermore, although the general line shapes obtained experimentally conform to theoretical expectations the line width, in practice, is usually determined by the uniformity of the C field and is considerably broader than predicted theoretically.

Two different types of magnetic dipole transitions, usually designated by π and σ, can be induced depending on whether the R.F. magnetic field is applied perpendicular or parallel to the C field (H, always assumed in the z direction). The "selection rules" governing these transitions can be determined, for low and high values of H, by noting that for any reasonable quantum mechanical treatment the transition probability depends on the matrix element of the perturbation causing the transition between eigenfunctions characterizing the initial and final states.

A field oscillating at frequency $\nu = \omega/2\pi$ along an arbitrary x axis (perpendicular to the z axis) can be expressed as

$$H_{rf}(\perp) = H_{rf}(e^{i\omega t} + e^{-i\omega t})\hat{i} = H_{\omega}\hat{i}$$

while for a field oscillating along the z axis

$$H_{rf}(\parallel) = H_{rf}(e^{i\omega t} + e^{-i\omega t})\hat{k} = H_{\omega}\hat{k} \quad .$$

Hence the corresponding perturbation Hamiltonian can be written (see Eq. (42))

$$\mathcal{H}_{rf}(\perp) = -g_J \frac{\mu_o}{h} H_{\omega} J_x - g'_I \frac{\mu_o}{h} H_{\omega} I_x \qquad (48)$$

$$\mathcal{H}_{rf}(\parallel) = -g_J \frac{\mu_o}{h} H_{\omega} J_z - g'_I \frac{\mu_o}{h} H_{\omega} I_z \quad . \qquad (49)$$

Now for low H the eigenstates of the Hamiltonian are characterized by the q.n.'s IJF and m_F. Taking matrix elements of Eqs. (48) and (49) in this representation we get[8]

$$\langle IJFm_F | \mathcal{H}_{rf}(\perp) | IJF'm'_F \rangle = 0 \quad \text{unless } F' = F \pm 1 \text{ or } F' = F$$

$$\text{and } m'_F = m_F \pm 1$$

$$\langle IJFm_F | \mathcal{H}_{rf}(\parallel) | IJF'm'_F \rangle = 0 \quad \text{unless } F' = F \pm 1 \text{ or } F' = F$$

$$\text{and } m'_F = m_F \, .$$

Similarly, as mentioned above, for high H the eigenstates of the Hamiltonian are specified by IJm_I and m_J. Taking matrix elements in this representation we get[8]

$$\langle IJm_I m_J | \mathcal{H}_{rf}(\perp) | IJm_I' m_J' \rangle = 0 \text{ unless } m_I' = m_I \pm 1 \text{ or } m_J' = m_J \pm 1$$

$$\langle IJm_I m_J | \mathcal{H}_{rf}(\parallel) | IJm_I' m_J' \rangle = 0 \text{ unless } m_I' = m_I' \text{ and } m_J = m_J' \ .$$

Therefore we have the following magnetic dipole transition selection rules

for low fields	for high fields	
$\Delta F = 0, \pm 1$ and $\Delta m_F = \pm 1$	$\Delta m_I = \pm 1$ or $\Delta m_J = \pm 1$	for R.F. field $\perp$ to H
$\Delta F = 0, \pm 1$ and $\Delta m_F = 0$	$\Delta m_I = 0$ and $\Delta m_J = 0$	for R.F. field $\parallel$ to H .

(50)

Since the Hamiltonian of Eq. (42) is diagonal in neither of the representations mentioned above for intermediate fields, simple selection rules like the above cannot be written down for this case.

By convention, transitions for which $\Delta F = \pm 1$ are called "direct transitions." It can be shown, for atoms with I and $J > 1/2$ and J half odd integral, that there are at least two types of $\Delta F = 0$, $\Delta m_F = \pm 1$ low field transitions which are observable by the atomic-beam flop-in method. These are referred to below as α and β transitions and occur in the $F = I + J$ and $F = I + J - 1$ hyperfine levels, respectively.

D. Spin Determination

The determination of nuclear spins, by the atomic-beam method, is based on Eqs. (44) and (45) for the frequencies of $\Delta F = 0$, $\Delta m_F = \pm 1$ transitions at low fields. In using Eq. (44) the term involving g_I' is temporarily ignored since $g_I'/g_J \approx 1/1836$. If J and g_J are known, for example from optical spectroscopy work, then g_F is a function of only two unknown quantities, the discrete parameters I and F. Assuming that $F = I + J$ (for α transitions) or $F = I + J - 1$ (for β transitions) reduces g_F to a function of I only and leads, for a given value of H, to different α and β transition frequencies for each discrete value of I (via Eq. (45)). The correct value, for a given nuclear species, is obtained by successively setting the R.F. field at all frequencies corresponding to reasonable values of I and noting for which particular value a resonance is registered at the detector (conducting a "Spin Search"). The identity of the nuclide for which a resonance is obtained is then ascertained (for radioactive detection) by noting the decay rate of the deposit on the collector surface and comparing this to known radioactive half-life data.

After a tentative value of I has been obtained by the above method full resonance curves are traced out (whenever possible) at several (weak) values of magnetic field for both the α and β transitions to illiminate the possibility of overlap (i.e. different transitions giving rise to the same value of ν for different I). This process usually suffices definitely to determine the spin.

If, as in the case for many atoms, J and g_J are also unknown, Eqs. (44) and (45) can be used to determine these quantities (as well as I) by a slightly more complicated procedure involving a continuous scanning of R.F. frequencies at a very low value of H. Resonance frequencies so determined are analyzed on the basis of all reasonable combinations of I, J and g_J, and possible values of these parameters extracted. All sets of such values are then used, in turn, to predict resonance frequencies at a different field and a discrete search, such as the one described above, is carried out. The particular set of values which lead to correct predictions of resonance frequencies at a number of arbitrary magnetic fields, is then taken as representing the actual values.

E. Hyperfine Structure Determination

To determine the hyperfine structure interaction constants, that is the values of "a" and "b", for a given (radioactive) atomic species the observable α and β (and perhaps additional) resonances are first observed at a sufficiently weak magnetic field to allow their frequencies to be predicted accurately by Eq. (45). The field is then increased (usually doubled) and new resonances sought on the basis of this equation. This process is repeated until the "weak field" criterion used in the derivation of Eq. (43) is violated to the extent that predictions based on it are no longer valid and the actual resonance frequencies are "shifted" from the linear Zeeman predictions by amounts necessitating extensive resonance searches. At this point, in order to obtain more reliable predictions, it is necessary to utilize perturbation theory of higher order than the first. Second order perturbation theory, however, requires a knowledge of the unperturbed energy level separation of the system under consideration. In the present case these are the zero field hyperfine structure levels of Eq. (19), which depend on the unknown parameters "a" and "b". Therefore the only way that more accurate predictions can be obtained is to make

guesses for "a" and "b" based on previously collected resonance data and to use these values either in a higher order perturbation calculation or for a direct diagonalization of $\mathcal{H}_{hfs}$ (see Eq. (42)).

Two Digital Computer Programs have been written to perform most of the computational work involved in hyperfine structure determinations by the method here described. The first, to be referred to hereafter as "Hyperfine," is written for the I.B.M. 704 and is described in detail in Reference 14. Given a set of experimental resonance data, this program determines the best values of "a" and "b" (and if desired g_I' and g_J) consistent with these data. This is done by first diagonalizing $\mathcal{H}_{hfs}$ for appropriate values of H using some "tentative" values of "a" and "b", which are supplied as input to the program. In this way tentative theoretical transition frequencies are obtained for all resonance lines represented in the data set. On the basis of the resulting residuals (that is the experimentally measured resonance frequencies minus the corresponding theoretical predictions) corrections are made to "a" and "b" and the diagonalization procedure is repeated. This iteration process is continued until the best least squares fit is obtained. The latter condition is realized when further changes in "a" and "b" yield only insignificant reductions in the goodness of fit parameter χ^2. In this way the values of "a" and "b" which lead to the best theoretical fit of the experimental resonance data are obtained.

The program requires as inputs: 1) various numerical constants and control words 2) calibration data used in the determination of the fields and field uncertainties for each experimental resonance point, 3) I, g_I', and "a" for a "comparison isotope" of the same element as that under consideration, 4) I, J, g_J, and tentative values of "a" and "b" for the particular isotope under consideration and finally, 5) resonance frequencies, resonance frequency uncertainties, associated low field q.n.'s, and calibration isotope frequencies for each resonance line that it is desired to fit. As output the program gives: 1) the best values of "a" and "b", 2) the uncertainties in these values, taken as one standard deviation, 3) the resonance frequencies and residual calculated on the basis of the best values of "a" and "b", 4) the value of the χ^2 goodness of fit parameter, 5) the value of g_I' obtained using Eq. (26) in conjunction with the comparison isotope data.

As indicated above "Hyperfine" also has the options of allowing g_I' and/or g_J (as well as "a" and "b") to vary during the fitting process. In this case the comparison isotope data is used first to calculate a tentative value of g_I' and/or the initial input value of g_J is also considered as tentative. These parameters are then improved by iteration in exactly the same way as "a" and "b", and are given as output along with their uncertainties.

The initial, tentative, values of "a" and "b" necessary as input to "Hyperfine" are determined, prior to the program's first application to a given case, by noting the shifts from the predictions of Eq. (45) and performing a 2nd or 3rd order perturbation calculation based on these. A discussion of the way in which this is done and the pertinent equations needed are given in Appendix C.

The other necessary program, which is written for the IBM 653 and is called "JO-9", is also described in detail in Ref. 14. Its purpose is, given a, b, I, J, g_I' and g_J', to generate a table of resonance frequencies vs. field for arbitrary hyperfine transitions. This is done by direct diagonization of Eq. (42) in the I J F m_F representation.

After initial guesses for "a" and "b" have been made based on shifts from the frequency predictions of Eq. (45) and using the formulae of Appendix C, the "Hyperfine" program is used, in conjunction with all data collected up to that time, to improve these values. Then the "JO-9" Program is used to predict higher field $\Delta F = 0$ (α and β) transition frequencies. Resonance searches, centered at the predicted frequencies, are then conducted and more resonance data is obtained. Using the last "Hyperfine" results for "a" and "b" as the new "tentative" values and adding the new resonance data to that previously obtained, "Hyperfine" is again used to improve "a" and "b" still further. This successive improvement process is continued until "a" and "b" are known sufficiently well to enable a search to be conducted for observable $\Delta F = \pm 1$ (direct) transitions (usually initially at low H). Finally, after all observable low field π and σ direct transitions have been found and "a" and "b" correspondingly improved, searches for any existing observable "field independent" direct transitions can be undertaken. The frequencies of these transitions, which are to first order independent of H, can be determined by the use of "JO-9" and occur when the derivative of the corresponding transition frequency with respect to H vanishes.

F. g_I' Direct Determination

Although the value of g_I' can be determined from the value of "a" using Eq. (26), it is not possible to determine the sign of either quantity by the method described above, without considering the direct effect of the g_I' term in Eq. (42). This can be seen by noting that $_{hfs}$ is diagonal in m_F so that, ignoring the g_I' term, reversing the signs of "a" and "b" results in a Hamiltonian who's eigenvalues are related to those of Eq. (42) by

$$W_{reversed}(m_F) = -W(-m_F) \quad .$$

Since, however, in the method described above we only observe the differences between energy states corresponding to $\Delta m_F = \pm 1$ the observed R.F. spectrum would be the same for either Hamiltonian. Therefore only the relative signs of "a" and "b" can be determined and hence the sign of g_I' cannot be determined by Eq. (26). Including the g_I' term in Eq. (42), however, removes this ambiguity. Although g_I' is usually much smaller than g_J it is often possible, with good C field uniformity and time stability, to determine its sign by noting the effect that changing it has on the fit of the experimental data (that is the effect on χ^2 and the frequency residuals). Furthermore a rough value of this parameter, including sign, can often be obtained, using high precision resonance data, by allowing g_I' to vary freely in the "Hyperfine" Program as described above.

III. NUCLEAR MODELS

A. Introduction

It is not possible, as in the case of the atomic system treated in Section I, to write down a Hamiltonian such as Eq. (1) for a complexed nuclear system because the form of nucleon-nucleon interaction, within a nucleus, is not yet well understood. Furthermore, even if such a Hamiltonian could be written down we would probably have to deal with a prohibitably difficult mathematical problem because of the many body nature of the nuclear system. Therefore the best that one can hope to do is to formulate some "model" of the nucleus which can be dealt with mathematically and on the basis of which various nuclear properties can be predicted. The two such models which have been most successful in their respective spheres of applicability are discussed briefly below.

Discussions of the measured nuclear properties of Lu^{176m}, Br^{80}, Br^{80m}, and I^{132} are given, in subsequent Sections, in terms of these models and thus their applicability further tested. It was with this in mind that the experimental measurements reported in this paper were undertaken.

B. The Shell Model

Odd A Nuclei:

The Nuclear Shell Model[15] of Mayer, Haxel, Jensen and Suess was originally formulated in an attempt to account for the occurrence of the unusually stable "Magic Number" nuclei. It replaces the complex nuclear potential by the approximation that each nucleon exhibits a strong negative spin-orbit interaction and moves in a spherically symmetric effective potential, $U(r_i)$, essentially independently of the other nucleons. This potential varies from a harmonic oscillator type for light nuclei to a square well type for heavy nuclei. Hence a nuclear Hamiltonian of the form

$$\mathcal{H}\,(\text{Shell Model}) = \sum_{i=1}^{A} \frac{p_i^2}{2M} + U(r_i) - f(r_i)\,\vec{l}_i \cdot \vec{s}_i \qquad (51)$$

is assumed. The exact forms of $U(r_i)$ and $f(r_i)$ are determined in such a way as to fit empirical nuclear data, $f(r_i)$ being always taken as positive.

The complete solution of the Schrodinger's Equation resulting from Eq. (51) consists of a product of single nucleon eigenfunctions, each characterized by the q.n.'s n, ℓ, j and m_j where n, the harmonic oscillator q.n., determines their radial dependence. Each single particle eigenstate is $2j + 1$ fold degenerate if direct interactions between nucleons are ignored. Taking these interactions into account lifts this degeneracy and consequently determines the order of filling of the states. It is to be noted that this situation is the exact opposite of that occurring in the atomic case where the electronic interaction term is greater than the spin orbit coupling. Thus, instead of exhibiting something approximating L-S coupling the nuclear system usually exhibits j-j coupling.

The ground state configuration of a given nucleus, which for j-j coupling is designated by giving the n, ℓ, and j of all occupied nuclear levels, is determined by filling these levels in a manner consistant with the Pauli Principle (neutrons and protons being considered as non-identical particles). With the added assumptions that $f(r_i)$ decreases with increasing n and that the tendency of equivalent nucleons (i.e. those having the same n, ℓ and j) to pair to states characterized by $j(\text{total}) = 0$ is enhanced with increasing j, this model not only predicts correctly the occurrance of magic number nuclei at the closing of widely spaced nuclear "shells" but is also capable of predicting the ground state spin and parities of most odd A nuclei. This is done by determining the appropriate Shell Model wave functions using the following angular momentum "coupling rules";

S1. The ground states of all nuclei with an even number of protons and neutrons have zero angular momentum and even parity.

S2. In nuclei consisting of an even number of neutrons (protons) and an odd number of protons (neutrons) the ground-state properties are determined by the protons (neutrons) alone.

S3. In a nucleus of odd A, the nucleons of the type which is present in odd number will usually couple their spins in such a way that the total nuclear angular momentum is that of the last partially filled orbit, j [normal coupling] .

These rules are supported both by emperical nuclear data and by calculations based on reasonable assumptions concerning nucleon-nucleon interactions. The "usually" occurring in S3. refers to the fact that for several odd neutrons or protons in a partially filled subshell (specified by

j), the nucleon angular momenta sometimes prefer to couple to some value less than j. This is explainable on the basis of finite range nuclear forces and also on the basis of the Collective Nuclear Model, to be discussed below. The discussion below will, for the most part, be restricted to the Extreme Single Particle Shell Model. That is, it will be assumed (as implied by S3.) that all nuclear properties are determined by the configuration of the last odd nucleon.

Nuclear Moments:

Once the nuclear wave function has been approximated by the method described above this can be used, after anti-symmetrization, to determine the expectation values indicated in Eqs. (20) and (21). Using the expression given in Eq. (21) for the electric quadrupole moment operator and the expression

$$\vec{\mu} = \sum_{i=1}^{Z} (g_{sp}\,\vec{s}_p + g_{\ell p}\,\vec{\ell}_p)_i + \sum_{j=1}^{N} (g_{sn}\,\vec{s}_n + g_{\ell n}\,\vec{\ell}_n)_j \qquad (52)$$

where

$$g_{sp} = 5.596, \quad g_{\ell p} = 1, \quad g_{sn} = -3.826, \quad g_{\ell n} = 0$$

for the magnetic dipole moment operator, we get for the nuclear magnetic dipole moment

$$\mu_I = g_{jr} j_r = g_{sr} \frac{j_r(j_r+1) + s_r(s_r+1) - \ell_r(\ell_r+1)}{2(j_r+1)} + g_{\ell r} \frac{j_r(j_r+1) + \ell_r(\ell_r+1)}{2(j_r+1)} \frac{-s_r(s_r+1)}{} \qquad (53)$$

where for odd Z, even N; r = p and n, ℓ, and j designate the configuration
for odd N, even Z; r = n of the last odd nucleon.

In deriving Eq. (53) it is assumed that the "normal coupling" condition of S3 holds and that the nuclear system exhibits pure j-j coupling.

Also for the electric quadrupole moment we get

$$Q_p = -\frac{2j+1-2\lambda}{2(j+1)} \langle r^2 \rangle \quad \text{for N even; Z odd}$$
$$Q_n \approx \frac{Z}{(A-1)^2} Q_p \quad \text{for N odd; Z even} \qquad (54)$$

In these equations, λ denotes the occupation number of the unfilled odd nucleon level characterized by j (= I), and $< r^2 >$ is usually taken as equal to 3/5 (nuclear radius)^2.

Equations (53) constitute analytical expressions for the so-called "Schmidt Lines" and reproduce fairly well the algebraic signs and general quantitative trends of most Odd A nuclear magnetic moments. Though most known magnetic moments deviate considerably from the Schmidt lines (usually by $\approx$ 1/2 to 1 nuclear magnetons) for a given type odd nucleon the values tend to cluster near either the line corresponding to $j = \ell + 1/2$ or the one corresponding to $j = \ell - 1/2$. Hence if $I = j$ is known Eq. (53) suffices to determine ℓ and hence the parity of the nuclear state. Ground state parities, found in this way, agree very well with determinations by other methods. Furthermore, if the simple angular momentum coupling rule S3 is abandoned and all nucleons occupying unfilled j levels allowed to contribute to the magnetic moment and, in addition, the effects of "mixed configurations" (such as were discussed above for the atomic case) are considered, calculations based on the Shell Model can account for most known odd-A magnetic moment data.

Equations (54), for the electric quadrupole moment, give quantitatively accurate results only near closed j shells and, in fact, the Shell Model is incapable, even with configuration mixing, etc., of explaining the large Q values found experimentally for some nuclei (10-20 times the Shell Model estimates). However, Eqs. (54) do give the signs of most odd-A quadrupole moments correctly and, in particular, predict that for a j level less than half full ($\lambda < \frac{2j+1}{2}$) Q should be negative while for a j level more than half full Q should be positive.

Odd-Odd Nuclei:

For odd-odd nuclei the Shell Model implies that the odd neutrons and odd protons (that is those outside closed j subshells) act as independent, superimposed, systems in determining the nuclear characteristics. Before attempting to predict these characteristics we must have some rules for coupling the angular momentum of the proton system, J_p, and that of the neutron system, J_n, to give the total spin I of the nucleus. Nordheim[16] has proposed two rules governing this coupling process in the case where the "normal" coupling rules S1-S3 are obeyed separately by the two systems. They are

N1. If $j_n = \ell_n \pm 1/2$ and $j_p = \ell_p \pm 1/2$, then $|j_n - j_p| < I \leq j_n + j_p$. That is j_n and j_p tend to add, but not necessarily to the highest possible value.

N2. If $j_n = \ell_n \pm 1/2$ and $j_p = \ell_p \mp 1/2$, then $I = |j_n - j_p|$.

Both these rules reflect the tendency of the nucleon spins to allign themselves parallel (as evidenced by the ground state of the deuteron) and of the nucleon orbital angular momenta to allign themselves antiparallel. In the case of N2 (Nordheim's Strong Rule) both these conditions can be satisfied simultaneously while in the case of N1 (Nordheim's Weak Rule) there is a competition between the two tendencies. N2 is well satisfied in general but N1, in addition to being quite non-definitive as stated, is often violated.

Recently Brennan and Bernstein[17] have proposed three coupling rules which are well born out by empirical nuclear data and which strengthen the Nordheim Weak Rule. These rules distinguish between particles and holes (i.e. particles missing from nearly filled j subshells) and can be stated as follows.

If both systems contributing to the angular momentum are either particles or holes, then

BB1. $I = j_p + j_n$, for $j_p = \ell_p \pm 1/2$ and $j_n = \ell_n \pm 1/2$

BB2. $I = |j_p - j_n|$, for $j_p = \ell_p \pm 1/2$ and $j_n = \ell_n \mp 1/2$

and if one of the systems contributing to the angular momentum is made up of particles while the other is made up of holes

BB3. $I = j_p + j_n - 1$ (This rule only reflects a tendency and is violated in some cases).

It is seen that while N2 remains unchanged the above replaced N1 by a much stronger rule plus an additional weak condition. These rules are supported, theoretically, by calculations made by Schwartz[18] assuming a spin dependent delta function interaction between the odd neutron and proton.

Nuclear Moments:

Having decided on the angular momentum coupling scheme we can now present Shell Model expressions for the nuclear moments of odd-odd nuclei. In the case of the magnetic dipole moment we must take the expectation value of the z component of Eq. (52) in a nuclear eigenstate specified by $|J_n J_p \; II>$. Assuming that the proton and neutron systems are independent and both exhibit pure j-j coupling this gives[19]

$$\mu_I = I\, g_I = g_{jp}\, \frac{I(I+1)+j_p(j_p+1)-j_n(j_n+1)}{2(I+1)} + g_{jn}\, \frac{I(I+1)+j_n(j_n+1)-j_p(j_p+1)}{2(I+1)} \qquad (55)$$

where g_{jp} and g_{jn} are given by Eq. (53) with the substitution $r \rightarrow p$ and $r \rightarrow n$ respectively.

Comparing the results obtained using Eq. (55) with the experimentally measured moments of odd-odd nuclei reveals that it predicts these moments with about the same accuracy as Eq. (53) does the moments of odd-A nuclei. This is to be expected if the assumed independent nature of the proton and neutron systems has any validity.

Schwartz[20] has suggested that for predicting the magnetic moments of odd-odd nuclei, "empirical" nucleon magnetic moments be used. This means that for a given odd-odd nucleus, characterized by N_o and Z_o, instead of using Eqs. (53) to determine the g_{jn} and g_{jp} of Eq. (55), one uses the measured value of μ_I for an even-odd nucleus having $N = N_o$, $Z = Z_o \pm 1$ to determine g_{jn} and μ_I for an odd-even nucleus having $N = N_o \pm 1$, $Z = Z_o$ to determine g_{jp}. With this technique much better predictions for odd-odd magnetic moments are obtainable.

To get an expression for the electric quadrupole moment of an odd-odd nucleus we must evaluate the matrix element of Eq. (21) for an eigenstate specified by $|\, j_n j_p\ II\rangle$. Noting that the quadrupole moment operator is the $\mu = 0$ component of the tensor operator $\bar{Q}^{(2)}$ and that this operator, in the present case, only involves the coordinates of the independent proton system characterized by angular momentum j_p, we see that this matrix element can be evaluated using Eq. (13). Making the proper identifications in this equation and noting the definition of the quadrupole moment, defined with respect to the proton system ~~above~~ alone we get[19]

$$Q_{\text{odd-odd}} \frac{(2I+1)!}{2j_p!} \left[\frac{(2j_p-2)!\ (2j_p+3)!}{(2I-2)!(2I+3)!} \right]^{1/2} W(j_p I\ j_p I;\ j_n 2)(-1)^{(j_p-j_n-I)} Q_p \qquad (56)$$

where Q_p is given by Eqs. (54).

C. The Collective Model

Odd A Nuclei:

The Bohr-Mottelson Collective Model of the nucleus is essentially

an extension of the Shell Model, in which not only the motion of nucleons in unfilled shells is considered but also collective motions of the nuclear core. This core, which in the Shell Model is considered only as an inert source of the effective nuclear potential in which the "loose" nucleons move, is considered now as capable of executing surface vibrations and rotations which can contribute to the total angular momentum and other properties of the nucleus. Instead of Eq. (51) we now have for the total nuclear Hamiltonian

$$\mathcal{H}(\text{collective}) = \mathcal{H}(\text{core}) + \mathcal{H}(\text{Shell Model}) + \mathcal{H}(\text{interaction}) \quad (57)$$

where the first term involves the collective coordinates of the nuclear core, the second term is the same as Eq. (51), and the last term is an interaction Hamiltonian which expresses the coupling between the collective degrees of freedom and the individual particle degrees of freedom.

Hence for zero coupling the oscillating core and nucleons outside the core are essentially independent systems and in the nuclear ground state (where the collective motion vanishes) we are back to a conventional Shell Model description. For weak coupling the two systems are still almost independent and the effect of surface coupling on the Shell Model states can be described by usual perturbation methods. Such surface coupling can, for example, explain many departures from the "normal" Shell Model angular momenta coupling rules. As the coupling is further increased a very complicated condition is reached (intermediate coupling) where the nuclear surface oscillations and the individual particle motion are so intermixed that they can in no sense be considered independent and the whole nucleus must be treated as one complex quantum mechanical system. Finally, as the coupling is further increased, a resimplification of the situation occurs in which the nuclear surface acquires a large deformation and consequently a certain stability in spatial orientation.

Under these conditions the motions of the individual particles are fast compared to the motion of the nuclear surface as a whole. Hence one can consider the problem quantum mechanically by a method similar to that used for treating diatomic molecules, that is by assuming that the "loose" nucleons move in an effective potential produced by a deformed core and then treating the slow vibrations and rotations of the core separately. This "strong coupling" situation has been considered in detail by Nilsson[22] and the discussions of experimental results given

in subsequent sections will be restricted to this aspect of the Collective Model. It is to be noted in passing that the adding of "loose" nucleons to a closed Shell Model configuration would be expected, according to the Collective Model[21], to lead to increasingly stronger surface coupling and hence to larger deformations. Therefore the strong coupling situation is expected to manifest itself far from closed Shell Model configurations, that is exactly at the places where the Shell Model itself is least applicable.

By assuming strong coupling the total nuclear wave function can be written as a properly symmetrized form of

$$\Psi = \chi \cdot \varphi_{vib} \cdot \mathcal{D}_{rot} \qquad (58)$$

where χ represents the intrinsic motion of the nucleons, φ_{vib} describes vibrations of the nucleus around its equilibrium shape and $\mathcal{D}_{rot}$ represents the collective rotation of the nucleus as a whole. Restricting ourselves to the vibrational ground state, the q.n.'s specifying the nuclear system are Ω_i, the projection of the angular momentum of each nucleon along the nuclear symmetry axis (Z' axis); I, the total nuclear angular moment; M its projection on a space fixed axis (Z axis); and K its projection on the Z' axis. It can be shown, by minimizing simultaneously explicit expressions for the intrinsic particle and rotational energies, that for the nuclear ground state the deformed nucleus tends to assume a cylindrically symmetric shape and that $I = K = \Omega = j$, where j is total intrinsic particle angular momentum with respect to the axis fixed in the nucleus and $\Omega = \sum_{i=1}^{A} \Omega_i$ (see Ref. 21).

Explicit forms for the intrinsic nucleon wave functions $\chi = \prod_i \chi_i$ have been obtained by Nilsson. He assumes each nuclear particle to move in a cylindrically symmetric harmonic oscillator potential of the form

$$V = M/2 \, (\omega_x^2 \, x'^2 + \omega_y^2 \, y'^2 + \omega_z^2 \, z'^2)$$

where $\omega_x^2 = \omega_o^2 \, (1 + 2/3\delta) = \omega_y^2$ (the primes denote coordinates with respect to axes fixed in the nucleus)

$\omega_z^2 = \omega_o^2 \, (1 - 4/3\delta)$

Hence δ, the so-called deformation parameter, is a measure of the departure of the nuclear potential (shape) from spherical symmetry. A Hamiltonian of the form

$$\mathcal{H}(\text{intrinsic}) = \frac{p_i'^2}{2M} + V + C\vec{\ell}_i \cdot \vec{s}_i + D\vec{\ell}_i^{\,2} \qquad (59)$$

is assumed for the intrinsic motion of each nucleon with respect to the deformed nucleus, where the $\vec{\ell}^{\,2}$ term is included to depress higher angular momentum states and has some of the features of an interpolation between a harmonic oscillator and square well potential. The C and D coefficients are chosen in such a way as to reproduce the usual Shell Model level ordering when $\delta = 0$. The matrix equation $\mathcal{H}(\text{intrinsic})\,\chi_i = E_i\,\chi_i$ is then solved for various values of δ, using a representation corresponding to eigenfunctions of a spherical harmonic oscillator. Results are given as tables of eigenfunctions and eigenvalues plus a "Nilsson Diagram" which gives, graphically, the energies associated with the various single nucleon eigenfunctions as a function of δ. (See Ref. 22). The eigenfunctions, thus generated, are characterized in general only by Ω_i and N (equals the total number of oscillator quanta). However, for small deformations, j is also a good q.n. while for very large deformations the states are specified by the so-called "asymptotic" q.n.'s $Nn_z\,\Lambda$ and Σ where n_z is the number of oscillator quanta along the Z' axis while Λ and Σ are the projections on the Z' axis of the orbital and spin angular momenta of the intrinsic motion. These eigenfunctions are all two fold degenerate because intrinsic states with equal but opposite Ω_i have the same energy. This follows directly from the assumed cylindrical symmetry of the nuclear potential.

Using the Nilsson diagram it is an easy matter, for odd A nuclei, to determine the Nilsson wave function corresponding to the ground state odd nucleon configuration and consequently the predicted value of $I = \Omega$. One first locates the abscissa on the diagram corresponding to the appropriate value of δ. Then, noting the ordering of the Nilsson levels corresponding to that value of δ, the available odd-type nucleons are assigned, two at a time, to each successive energy state. The eigenstate into which the last odd nucleon falls then determines Ω, since all Ω_i's associated with lower states have been paired to zero. Furthermore the total intrinsic wave function χ, thus generated, can be used in conjunction with the collective contributions indicated in Eq. (58), to calculate expectation values of quantum mechanical operators.

Mottelson and Nilsson[23] have deduced, using the above method, the spins and many other nuclear properties of odd A nuclei lying in the

mass ranges $A \approx 25$, $150 < A < 190$, and $A > 220$. These are the A value ranges where the strong coupling Collective Model is most likely to be applicable, as evidenced by direct observations of nuclear rotation band spectra in these regions. Their results, for the most part, are in better agreement with available experimental results than predictions using the Shell Model, especially in regard to electric quadrupole moments.

Nuclear Moments:

To obtain an explicit expression for the magnetic dipole moment of an odd A nucleus, using the Collective Model, we must take the expectation value indicated in Eq. 20, in a Collective Model ground state of the type indicated in Eq. (58). To the magnetic dipole moment operator of Eq. (52) we must now add a term $g_R \vec{R}$, where $\vec{R}$ designates the angular momentum of the nuclear surface and $g_R \cong Z/A$ for a uniformly charged nucleus. When this is done the following result is obtained for the nuclear ground state[22]

$$\mu_I = \frac{I}{I+1}\left[(g_{sr}-g_{\ell r})\frac{1}{2}\sum_{\ell_r}(a^2_{\ell_r\,\Omega_r-1/2} - a^2_{\ell_r\Omega_r+1/2}) + g_{\ell_r} I + g_R\right] \quad \text{for } I \neq 1/2 \qquad (60)$$

where r = n for odd N nuclei, r = p for odd Z nuclei, and the a's refer to expansion coefficients for appropriate Nilsson wave functions and are given in Ref. 22. For I = 1/2 a slightly more complicated expression, given in the above mentioned reference, holds. For very strong (asymptotic) coupling Eq. (60) reduces to the simpler form

$$\mu_I = \frac{I}{I+1}\left[g_r \Lambda_r \pm g_{sr}/2 + g_R\right] \qquad (61)$$

where Λ refers to the asymptotic q.n. of the unpaired odd nucleon and the upper sign holds if $\Omega_r = \Lambda_r + 1/2$ while the lower sign holds if $\Omega_r = \Lambda_r + 1/2$.

In the case of the electric quadrupole moment we not only have to deal, as in the Shell Model case, with a contribution from the intrinsic motion of the nucleons, but also with a (usually much larger) contribution from the deformed nuclear core. Hence

$$Q = Q_p + Q_c \qquad (62)$$

where Q_p is the single particle contribution and Q_c is the core contribu-

tion. It is the presence of Q_c, which is due to the combined action of many nucleons, that enables the Collective Model to explain the large observed Q's for nuclei with A's in the ranges mentioned above. Using an eigenfunction of the form given in Eq. (58) and taking the expectation value of an appropriate collective model quadrupole moment operator, gives for the nuclear ground state[21,23]

$$Q_c = P_Q \, Q_o \tag{63}$$

where

$$Q_o = 4/5 \;\; \delta \, Z \, R_o^{\,2} \, (1 + \tfrac{1}{2} \;\; \delta \;\;) (R_o = \text{nuclear radius}) \tag{64}$$

$$P_Q = \frac{I(2I - 1)}{(I+1)(2I+3)} \; . \tag{65}$$

Here Q_o is just the classical expression for the quadrupole moment of an ellipsoidal nucleus, evaluated with respect to the axis fixed in the nucleus. P_Q is a "projection factor" giving the projection of this quadrupole moment on the space fixed axes, and is, in general, a function of the nucleon surface coupling. It varies from 1, for zero coupling, to the value of Eq. (65) for very strong coupling. Q_c is usually much greater than Q_p for nuclei conveniently describable by the Collective Model so that normally the latter is ignored in calculations. If it is assumed that the strong coupling situation is fully realized and that $Q_p \ll Q_c$, Eqs. (62)-(65) provide a method of determining δ from the measured Q value.

Odd-Odd Nuclei:

To treat odd-odd nuclei using the strong coupling Collective Model the same initial assumption is made concerning the interaction of the intrinsic neutron and proton systems as is made in applying the Shell Model. That is, the neutrons and protons are treated as completely independent superimposed systems. It is, however, further assumed that the collective aspects (i.e. the value of δ) are due to the combined effects of the neutrons and protons in the nuclear core so to this extent the existence of one type of nucleon can influence the intrinsic motions of the other type. (This is true, in fact, even if one type occurs in even number.) Under these assumptions, once the value of δ has been decided upon, the neutron and proton configurations can be determined separately by the method described above for odd A nuclei.

In the case of odd-odd nuclei, however, even after these configurations have been determined it is still not possible to predict the total ground state nuclear spin, on the basis of the Collective Model only, because on this Model the two combined nucleon states characterized by $\Omega = \Omega_p + \Omega_n$ and $\Omega = \Omega_p - \Omega_n$ are degenerate. Here Ω is the total (neutron plus proton) intrinsic angular momentum projection along Z'. Hence to determine $I = \Omega$ we must decide between the two possibilities above on the basis of direct nuclear forces. Gallagher and Moszkowski[24] have successfully accounted for the spins (and other nuclear properties) of many odd-odd nuclei (some of which lie far outside the range of A values for which the Collective Model would be expected to hold) by using two angular momentum coupling rules involving the asymptotic q.n.'s mentioned above. They are

GM1. $I = \Omega_p + \Omega_n$ if $\Omega_p = \Lambda_p \pm 1/2$ and $\Omega_n = \Lambda_n \pm 1/2$

GM2. $I = |\Omega_p - \Omega_n|$ if $\Omega_p = \Lambda_p \pm 1/2$ and $\Omega_n = \Lambda_n \mp 1/2$.

These rules are obvious extensions of the Nordheim Rules to the case of collective nuclei and are based on essentially the same theoretical grounds.

Nuclear Moments:

An expression for the magnetic dipole moment of an odd-odd nucleus, based on the Collective Model, can be obtained by an obvious extension of Eq. (64). This expression can be written as follows

$$\mu_I = \frac{I}{I+1}\left[(g_{sp}-g_{\ell p})\,1/2\sum_{\ell_p}(a^2_{\ell_p\Omega_p}-1/2-a^2_{\ell_p\Omega_p}+1/2)+g_{\ell_p\Omega_p}\right.$$

$$\left.\pm g_{sn}\,1/2\sum_{\ell_n}(a^2_{\ell_n\Omega_n}-1/2-a^2_{\ell_n\Omega_n}+1/2)+g_R\right] \qquad (65)$$

where: the upper sign holds if $I = \Omega_p + \Omega_n$

the lower sign holds if $I = \Omega_p - \Omega_n$

and all terms, with the exception of g_R, are reversed in sign and the lower sign used if $I = \Omega_n - \Omega_p$. For very strong (asymptotic) coupling Eq. (65) can be simplified to yield an expression, analogous to Eq. (61), for odd-odd nuclei[24]

$$\mu_I = \frac{I}{I+1}\left[g_{\ell_p} \Lambda_p + g_{sp/2} \Sigma_p \pm g_{sn/2} \Lambda_n + g_R \right] \qquad (67)$$

with the same sign conventions as in Eq. (65). The value of μ_I obtained using Eq. (67) agrees with that obtained using Eq. (65) to within about 10% for $\delta \approx 0.3$. For smaller values of δ Eq. (66) should be used.

Calculation of the electric quadrupole moments of odd-odd nuclei, using the Collective Model, proceeds in exactly the same manner as for the odd A case and an expression like Eq. (62) is obtained. It is seen from this equation and equations (63) - (65) that if we ignore the Q_p contribution to the total Q, the measured quadrupole moment should depend primarily on the nuclear deformation, δ, and the spin. Furthermore isotopes of the same element would be expected to exhibit almost equal values of Q_o since such isotopes have the same Z and usually about the same δ. Therefore the Q/P_Q ratios for an isotopic series having A's in the region where collective effects dominate, should be almost constant and equal to Q_o. This does, in fact, seem to be the case for many isotopic series exhibiting especially large Q values. [See for example the Q_o values of Lu^{176}, Lu^{175} and Lu^{177} given in Table 5 of Section V.H.]. This lends strong support to the Collective Model explanation for the existence of these large moments.

IV. THE ATOMIC BEAM MACHINE AND AUXILIARY EQUIPMENT

A. Introduction

Three, essentially different, atomic-beam machines were used to perform the experimental measurements considered in this paper. All of the work on I^{132} as well as the early work on Lu^{176m} and Br was done using what will henceforth be called machine no. 1. This machine is of the inside-out flop-in type and has been described in detail elsewhere.[25]

The majority of the work on Br^{80}, Br^{80m}, and Lu^{176m} was done using machine no. 1 after it had been completely redesigned and correspondingly altered. The resulting apparatus, although retaining many features of the original machine, differs from the latter in a number of important ways and, for the sake of discussion, will be referred to as machine no. 2. Since this redesigning operation was carried out during the course of the experiments reported here, a rather detailed discussion of machine no. 2 will be given below. The discussion will mostly be restricted to characteristics which were changed by the redesign. Features not explicitly mentioned are identical to the corresponding features of machine no. 1 and are described in Reference 25.

Some of the later work on Lu^{176m} was performed in collaboration with Dr. V. W. Cohen and his group at B.N.L. The machine used at Brookhaven (machine no. 3) is described elsewhere so no further mention will be made of it here.[26]

B. Machine Geometry

The overall geometry of machine no. 2 is very similar to that of machine no. 1. The main differences are: 1) A four inch buffer chamber has been added between the oven and detector chamber. 2) The C magnet has been lengthened. 3) The various beam defining slits and stops within the machine have been changed in number and in width to accommodate the increased machine length. In Fig. 4 is given a photograph of machine no. 2 while Fig. 5 and Table 1 give the positions and optimum widths of the various slits and stops as well as important linear dimensions along the beam direction. The widths given in the table were chosen as those which maximize the resonance signal to noise ratio for a beam of K atoms and at the same time lead to a resonance signal height of easily detectable magnitude (1.5-2% of the full beam).

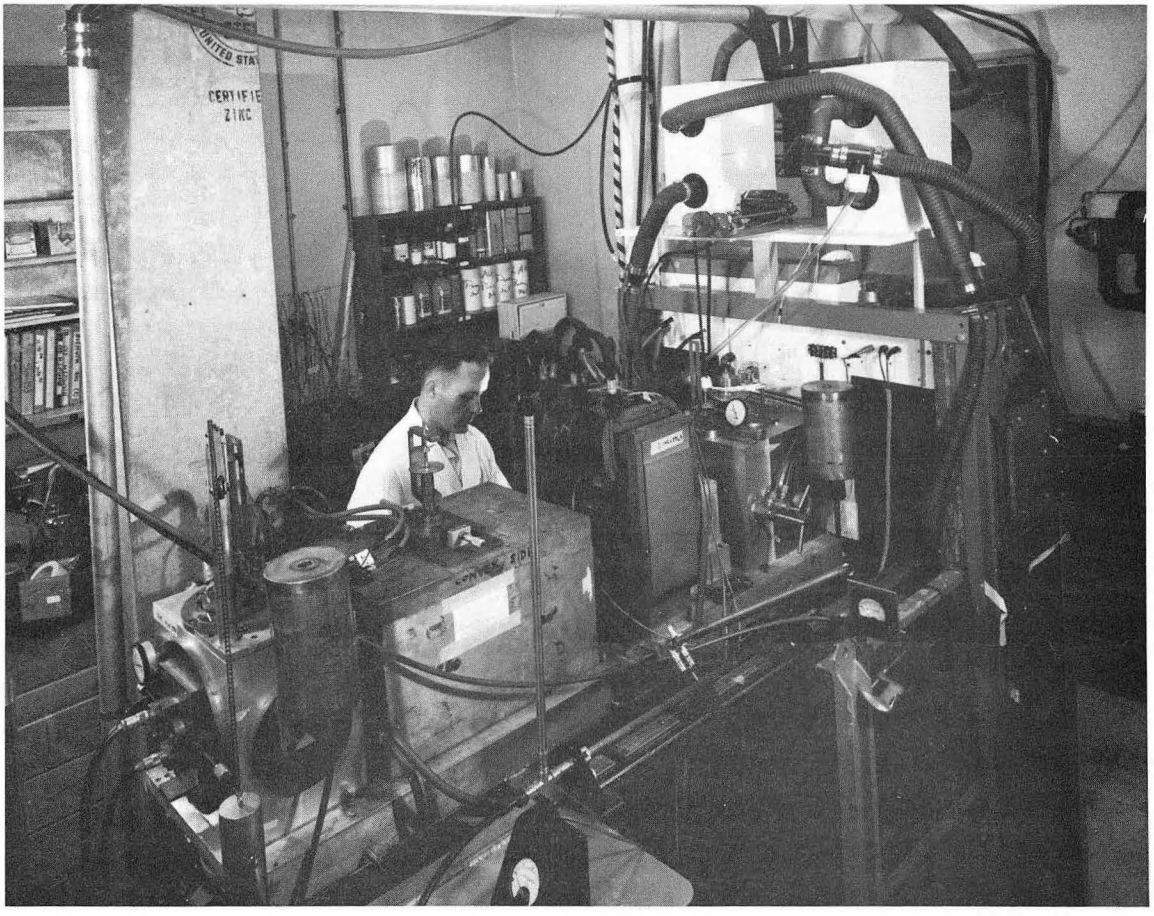

ZN-3401

Fig. 4. Photograph of atomic-beam machine no. 2

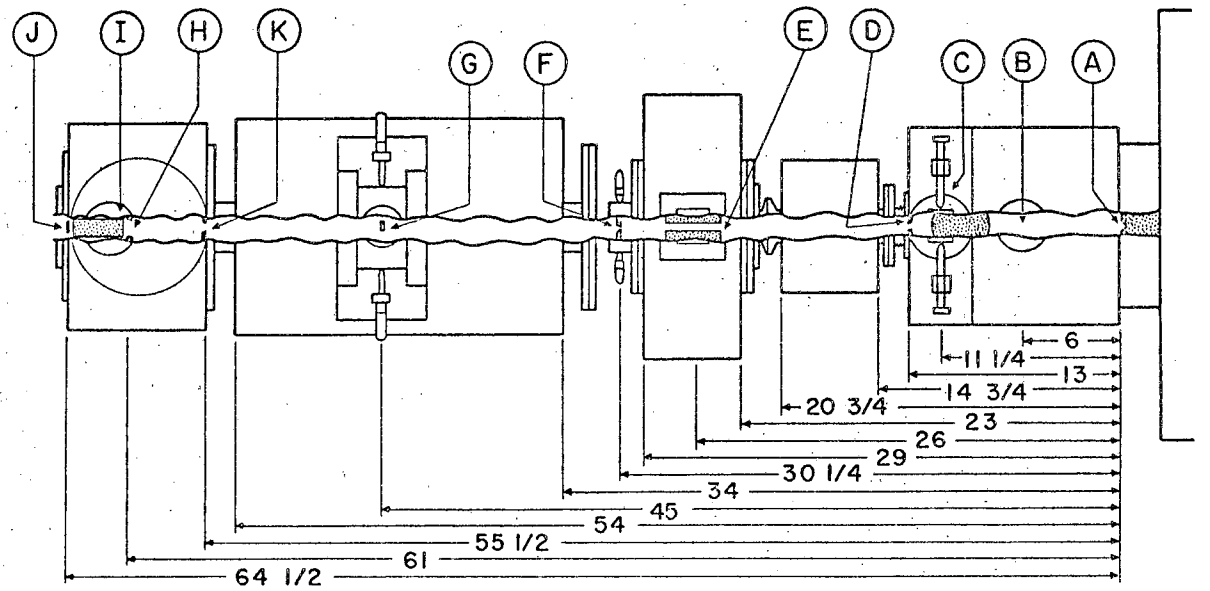

Fig. 5. Schematic diagram of atomic-beam machine no. 2 showing important linear dimensions. (see Table 1)

Table 1. SLIT AND STOP WIDTHS

Designation	Description	Width (mils)
A	Source Slit	15
B	Beam Flag	--
C	K oven Slit	40 (diam. of hole)
D	Buffer Chamber Slit	60
E	R.F. Hairpin	60
F	Collimator Slit	27
G	Stop Wire	40 1/2
H	Cold Trap Slit	250
I	Collector Button	250
J	Hot Wire	65
K	Detector Slit	50

C. The Vacuum System

The vacuum system of machine no. 2 is described by the following table, which gives the types of vacuum pumps used and the purpose that each of them serves.

Numberical Designation	Type of Pump	Use
1	PMC 721 oil diffusion	Pumps directly on oven can.
2	PMC 721 oil diffusion	Pumps directly on detector can near detector position.
3	MCF 300 oil diffusion	Pumps directly on buffer chamber.
4	MCF 300 oil diffusion	Pumps directly on C magnet can.
5	VMF 10 oil diffusion	Backs pumps nos. 2, 3, and 4.
6	VMF 10 oil diffusion	Acts as D.P. stage of button holder pumpout.
7	Welsch 5 cfm mechanical	Backs pump no. 5.
8	Welsch 5 cfm mechanical	Backs pump no. 1.
9	Welsch 3/4 cfm mechanical	Acts as mechanical pump stage of button holder pumpout.
10	Welsch 3/4 cfm mechanical	Manifold pump out.

Using this system of pumps operating pressures of about 5×10^{-7} mm are obtainable in the detector and buffer chambers while a pressure of 5×10^{-7} mm - 1×10^{-5} mm is obtainable in the oven chamber. Normal forevac pressure is between .5 and 1 micron. The vacuum system is sufficiently tight, that all chambers of the machine remain at pressures of less than .5μ for about one hour after all pumps (D.P. and mechanical) have been turned off.

Rapid action vacuum values enable the oven D.P. to be isolated from the oven chamber as well as from the oven forevac mechanical pump. A bypass vacuum line then enables the oven forvac pump to pump directly on the oven can. This allows the oven can to be "roughed down" to forevac pressure after introduction of beam materials. During this operation the oven chamber is also isolated from the rest of the high vacuum system by closing a rapid action valve on the oven end of the buffer chamber.

The buffer chamber, in addition to allowing isolation of the oven chamber and providing a "buffer zone" between the oven and detector chambers, is also very convenient because it can be completely isolated from the rest of the machine. The K calibration oven, since it is contained in this chamber, can therefore be removed and its supply of K replenished without disturbing the rest of the vacuum system.

D. The Magnet System

Some salient information regarding the A, B, and C magnets of machine no. 2 is given in the following table.

Magnet	Material	Gap Width (mills)	Length (in.)	Approx. No. of Turns per coil	Diam. of coil wire (mills)	D.C. Resistence per coil (Ω)	Approx. Induct. per coil (henries)	Supply Current Regulation
A	Permendur	100	2 1/2	300	40	3.2	.38	1 part in 10^4
B	Armco	415	21 1/2	3750	40	80	3.8	1 part in 6×10^4
C	Armco pole pieces with Hypernom pole tips	500	6	10,500	20	520	---	1 part in 10^5

The C magnet of machine no. 2 is perhaps the greatest single feature that distinguishes it from machine no. 1. This magnet has pole pieces made of Armco and pole tips which are 1/2" hypernom plates accurately spaced by quartz spacers. The magnet is powered by three coils whose characteristics are given above. These coils are connected in parallel and current is supplied by a transistorized D.C. current regulated power supply which provides from zero to 200 ma of current. With this arrangement C fields ranging from 0-1000 gauss are obtainable. A curve giving the C field vrs. the current through the windings is given in Fig. 6. All experimental points shown in this figure were taken after carefully cycling down the C magnet in order to eliminate as much of its residual magnetism as possible. Water cooling of the C magnet coils, although provided for in the machine design, does not seem to be necessary.

Great care was taken to get the hypernom pole tips of the C magnet accurately parallel and consequently a very homogeneous C field has resulted. At 500 gauss the field, along the beam direction, varies by less than .02 gauss per inch (less than .004% per inch.). This estimate of the inhomogenuity of the C field is based on the assumption that the entire K resonance line width (of about 40 KC at 500 mc) is due to variations in the C field while actually the "natural line width" is about 27 KC. Hence this estimate is probably quite pessimistic. The K line width changes very little as the C field varies from 0 to 500 gauss, which further indicates that most of the line width is due to causes

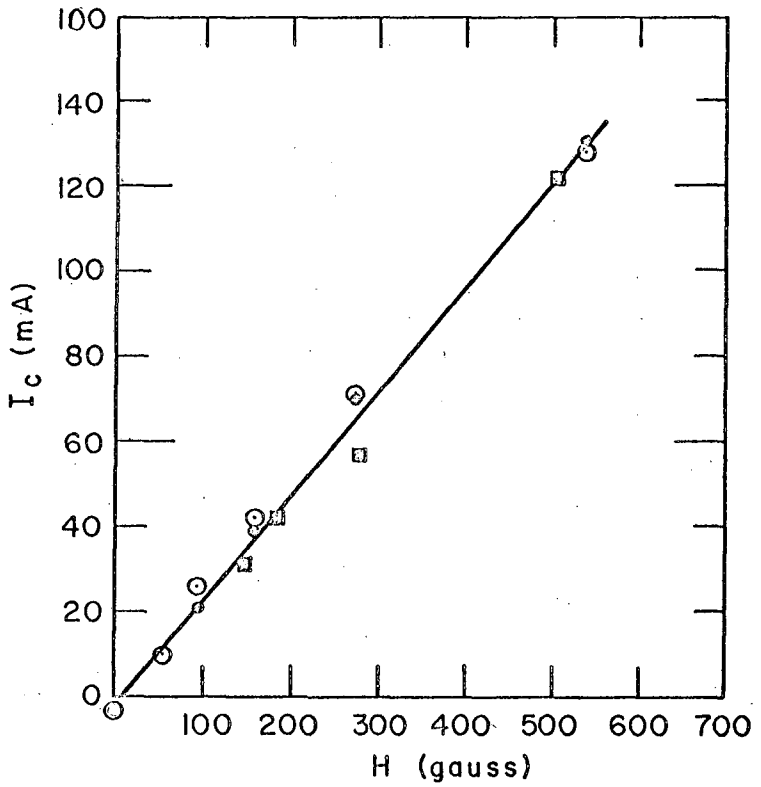

MU-27380

Fig. 6. "C" field calibration curve

⊙ → I_A = 0.85 amp I_B = 0.5 amp

● → I_A = 1.30 amp I_B = 0.75 amp

▩ → I_A = 2.55 amp I_B = 1.5 amp

other than field inhomogeneity. Fringing of the A and B fields into the C field region does not seem to have much effect on the line width as long as care is taken to keep all these magnetic fields in the same direction. This conjecture is supported by the fact that increasing or decreasing the strength of A and B fields effects the resonance signal to noise but not the line width. Figures 24, 36, and 37 show resonance lines in Lu^{176m}, Br^{80}, and Br^{80m} traced out both on machines no. 1 and no. 2. The dramatic improvement in line width due to the new C magnet is obvious.

The A and B magnet pole pieces for machine no. 2 are the same as those for machine no. 1 but the coils that drive the magnets are different. Figure 7 is a diagrammatical cross section of the B magnet pole tips. The A magnet design is similar but smaller in scale. For the B magnet the field gradient to field ratio $\frac{(\nabla H)_B}{(H)_B}$ (which is determined by the pole tip geometry) is 1.2 cm^{-1} while $\frac{(\nabla H)_A}{(H)_A} \approx 5\ cm^{-1}$ for the A magnet.

The A and B magnets are powered by two coils each and can be driven either by separate current-regulated power supplies or both in series by the B magnet power supply. The later procedure is preferable for accurate work due to the greater regulation capacity of the B supply as compared to the A supply. At high magnetic fields ($H > 200$ gauss) the K resonance line width using separate A and B supplies was found to be from 2-3 times greater than when only the B supply was used to drive both magnets. These power supplies, which have been described elsewhere,[27] are capable of delivering 0-5 amps through the A and B magnet coils. Care must be taken, however, not to drive more than 2 amps through the B magnet coils and 4 amps through the A magnet coils because they become overheated at higher currents. Both the magnet coils are cooled by circulating tap water over the surface of the coil forms.

Appropriate A and B magnet currents to use during machine operation were determined by maximizing the resonance signal to noise ratio for K. After much experimentation the optimum values:

$$I_A(K) = 0.85 \text{ amp}$$

$$I_B(K) = 0.50 \text{ amp}$$

were decided upon. For atoms other than K, the A and B currents were set

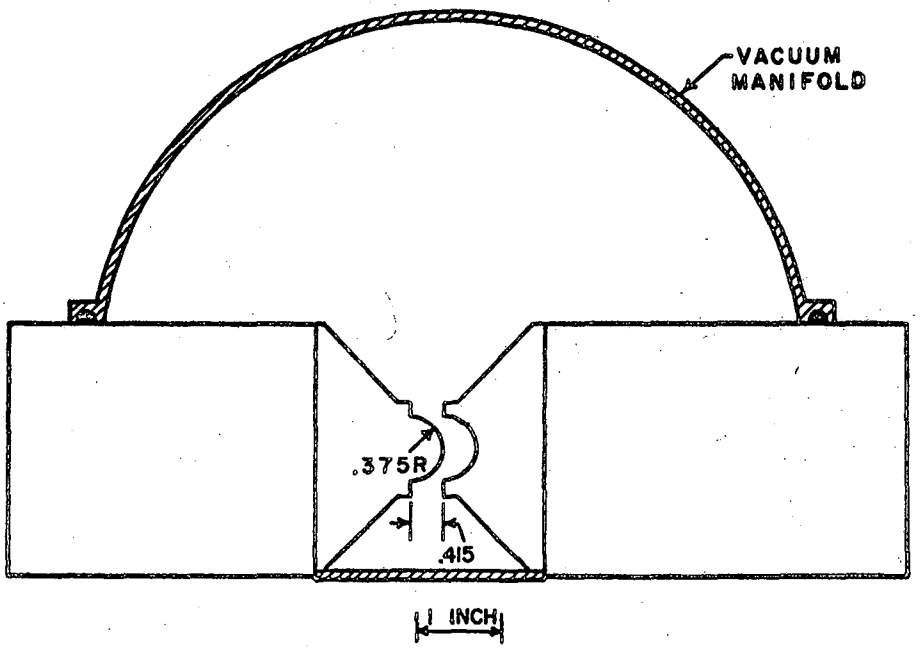

CROSS SECTION B POLE TIPS

MU-18036

Fig. 7.

in accordance with the following expressions.

$$I_A(x) = I_A(K) \frac{g_J(K)}{g_J(X)}$$

$$I_B(X) = I_B(K) \frac{g_J(K)}{g_J(X)} \quad .$$

Such a procedure works satisfactorily for Br, Lu^{176m}, and Er and seems reasonable in view of Eq. (47).

E. C Field Calibration System

The C field was calibrated by observing $\Delta F = 0$, $\Delta m_F = \pm 1$ resonances in a K^{39} atomic beam. The oven, from which the K beam emerged, is located within the buffer chamber in front of the radioactive beam source as indicated in Fig. 5. It was raised out of the way, by means of a small electric motor, between C field calibrations. The K oven was operated at temperatures ranging from 55°C to 120°C depending on the amount of K present in the oven. The heating of the stainless steel oven was accomplished by passing an electric current of from .6 amp (14 volts) to 15 amp (25 volts) through a 3 1/2 in. length of 13 mil diameter ni-chrome wire, which is wound on a ceramic form and placed in close proximity to it. The K beam was detected using a 65 mil wide 2 mil thick rhenium hot wire in conjunction with a Vibrating Reed Electrometer Model 31. The hot wire was maintained at a dull red heat (I = 2.0 amp, V = .5 volts) during operation. Before and after each use the hot wire was "flashed" to a bright orange temperature (A = 8.0 amp, V = 3.2 volts) to clean it off. The ion collector plate was kept at a potential of -22 1/2 volts with respect to the hot wire.

Using the above arrangement ion currents of $(1\text{-}5) \times 10^{-9}$ amps were obtained for 100-125 hours of continuous operation. Since K resonance heights were typically 1.5-2% of the full beam, this provided conveniently detectable K resonance signals for calibration purposes.

F. R.F. Loops and Signal Generating Equipment

In the following table a list is given of the R.F. equipment used during the course of the experiments reported in this paper. The frequency ranges over which these instruments were used are also given. Equipment used at B.N.L. but not at Berkeley is not included in the table. A description of ~~this~~ that R.F. equipment is given in Reference 26.

Instrument	Frequency range Mc/sec
Oscillators	
General Radio 805	0.016 - 50.0
Tektronix 190A	0.35 - 50.0
Hewlett-Packard 608A	10.0 - 500.0
General Radio 1208B	65.0 - 500.0
General Radio 1209B	250.0 - 920.0
General Radio 1218A	900.0 - 2000.0
Rhode and Schwartz SLRD	275.0 - 2750.0
Amplifiers	
IFI 500 wide-band amplifier	0.5 - 240.0
IFI 510 wide-band amplifier	0.5 - 240.0
Frequency measuring instruments	
Hewlett-Packard 524B frequency counter	0.0 - 10.0
Hewlett-Packard 524A frequency converter unit	10.0 - 100.0
Hewlett-Packard 524B frequency converter unit	100.0 - 220.0
Hewlett-Packard 540A transfer oscillator	100.0 - 220.0
Auxilliary Equipment	
Weston r.f. milliometer model 425	
Weston D.C. microameter model	
General Radio 874 Adjustable Line	
General Radio 874-LBA slotted line	
General Radio 874-D50 50 cm adjustable stub	
Federal Cable Co. 50 Ω cable	
General Radio fittings	

The uncertainties in all frequency measurements were less than 2 Kc/sec, which is only a small fraction of a line width for any of the resonances observed. Hence frequency measurement errors would be expected to make only a small contribution to the total experimental error associated with any of the experiments.

Figure 8 is a schematic diagram of the dual purpose R.F. loop used for the initial work done using machine no. 1. This loop, as indicated in the diagram, can be used either to excite π or σ transitions. Figure 9 gives schematic diagrams of the π and σ loops used at B.N.L.

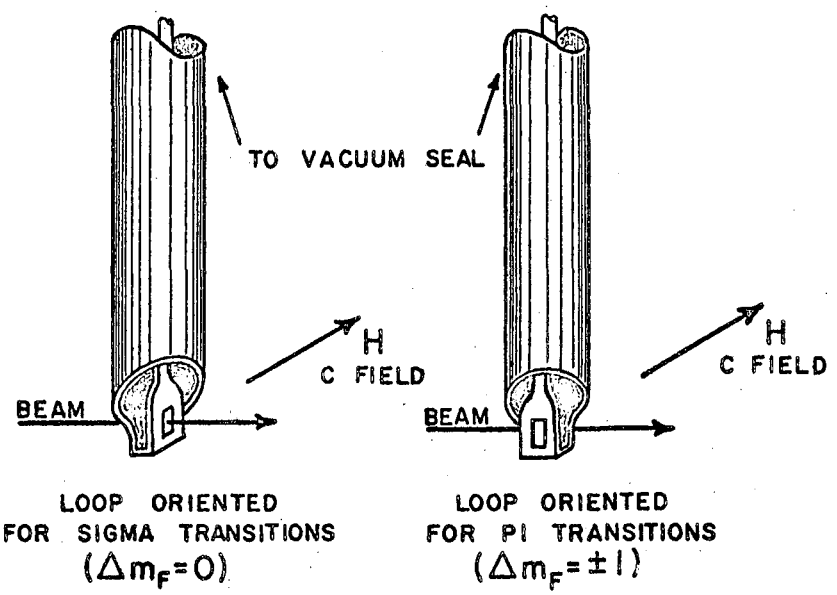

MU-18042

Fig. 8. Dual purpose R.F. loop.

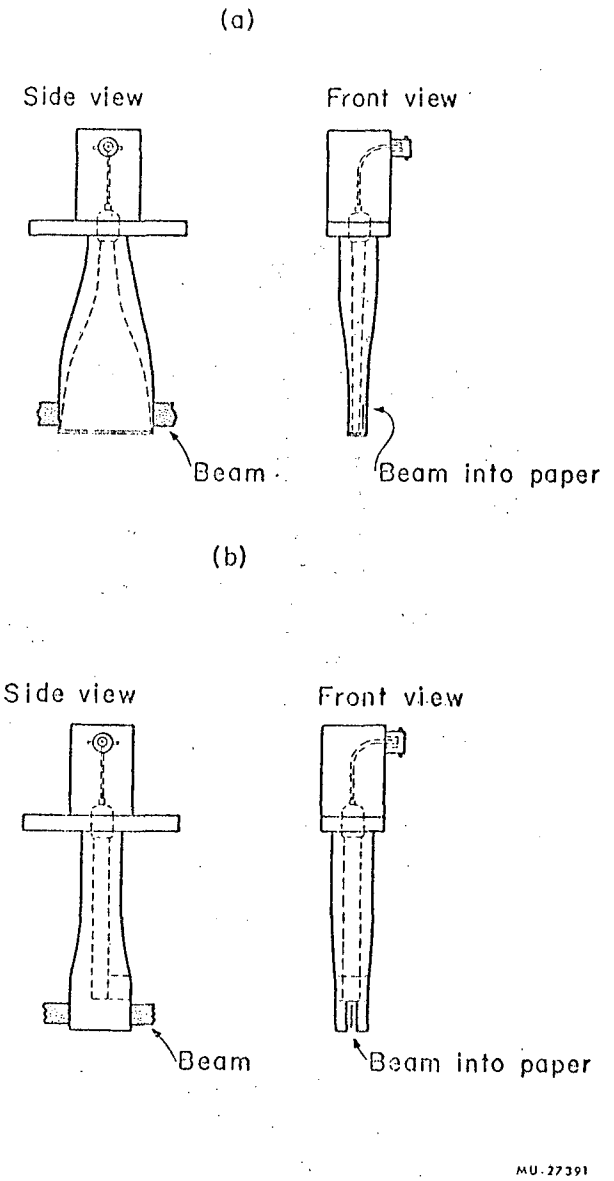

Fig. 9. R. F. Loops used at B.N.L. (a) Pi Loop (b) Sigma Loop
Uniform C-field is taken as into paper.

The π loop of this diagram was also the type used at Berkeley for the work done using machine no. 2. The actual π loop extends a distance of 3/4" along the beam direction and contains a 62 mil x 500 mil canal through which the beam passes. This 3/4" long R.F. region leads to a natural line width of about 27 Kc/sec for K, as mentioned above.

The R.F. current to the loop was monitored, at frequencies of less than 200 mc/sec, by a Weston R.F. milliameter in conjunction with a trombone-type line stretcher. The line stretcher was used to produce a standing wave current antinode at the position of the ammeter. For frequencies > 200 mc/sec a General Radio 874-LBA slotted line and adjustable tuning stubs were used in conjunction with a rectifier crystal pick-up probe and a D.C. microameter. Both of these methods furnish only a qualitative indication of the R.F. current actually getting to the loop. The method used to determine what current to use for exciting a given transition in a radioactive nuclide was to: 1) Obtain a resonance in K at the expected resonance frequency of the radioactive nuclide. 2) Vary the R.F. power until this K resonance exhibited its maximum height. 3) Note the R.F. current by one of the methods described above and use this same current when searching for the radioactive nuclide resonance.

This method met with considerable success in the case of Lu^{176m} but always led to overpowering when applied to the Br isotopes. A typical overpowered Br^{80m} resonance curve is compared with one obtained using the correct R.F. power in Fig. 10. It is seen that the resonance is broadened and lowered in intensity by application of too much power. For this reason a two pass method was used for the Br isotopes. In the first pass the R.F. current indicated by the above method was used until a broad, weak resonance pattern (such as the overpowered one of Fig. 10) had been obtained. Then the power was reduced a little at a time and the resonance pattern retraced until a curve of 40-50 Kc/sec half width was obtained.

G. Radioactive Decay Counters

The two methane continuous flow proportional β counters used for these experiments are the same as those described in detail elsewhere[25] and so will only be mentioned briefly here. Figure 11 shows a photograph of the counter system (i.e. scalers, amplifiers, and lead shielded ionization chambers) while Fig. 12 shows a diagrammatical cross sectional view of one of the counters. One of the counters was used to count full-

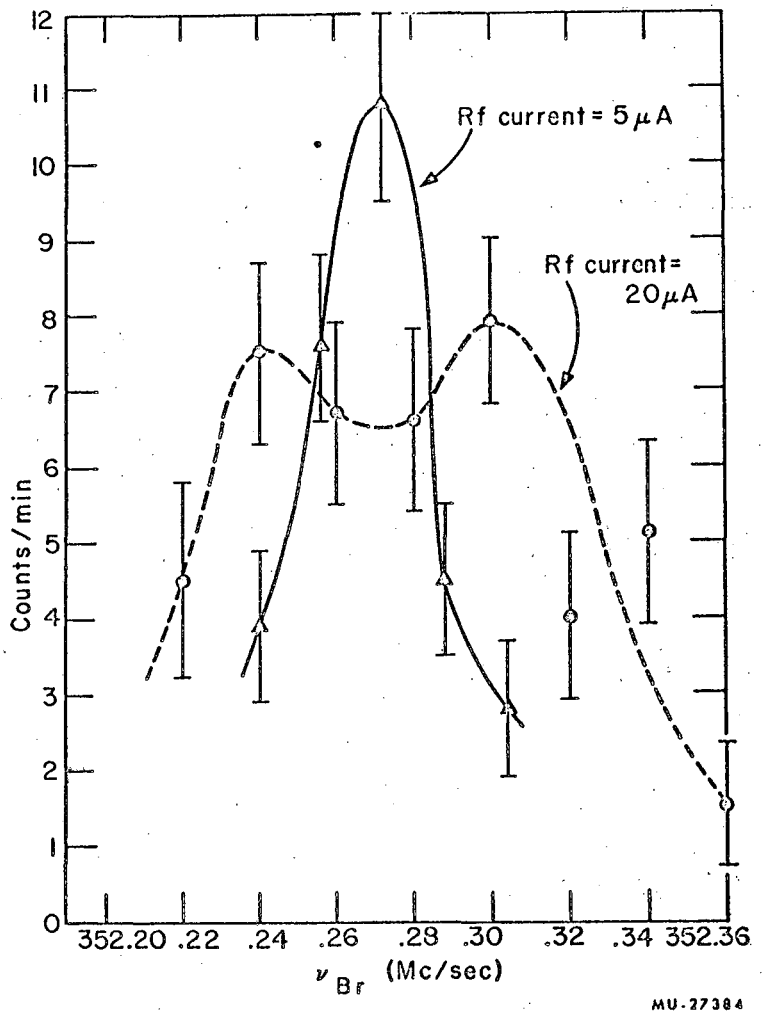

Fig. 10. Br^{80} resonance curves showing the effect of over-powering β transition (ν_K = 400.0 mc/sec).

beam and direct-beam buttons for the purpose of beam normalization and had a background of 5-10 counts per minute.* The other one was used to count comparably lower counting resonance buttons and had typically a background of 2-4 counts per minute. Both counters were left running on background when not in use after it was found that turning them off for extended periods of time seemed to lead to higher background counting rates.

---

* It is convenient, for the experimental discussions of subsequent sections, to adopt a nomenclature pertaining to beam exposures taken under various specialized experimental conditions. For the purposes of this paper the following definitions will suffice.

Full-beam Exposure: Taken with stop-wire out, deflecting fields off.

Direct-beam Exposure: Taken with stop-wire out, deflecting fields on.

Resonance Exposure: Taken with stop-wire in, deflecting fields on, R.F. field on.

Background Exposure: Same as Resonance Exposure except the R.F. field is turned off.

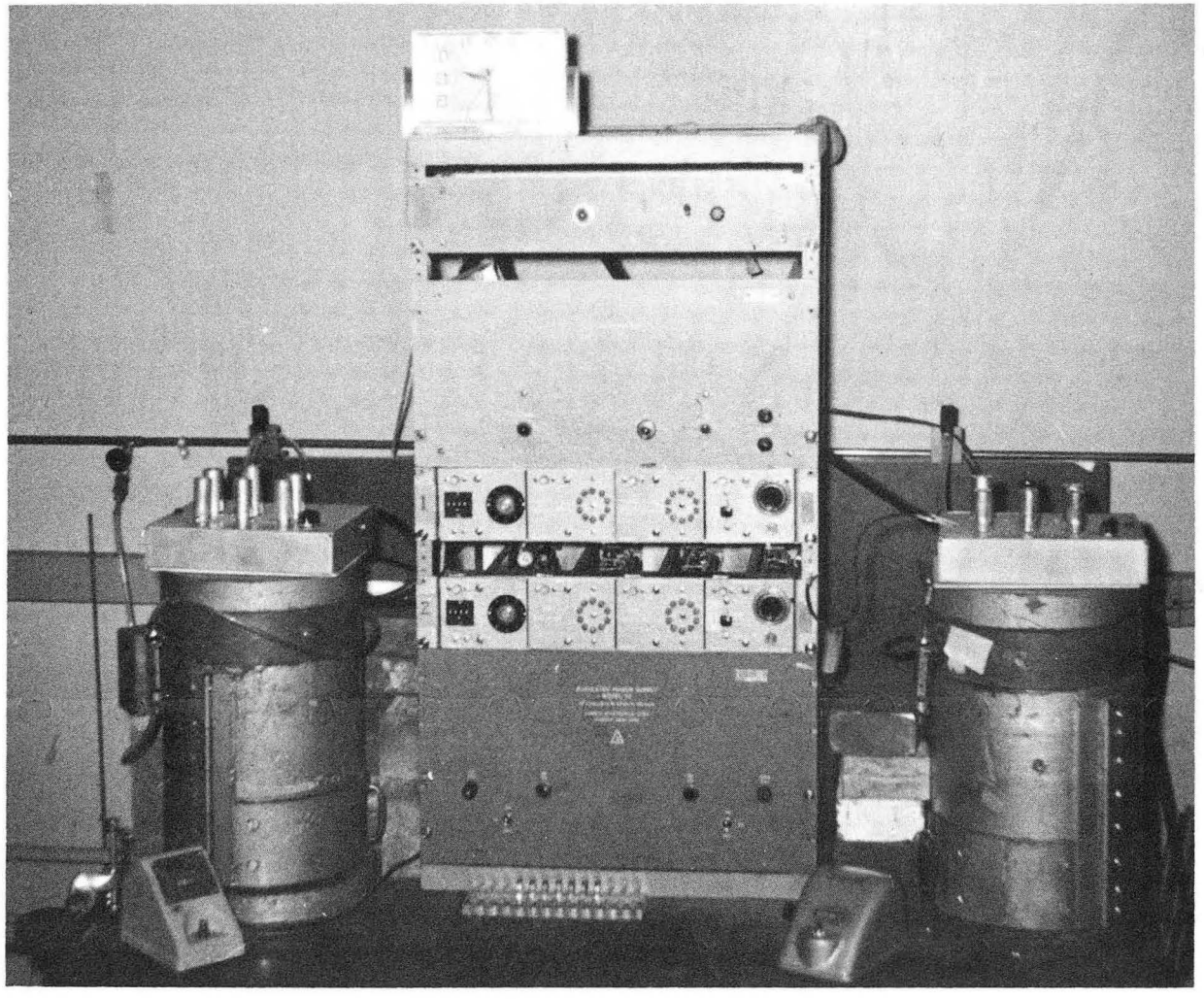

ZN-2214

Fig. 11. Photograph of proportional Beta counter system.

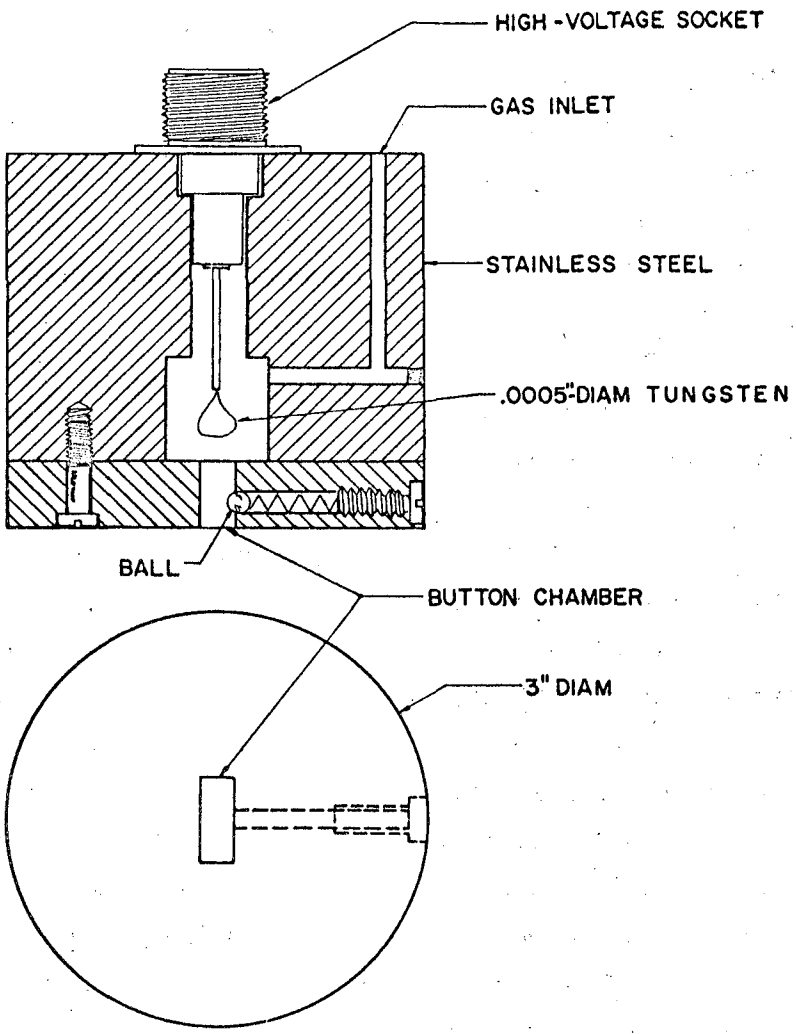

Fig. 12. Diagrammatical cross section of a Beta particle counter.

V. THE Lu^{176m} EXPERIMENT

A. Introduction

Although part of the later work on Lu^{176m} was done at B.N.L. the spin measurement and most of the hyperfine structure measurement (to the accuracy reported in this paper) were performed at the L.R.L. Atomic-beam Laboratory. More accurate measurements of the hyperfine structure separations are now being carried out at B.N.L. and the results of these measurements together with a description of the experimental equipment and technique used will be published soon. For these reasons the discussion given below in Section B and C will be restricted to the L.R.L. operation and in Section D only a brief description will be given of the experimental procedure used at B.N.L.

B. Isotope Production

The Lu^{176m} used was produced in a Lu^{175} (n,γ) Lu^{176m} reaction by bombarding natural 99.9% pure Lu metal with thermal neutrons. Forty to fifty mg. pieces of Lu metal were sealed in pyrex capsules which in turn were sealed in 99.999% pure aluminum capsule holders for additional safety in handling. These units were then transported to the pile for irradiation. The bombardments were done in the General Electric Test Reactor at the Vallecitos Atomic Laboratory in Pleasanton, California. The neutron flux was 9×10^{13} neutrons/cm.^{2} sec. and the sample was left in the pile for 4 hours before being transferred to L.R.L. by car.

Upon arrival at L.R.L. (usually about one hour after removal from the reactor) the aluminum capsule holder was opened and the pyrex capsule removed and broken. These operations were done, using manipulators, in a lead shielded "cave" of the type shown in Fig. 13. Although the β-γ radiation level at a distance of 1 foot from the bare Lu chunk was usually around 5R./hr., the radiation level at the front of the cave rarely exceeded 2 MR./hr. After decapsulation the Lu sample was transported, in a 2 inch thick lead "pig" to the atomic-beam machine.

C. Beam Production and Characteristics

Using a "glove box," which is attached to the oven end of the atomic-beam machine, for radiation protection, the Lu sample and a few Cs Cl crystals were loaded into an oven unit of the type shown schematically in Fig. 14. This unit consists of a tantalum crucible (3/8" long, 19/64" o.d., 1/32" thick wall) and a tantalum oven (1/2" long, 11/32" o.d., 1/32" thick wall) onto which 3 mil tantalum sheets

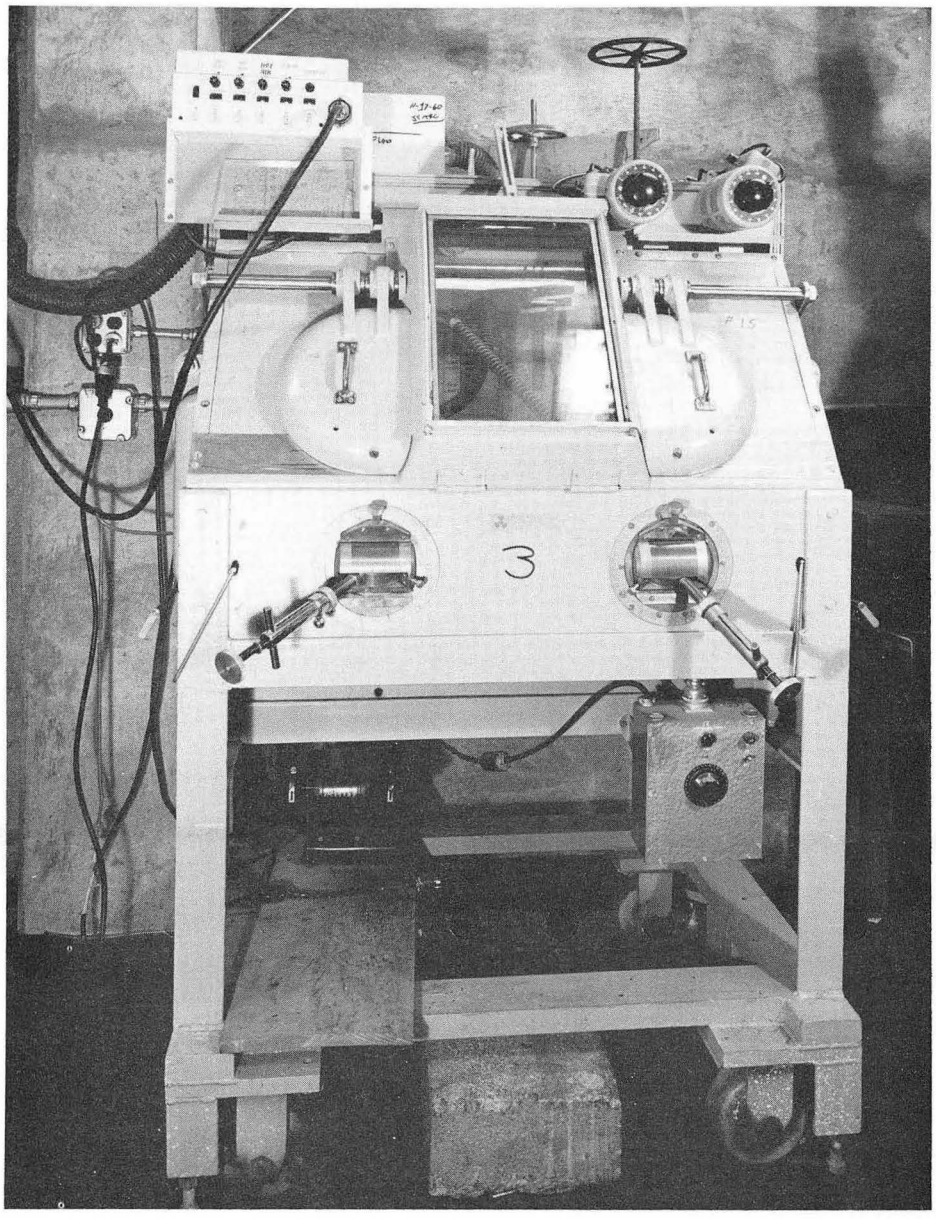

ZN-2677

Fig. 13. Lead shielded "cave" used for handling highly radioactive materials.

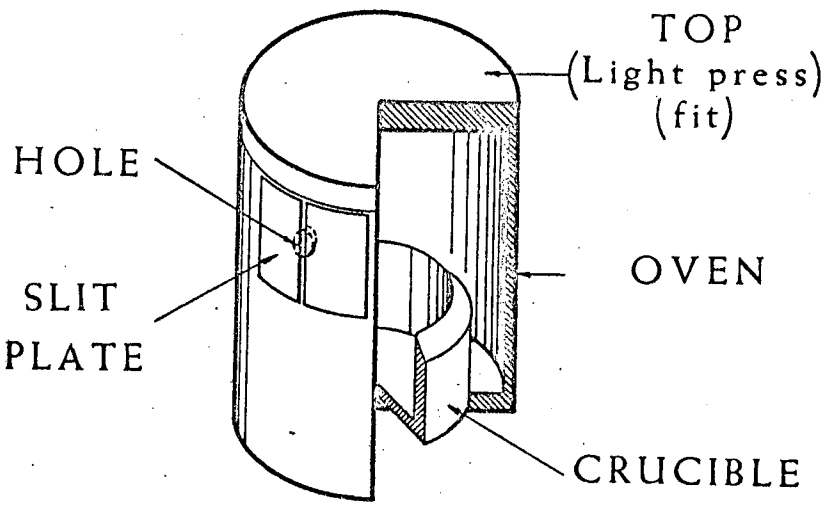

Fig. 14. Source oven unit for rare earths.

have been spot welded to form 15 mil wide slits. The crucible fits snug into the oven and has a sharp lipped upper edge to prevent "creep". The oven unit was mounted, as indicated in Fig. 15, on a water cooled oven holder assembly which was then attached to the beam machine in such a way that the Lu oven was vacuum sealed within the machine's oven chamber.

A useable Lu beam was produced by heating the oven to approximately 2000°C through electron bombardment. Two 15 mil diameter thoriated tungsten filaments, in close proximity to the oven (see Fig. 15) were heated by passing about 7 amps of electric current through each of them. The needed electron bombardment current of about 90-110 ma. was then obtained by holding the oven at a 1.0 - 1.2 kv. positive potential with respect to the filaments. In this way the 90-110 watts of power necessary for heating the oven could easily be supplied.

Before attempting to produce a Lu beam, the Cs Cl which had been put into the oven during the loading process was driven off by supplying about 4 watts of power to the oven. Thus a beam of Cs Cl molecules, which could be detected upon striking the hot wire, was produced. The oven holder assembly was then moved vertically and horizontally by means of exterior positioning screws until the Cs Cl beam reaching the hot wire registered a maximum. The Lu oven having thus been lined up, the power was slowly increased until all the Cs Cl was driven from the oven and finally until a Lu beam was obtained. This beam was collected on fired 2 mil platinum foils which were mounted during exposure to the beam on brass "buttons" as illustrated in Fig. 16. The presence of Lu was detected by counting the decay β particles in the β proportional counters mentioned in Section IV G. With the above method, Lu full-beam counting rates of about 2000 counts/minute after one minute exposure of the foil to the beam were easily attainable and this "size" beam was found to be most convenient.

Natural Lu metal is 97.4% Lu^{175}, which has a thermal neutron capture cross section of 18 barns, and 2.6% Lu^{176}, which has a corresponding cross section of 3800 barns. Hence one would expect an appreciable percentage of the full-beam activity to be attributed to the decay of Lu^{177} present in the beam. Calculation shows that for a four-hour irradiation, at the beginning of a run (1 hr. after removal from the pile) the ratio of Lu^{176m} activity to Lu^{177} activity in the beam is 7.1 while after 8 hours of running time this ratio is 1.65.

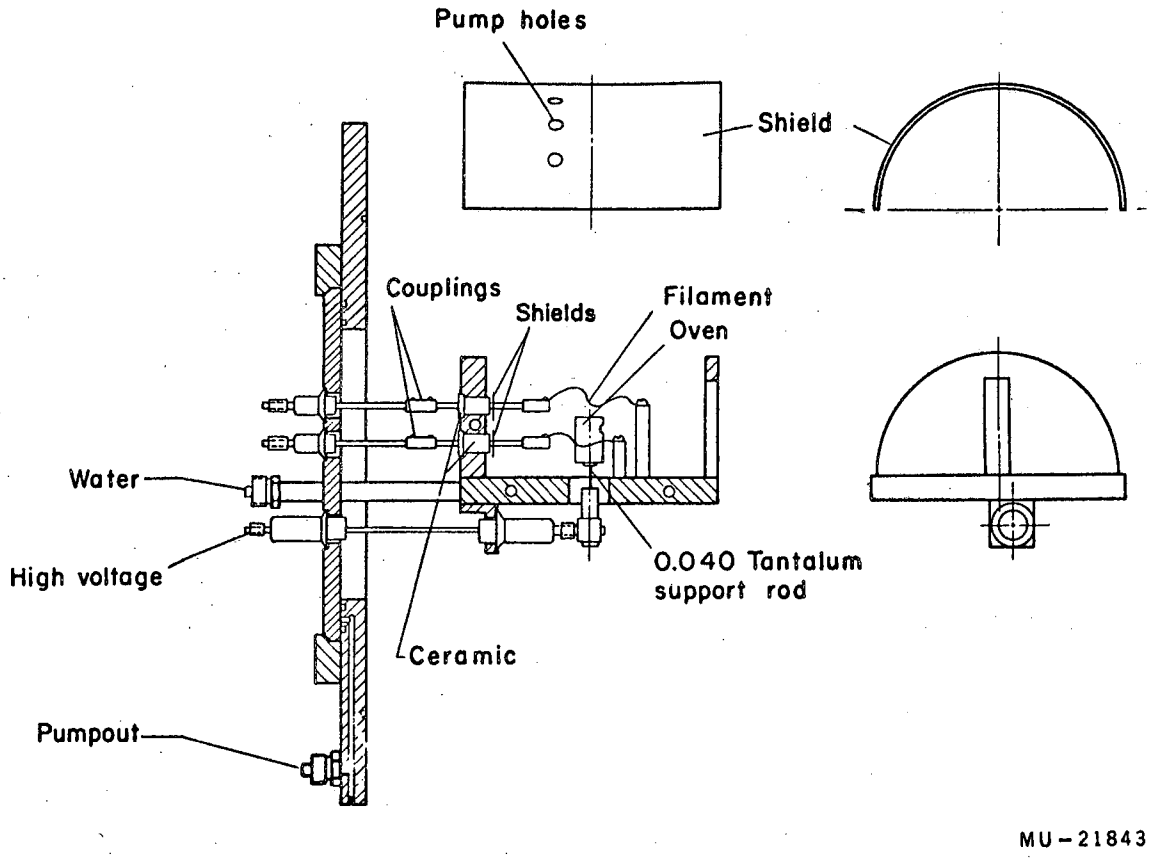

Fig. 15. Rare earth oven holder assembly.

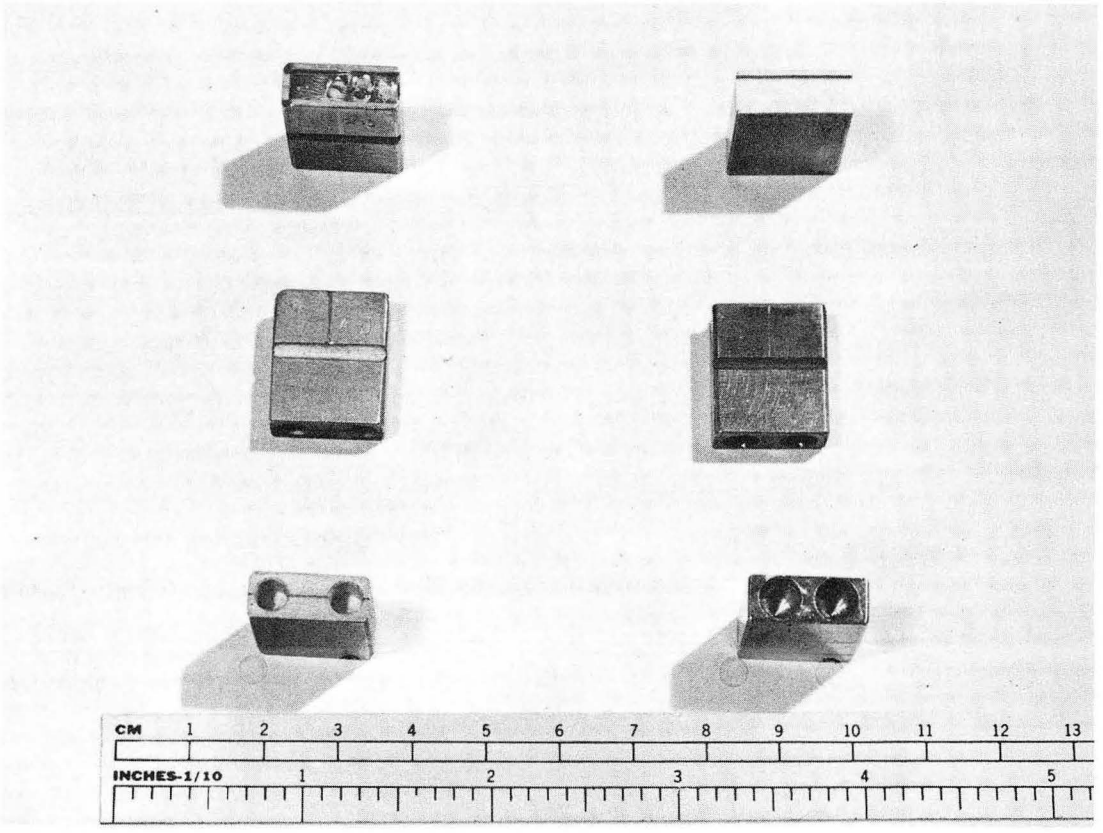

ZN-3400

Fig. 16. "Buttons" used for collection of the radioactive atomic-beam.
To the right: Silver plated buttons used for collecting Br and I.
To the left: Platinum foil holder used for collecting Lu and Br.

Therefore, although "beam sizes" of 2000 c/m were usually obtainable for considerably longer periods of time, after about 8 hours of operation most runs had to be discontinued because of prohibitally poor resonance signal to background ratios.

Using A and B magnet currents in accordance with the discussion of Section IV D throw-outs (i.e. the ratio of full-beam minus direct-beam to full-beam counting rates) of .75 - .80 were obtained. During resonance searches beam exposures were taken for 5 minutes each. The beam strength was checked from time to time by taking 1 minute direct-beam exposures. Experience showed that the beam was never sufficiently unstable to warrent taking a normalization exposure after every resonance exposure. The signal to background ratio, that is the ratio of the highest counting rate obtained during a resonance search to the counting rate for a machine-background exposure, ranged from 2.5/1 for $\Delta F = \pm 1$ transitions in the $2D_{3/2}$ atomic state and $\Delta F = 0$ transitions in the $^2D_{5/2}$ atomic state to 5/1 for low field $\Delta F = 0$ transitions in the $^2D_{3/2}$ state. The C field was checked after each resonance exposure to assure that no drift had taken place during the course of the exposure. Such drifts, though rare, were usually connected with the Bevatron's magnetic field, which fringed into the atomic-beam laboratory. This fringing was sufficiently strong to throw the C field completely off of a K resonance if the Bevatron was turned off or on during exposure of a foil.

D. Operating Procedure at B.N.L.

The Lu^{176m} experiment at B.N.L. was patterned after the one at L.R.L. and hence has many similar characteristics. For example, the oven units and oven holder assembly used at B.N.L. were exactly the same as those depicted in Figs. 14 and 15. Since the Brookhaven High Neutron Flux Research Reactor is located at B.N.L., the Lu samples, which were bombarded in this pile for 4-hour periods, could be transferred to the atomic-beam machine very rapidly and the Lu was usually inside the machine and the oven ready to be lined up within 30 minutes of removal of the sample from the pile. The lining up procedure was the same as that outlined above. Under operating conditions the Lu beam throw-out was about the same as at L.R.L. (.75 - .80) and useable Lu beams (direct beams of about 200 c/m for a 1 minute exposure) were obtained with around 160 watts of electron bombardment power. The Lu beam was collected on soot covered copper plates and resonance exposures were for about 200 sec at the beginning of a given run. The exposure time was augmented during the course of the run to compensate for the radioactive decay of

Lu^{176m} until about a 350 sec. exposure time was reached. At this point the beam was "raised" by applying more electron bombardment power and the exposure time augmentation process repeated. All exposed plates were counted for 10 minutes or longer in low background proportional Geiger Counters. The signal to background ratio at B. N. L. was typically between 2/1 and and 2.5/1. Because of the great stability of the C magnet current supply (and the absence of a Bevatron) the C field did not require constant monitoring as at L. R. L. and was only checked after a Lu resonance line had been traced out.

E. Spin Determination: Data and Results

Using what was referred to in Section IV A as machine no. 1, a spin search such as is described in Section II D was carried out for Lu^{176m}, by looking for low field α and β observable transitions in the $^2D_{5/2}$ atomic state. Since this state lies only 1993.9 cm^{-1} above the $^2D_{3/2}$ ground state[29], about 25% of the Lu^{176m} atoms in the beam would be expected to be in the $^2D_{5/2}$ state at any time. The results of the initial spin search are given in Table 2. It is seen from this table that frequencies which correspond to I = 1 resonances always lead to counting rates equal to at least double the background counting rate, and that this is not the case for the neighboring integral spin values. These data strongly indicate a spin of 1 for Lu^{176m}. Figures 17 and 18 show decay curves for a full-beam exposure and an I = 1 resonance exposure. These curves show first that most of the activity in the beam was caused by Lu^{176m} and second that the apparent I = 1 resonance is a Lu^{176m} resonance. Subsequently α and β resonances in the $^2D_{3/2}$ ground state of Lu^{176m} were also observed and again indicated I = 1. Figures 19 and 20 show α and β resonance curves for Lu^{176m} in both the $^2D_{5/2}$ and $^2D_{3/2}$ states.* These were obtained at a C field corresponding to ν_K = 6.0 mc/sec.

The above mentioned data together with the fact that this spin value is consistant with all the hyperfine structure data discussed in the next section, seems conclusively to indicate a spin of I = 1 for Lu^{176m}.

F. Hyperfine Structure Determination; Data and Results

As with the spin determination, the initial work on the hyperfine structure of Lu^{176m} was performed by observing transitions in the $^2D_{5/2}$ atomic state. Using the method described in Section II E, α and β resonances were traced out at progressively higher magnetic fields

*In Figure 20 and in all other resonance curves exhibited in this paper, points with horizontal lines drawn through them correspond to machine background exposure.

Table 2 . Lu^{176m}, J = 5/2 Spin Search Data

ν_K mc/sec	H gauss	F state	Counting Rate For I = 0	I = 1	I = 2	Machine background
1	1.418	7/2	19.8 ± 2.1	83.6 ± 4.8	20.6 ± 1.8	15.9 ± 1.8
1	1.418	5/2		44.9 ± 3.3		15.9 ± 1.8
3	4.201	7/2		55.4 ± 3.3		14.5 ± 1.8
3	4.201	5/2		32.5 ± 2.4		14.5 ± 1.8
6	8.248	7/2		65.3 ± 3.3		14.5 ± 1.8
6	8.248	5/2		25.2 ± 2.2		9.2 ± 1.5

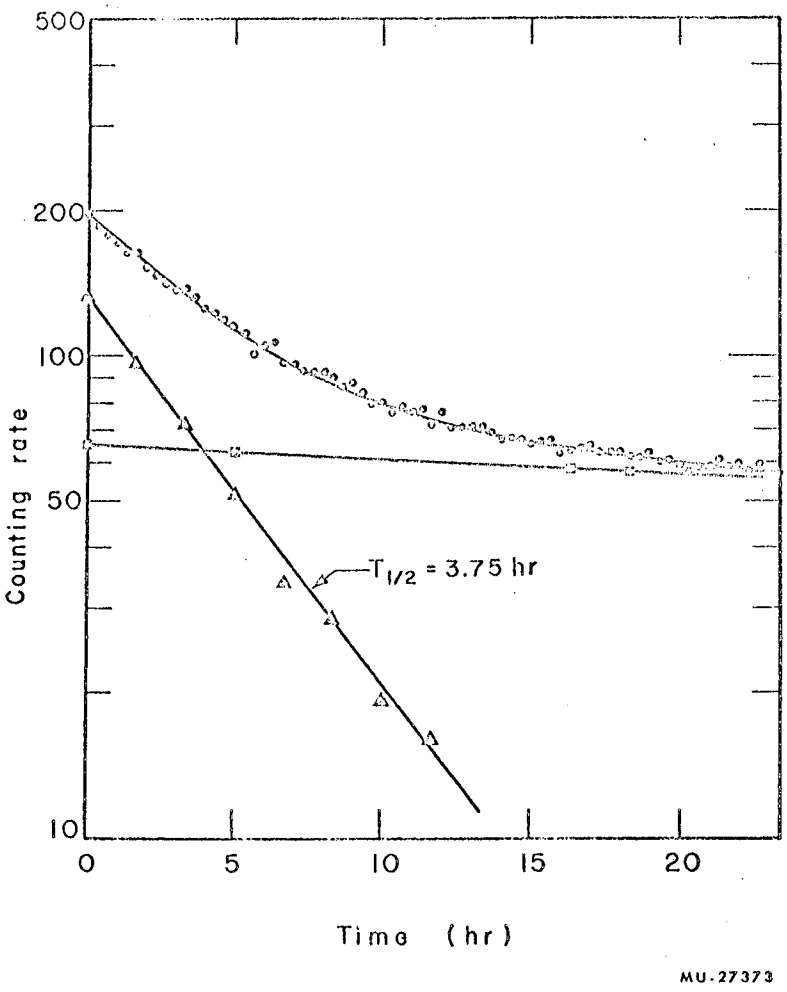

Fig. 17. Lu^{176m} full beam decay curve.

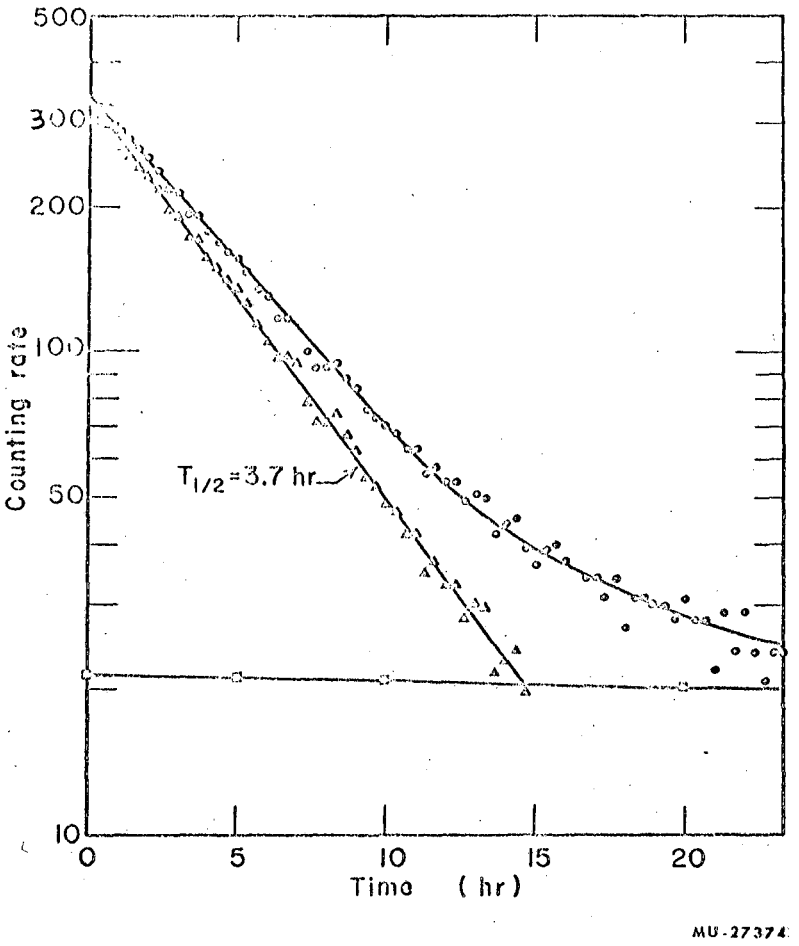

Fig. 18. Lu^{176m} I = 1 resonance decay curve ($^2D_{5/2}$ state).

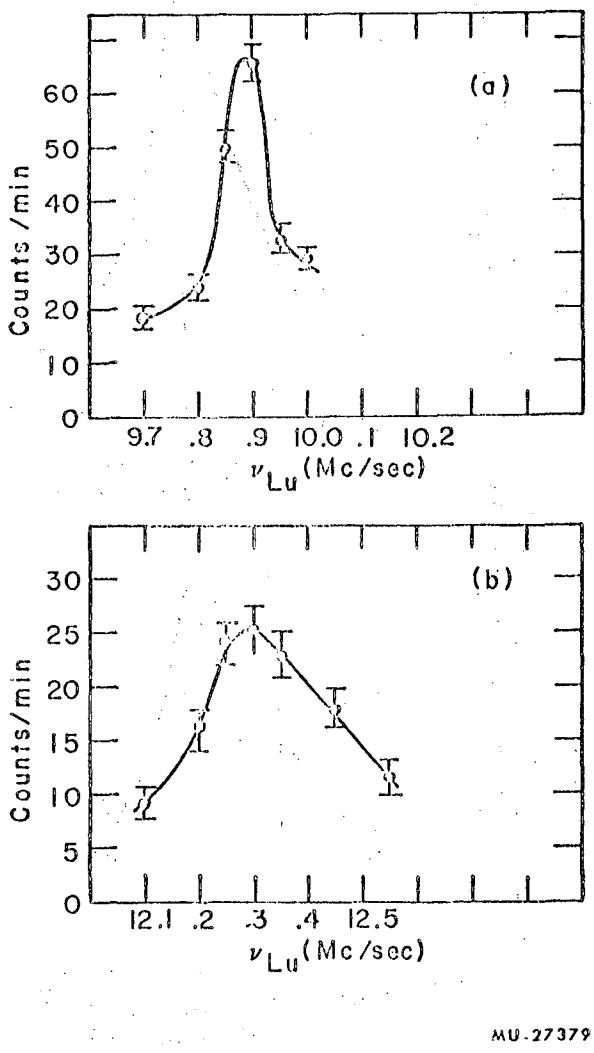

Fig. 19. Lu^{176m} low field $\Delta F = 0$ resonances ($^2D_{5/2}$ state)
(a) α transition (ν_K = 6.00 mc/sec) ν (Zeeman) = 9.89 mc/sec
(b) β transition (ν_K = 6.00 mc/sec) ν (Zeeman) = 12.27 mc/sec

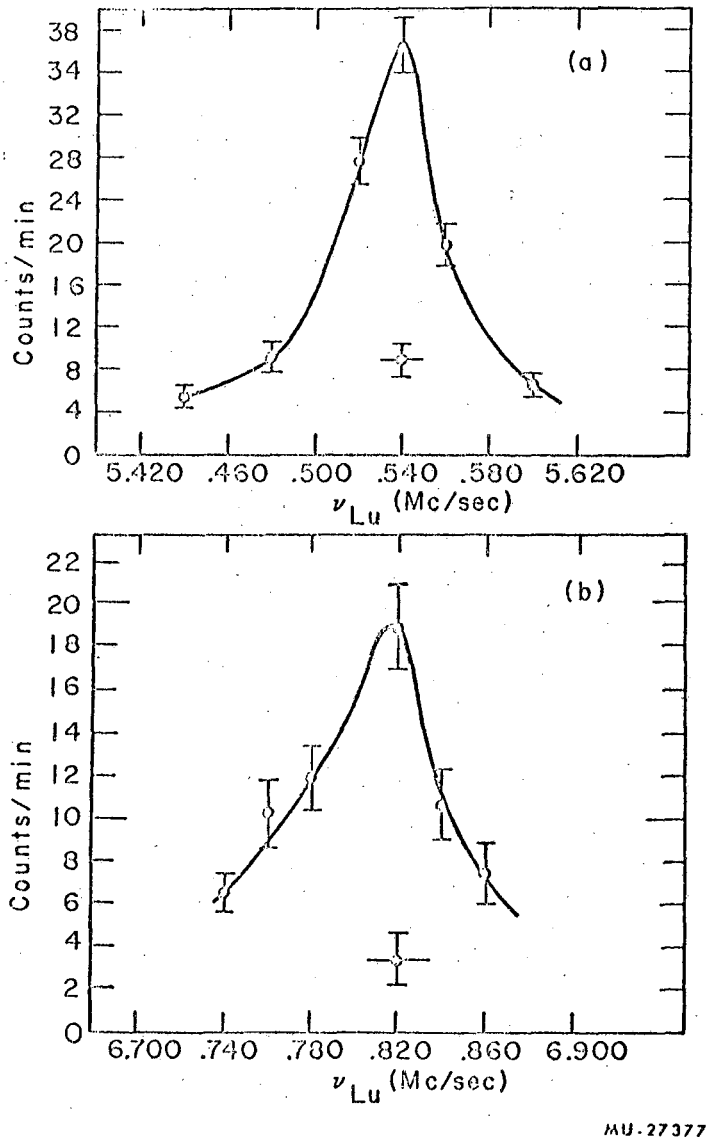

Fig. 20. Lu^{176m} low field resonances ($^2D_{3/2}$ state)
(a) α transition (ν_K = 6.00 mc/sec) ν(Zeeman) = 5.54 mc/sec
(b) β transition (ν_K = 6.00 mc/sec) ν(Zeeman) = 6.78 mc/sec.

until shifts from the linear Zeeman predictions of 3.3 mc/sec and 1.5 mc/sec were observed in the α and β resonances respectively. On the basis of these shifts initial guesses were made for "a" and "b" using the method outlined in Appendix C. These values, the necessary known comparison isotope and calibration isotope data (see Appendix A), and all Lu^{176m} resonance data which had been collected up to that time were supplied as input to the "Hyperfine" program and improved values of "a" and "b" sought. The program did not converge, indicating that something was wrong with the input data.

At this point it was decided to look for resonances in the $^2D_{3/2}$ ground state of Lu^{176m} in order to obtain an improved resonance signal to background ratio and consequently more reliable data. Again α and β resonance lines were traced out at higher and higher magnetic fields until appreciable shifts from the linear Zeeman predictions were observed in both the α and the β transitions. Guesses were then made for "a" and "b" and a "Hyperfine" run made based on the $^2D_{3/2}$ resonance data. Again the program could not converge to "a" and "b" values consistent with the experimental data.

In searching for the reason for this failure it was noticed that a plot of $\Delta f/H$ vrs. H, where Δf is the resonance shift from the linear Zeeman prediction, is (for moderate values of H) parabolic in shape for the α resonances and linear for the β resonances in both the $^2D_{3/2}$ and $^2D_{5/2}$ states. From Eqs.(7A) it is obvious that a parabolic shape is likely to result only if the magnetic quantum numbers involved in the α transition change sign but not magnitude, that is if $m_F(\text{initial}) = -m_F(\text{final})$. Therefore, in view of the low field selection rule $\Delta m_F = \pm 1$ for single quantum transitions, the α transition for the $^2D_{3/2}$ [$^2D_{5/2}$] state would be expected to take place between the two states $(5/2, 1/2) \leftrightarrow (5/2, -1/2)$ [$(7/2, 1/2) \leftrightarrow (7/2, -1/2)$] .

In Fig. 21b is given a schematic energy level diagram which indicates the correspondence between the low field (Zeeman) magnetic quantum levels (shown on the left side of the diagram) and the high field quantum levels (shown on the right side of the diagram) for the case I = 1, J = 3/2. The quantum numbers corresponding to the initial and final states associated with the observable α and β transitions are also shown on this diagram. It is seen that the α transition quantum numbers are not those expected on the basis of the above analysis. Figure 21a is the

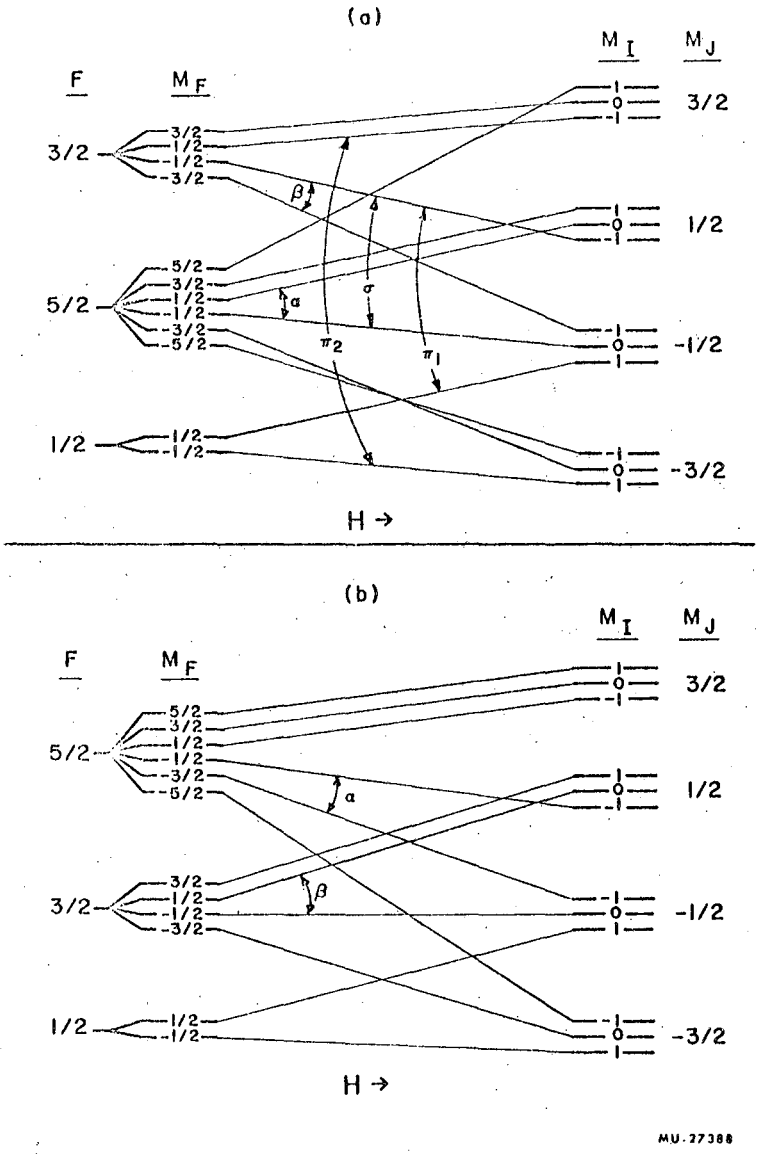

Fig. 21. Schematic energy level diagrams for J = 3/2, I = 1
(a) Inverted ordering (b) Normal ordering.

same as 21b except that instead of assuming normal zero field hyperfine level ordering (i.e. F = 5/2, 3/2, 1/2 in order of decreasing energy)as was done in Fig. 21b the inverted level ordering F = 3/2, 5/2, 1/2 is assumed. It is seen that in this case the expected α transition quantum numbers are obtained and that furthermore the $\Delta f/H$ vrs. H curve for the β transitions is predicted to be linear. Assuming,therefore, the ordering of Fig. 21a, starting values of "a" and "b" were calculated and these values, when used in conjunction with the quantum numbers:

$$(\alpha) \quad (5/2,\ 1/2) \leftrightarrow (5/2,\ -1/2)$$
$$(\beta) \quad (3/2,\ -1/2) \leftrightarrow (3/2,\ -3/2)$$

led to a good fit, by "Hyperfine," of all $^2D_{3/2}$ resonance data which had been gathered up to that time. Similar results were obtained for the $^2D_{5/2}$ data when a F = 5/2, 7/2, 3/2 inverted ordering was assumed.

Once an initial fit had been obtained the procedure described in Section II E was followed and the "J0-9" Program used in conjunction with "Hyperfine" to enable searches for higher field $\Delta F = 0$ transitions to be conducted. In this way a total of 13, $\Delta F = 0$ resonance lines in both the $^2D_{3/2}$ and $^2D_{5/2}$ atomic states were traced out at field ranging from 0 to 504.3 gauss. Then a B magnet coil of machine no. 1 shorted out and the redesigning procedure that led to machine no. 2 was undertaken. Two examples of intermediate field $^2D_{5/2}$ lines traced out on machine no. 1 are shown in Fig. 23. Figure 24 shows an intermediate field $^2D_{3/2}$ line as it appeared when traced out on machine no. 1 and also as it appeared when traced out on machine no. 2.

During the rebuilding of the machine at L.R.L. the work on Lu at B.N.L. was undertaken. First three $^2D_{3/2}$ intermediate field lines, which had been previously traced out at L.R.L, were retraced on the machine at Brookhaven (machine no. 3). Because of this machine's much more homogeneous C field, these lines were almost 40 times narrower than the original lines. An example of one of the $\Delta F = 0$ resonance curves obtained at Brookhaven is shown in Fig. 29 b. The refinement of the experimental data which resulted from the inclusion of these three lines enabled "a" and "b" to be determined with sufficient accuracy to allow a search for the observable field dependent $\Delta F = \pm 1$, $\Delta m = \pm 1$ direct transitions to be undertaken. Two such deservable transitions exist for the $^2D_{3/2}$ state of Lu^{176m}. They are indicated by π_1 and π_2 in Fig. 21 a and correspond to: $(3/2,-1/2) \leftrightarrow (1/2,\ 1/2)$ and $(3/2,\ 1/2) \leftrightarrow (1/2,-1/2)$ respectively. After much labor, indications of these lines were found at Brookhaven but at frequencies differing considerably

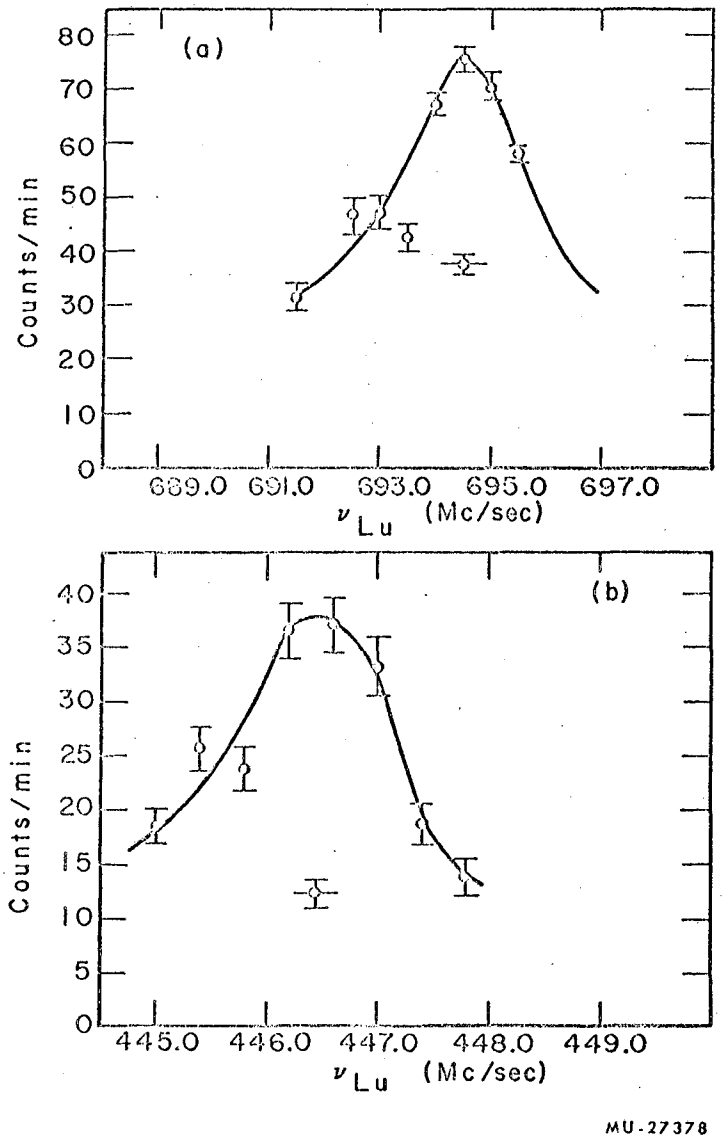

Fig. 22. Lu^{176m} intermediate field, $\Delta F = 0$, resonances ($^2D_{5/2}$ state)
(a) α transition (ν_K = 500.0 mc/sec)
(b) β transition (ν_K = 500.0 mc/sec).

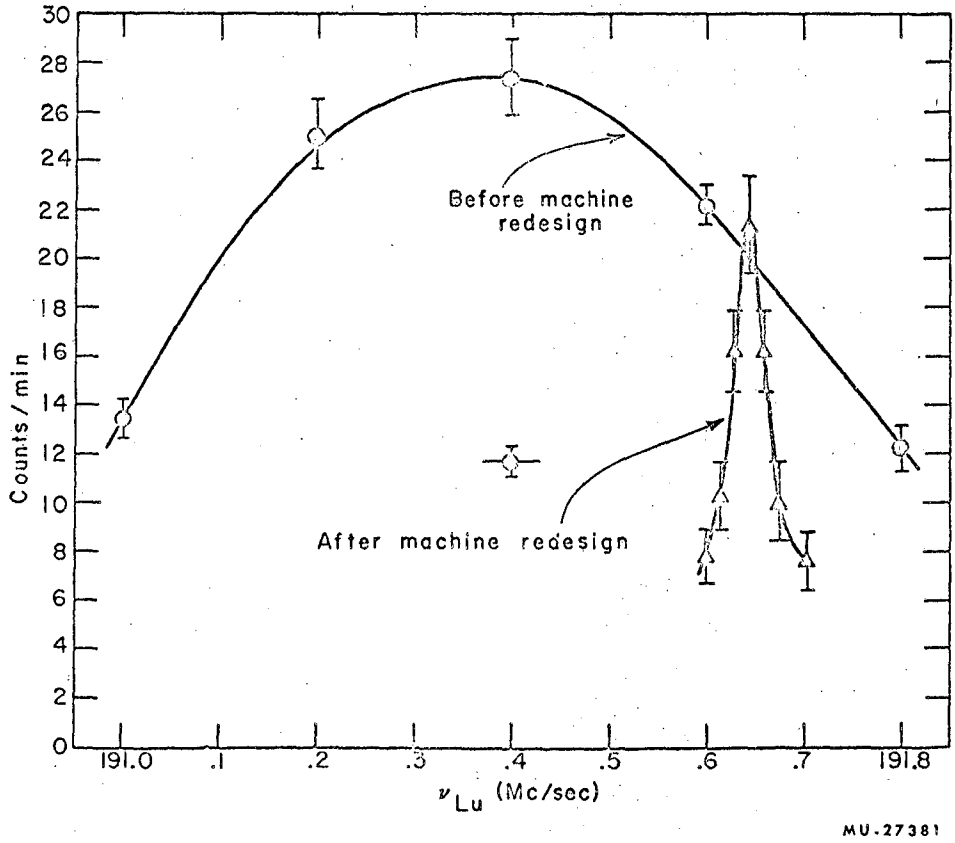

Fig. 23. Lu^{176m} α resonance curve as it appeared before and after the redesigning of machine no. 1 (ν_K = 500.0 mc/sec) .

from the resonance frequencies predicted on the basis of previously observed $\Delta F = 0$ transitions.

By this time machine no. 2 at Berkeley was in working order and an attempt was made, using this machine, to verify the π_1 and π_2 line frequencies found at B.N.L. The lines shown in Fig. 26(a) were obtained but at frequencies which lay considerably outside the Brookhaven lines and which also seemed inconsistent with existing $\Delta F = 0$ resonance data. The disagreement between the Brookhaven lines and the Berkeley lines was later removed by the discovery that the C magnet of machine no. 3 had been misaligned during the direct transition search at B.N.L. Also the apparent inconsistency between the $\Delta F = 0$ and $\Delta F = \pm 1$ resonance data was removed, as indicated below, when a slightly different value of g_J was used an input to "Hyperfine."

As indicated in Fig. 27 there is a value of field (H = 508 gauss) where the energy of the hyperfine level corresponding to $F = 3/2$, $m_F = -1/2$ and the energy of the level corresponding to $F = 1/2$, $m_F = 1/2$ vary at the same rate with respect to magnetic field. This means that the frequency of the π_1 direct transition, which corresponds to a transition between these two energy levels, is to first order independent of H at this value of field. After using the π_1 and π_2 field dependent resonance frequencies of Fig. 26(a) together with all the $\Delta F = 0$ data which had been obtained at B.N.L. to predict as accurate as possible values of "a" and "b", a search for this "field independent" direct transition was undertaken using machine no. 2. Subsequently the resonance line shown in Fig. 26(b) was obtained. Finally on the basis of all three $\Delta F = \pm 1$, $\Delta m_F = \pm 1$ lines the frequency of the $(3/2, -1/2) \leftrightarrow (5/2, -1/2)$, $\Delta F = \pm 1$ $\Delta m_F = 0$ line (which is specified by in Fig. 22) was predicted and this line was searched for at B.N.L. Ultimately the resonance curve of Fig. 29(a) was obtained.

A list of all resonance data obtained for the $^2D_{3/2}$ atomic state of Lu^{176m} is given in Table 3. At first, as mentioned above, difficulty was encountered in simultaneously fitting the $\Delta F = 0$ and the $\Delta F = \pm 1$ resonance data with the same "a" and "b" values. A fit was obtained, however, by allowing g_J as well as "a" and "b" to vary while trying to secure the fit. The value $g_J\ (^2D_{3/2}) = -.79931 \pm .000025$ was converged upon both when g_I was determined, by "Hyperfine," using the Fermi-Segre Formula (Eq. (26)) and when g_I was allowed to vary freely along with "a," "b," and "g_J". This value of $g_J\ (^2D_{3/2})$ agrees, within experimental error, with Ritter's[30] value of $g_J\ (^2D_{3/2}) = -.79921 \pm .00008$ but differs sufficiently from the latter to allow a fit of the Lu^{176m}

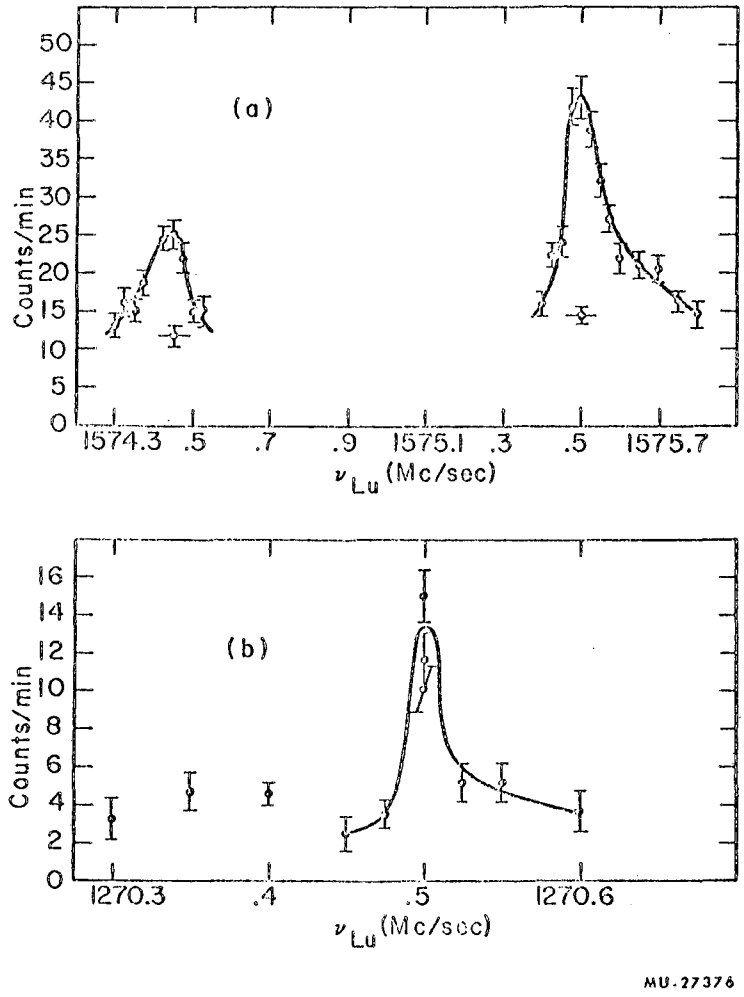

Fig. 24. Lu^{176m} pi direct transitions ($^2D_{3/2}$ state)
(a) Field dependent lines (ν_K = 280 Mc/sec)
(b) Field independent line (ν_K = 1110.0 Mc/sec).

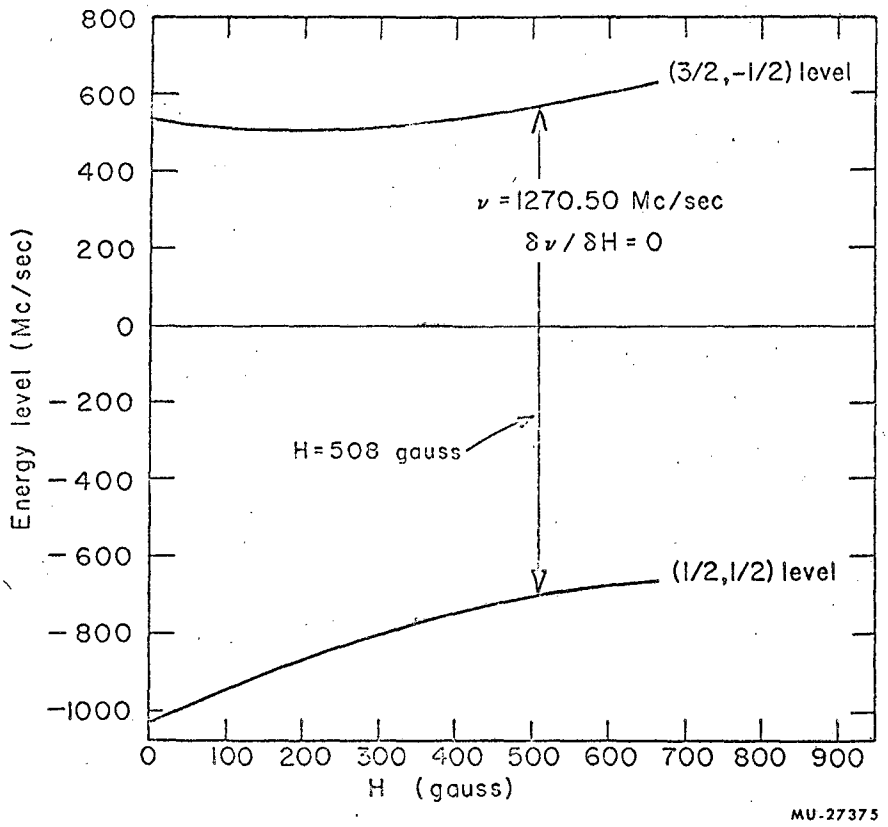

Fig. 25. Energy level diagram for determining the position of the field independent direct Pi transition.

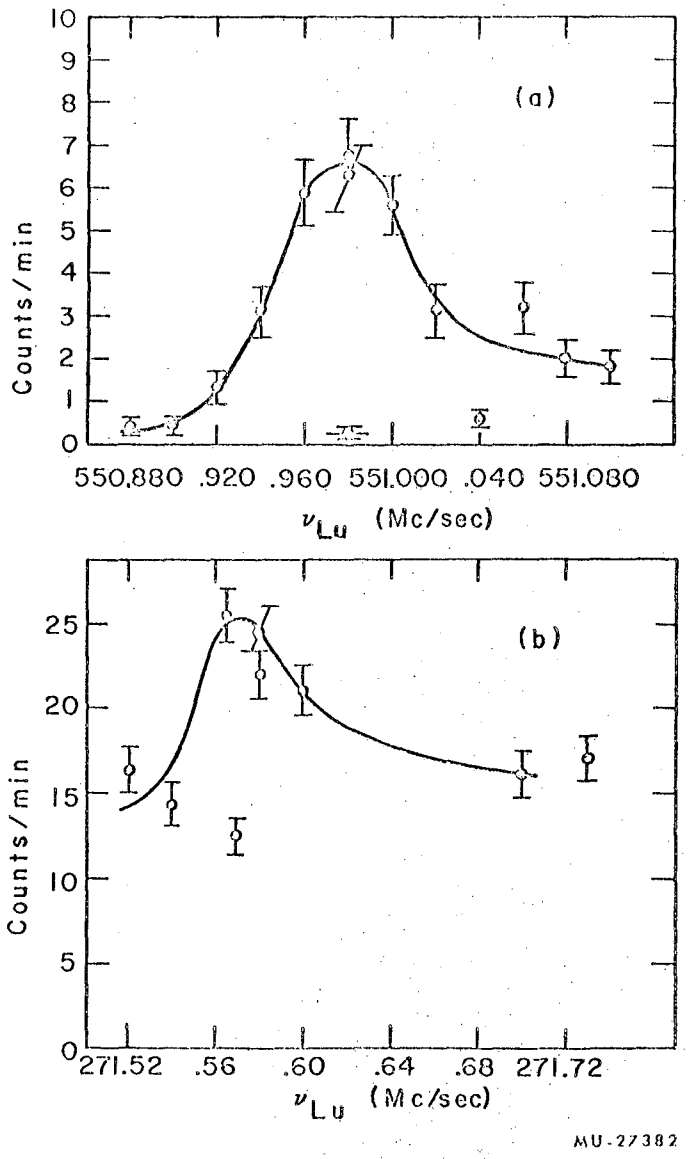

Fig. 26. Lu^{176m} resonances found at B.N.L. ($^2D_{3/2}$ state)
(a) Direct sigma transition (ν_K = 200.0 kc/sec)
(b) β transition (ν_K = 500.0 mc/sec) .

Table 3 . Lu^{176m}, J = 3/2 Resonance Data and Final Hyperfine Output

$a = 97.195 \pm .004$ mc/sec

$b = -635.191 \pm .005$ mc/sec $\qquad \chi^2 = 1.4$

$g_J = -0.799311 \pm .000023$

$g_I > 0$

Run No.	ν_K mc/sec	H gauss	ΔH gauss	ν_{Lu} mc/sec	$\Delta\nu_{Lu}$ mc/sec	Residual mc/sec	F_1	M_1	F_2	M_2	Weight factor
1	500.0	278.794	.008	271.57	.020	.009	3/2	-1/2	3/2	-3/2	2120.9
2	500.0	278.794	.008	191.645	.020	-.003	5/2	1/2	5/2	-1/2	2313.8
3	1100.0	504.321	.007	517.895	.030	-.007	3/2	-1/2	3/2	-3/2	1036.2
4	0.28	0.40	.03	1574.450	.030	.014	3/2	-1/2	1/2	1/2	424.5
5	0.28	0.40	.03	1575.500	.030	-.007	3/2	1/2	1/2	-1/2	423.4
6	1110.0	507.986	.007	1270.500	.015	-.001	3/2	-1/2	1/2	1/2	4444.4
7	0.28	0.29	.03	550.980	.020	.000	3/2	-1/2	5/2	-1/2	2473.0
8	6.0	8.25	.02	5.530	.015	-.006	5/2	1/2	5/2	-1/2	2482.1
9	6.0	8.25	.02	6.820	.015	.005	3/2	-1/2	3/2	-3/2	2006.7
10	2.0	2.81	.02	1.890	.015	-.002	5/2	1/2	5/2	-1/2	2373.5
11	40.0	46.08	.08	30.95	.10	.003	5/2	1/2	5/2	-1/2	76.9
12	100.0	93.04	.14	62.650	.07	.027	5/2	1/2	5/2	-1/2	72.4
13	200.0	149.71	.16	101.25	.10	.046	5/2	1/2	5/2	-1/2	43.9
14	300.0	196.28	.18	133.40	.14	.059	5/2	1/2	5/2	-1/2	28.9
15	1100.0	504.32	.25	365.40	.50	-.217	5/2	1/2	5/2	-1/2	3.4
16	12.0	15.92	.06	13.20	.10	-.040	3/2	-1/2	3/2	-3/2	78.7
17	24.0	29.84	.07	25.10	.04	-.005	3/2	-1/2	3/2	-3/2	187.5
18	40.0	46.08	.08	39.30	.05	.016	3/2	-1/2	3/2	-3/2	130.1
19	100.0	93.04	.14	82.20	.10	.014	3/2	-1/2	3/2	-3/2	36.7
20	200.0	149.71	.16	137.10	.10	-.116	3/2	-1/2	3/2	-3/2	26.9

resonance data.

The small value of 1.4 for χ^2, indicated in Table 3(when compared to the acceptable value[31] of 16.0) shows that the experimental frequency errors quoted in the table are for the most part quite pessimistic. For this reason the errors quoted there for a, b, and g_J (which are the same as those quoted directly by "Hyperfine") probably themselves constitute fairly pessimistic values. However to be absolutely safe, twice these values will be adopted as the experimental errors to yield final results for the $^2D_{3/2}$ state measurements of:

$$a(^2D_{3/2}) = 97.195 \pm .008 \text{ mc/sec}$$

$$b(^2D_{3/2}) = -635.19 \pm .01 \text{ mc/sec}$$

$$g_J(^2D_{3/2}) = -.79931 \pm .00005$$

and using Eqs. (9 a) and (10 a) of Appendix C in conjunction with the above results

$$\Delta\nu_{3/2,5/2} = -5/2a - 5/4b = (551.000 \pm .032) \text{ mc/sec}$$

$$\Delta\nu_{5/2,1/2} = 4\,a - b = (1023.97 \pm .04) \text{ mc/sec.}$$

The algebraic signs of "a" and "b" quoted above are correct if the g'_I of Lu^{176m} is positive. That this is in fact the case was established both by trying to fit the experimental data using the Fermi-Segre Formula to determine g'_I, while assuming that it is negative, and by starting with a negative initial g'_I and then fitting the experimental data by allowing it to freely vary. In the first case a fit was obtained but with a $\chi^2 = 54.8$ as compared to $\chi^2 = 1.4$ for positive g'_I. In the second case g'_I converged to a positive value consistent with that obtained using the Fermi-Segre Formula.

"a" and "b" in both the $^2D_{5/2}$ and the $^2D_{3/2}$ states have been measured for Lu^{175} by Ritter[30] and for Lu^{177} by Peterson.[32] The ratio's

$$\frac{a(^2D_{3/2})}{a(^2D_{5/2})} \quad \text{and} \quad \frac{b(^2D_{3/2})}{b(^2D_{5/2})}$$

were found to be the same for both of these Lu isotopes (as would be expected) and it was therefore felt that very little would be gained by doing an accurate measurement of a $(^2D_{5/2})$ and $b(^2D_{5/2})$ for Lu^{176m}.

Consequently no further work was done on the $^2D_{5/2}$ state at L.R.L. after the redesigning of machine no. 1. For the sake of completeness, however, the experimental data which were obtained for this atomic state are given in Table 4 together with the best values of "a", "b", and g_J converged upon by "Hyperfine" in attempting to fit these data. Doubling the errors quoted in this table and remembering that g_I' has been established as positive by the $^2D_{3/2}$ data, we arrived at the final results for the $^2D_{5/2}$ state:

$$a\,(^2D_{5/2}) = 77.6 \pm 4.8 \text{ mc/sec}$$

$$b\,(^2D_{5/2}) = -782.3 \pm 9.6 \text{ mc/sec}$$

$$g_J(^2D_{5/2}) = -1.2001 \pm .0006$$

and using the equations of Appendix C

$$\Delta\nu_{5/2,7/2} = -7/2a - 21/20b = (550 \pm 27) \text{ mc/sec}$$

$$\Delta\nu_{7/2,3/2} = 6a - 9/20b = (818 \pm 33) \text{ mc/sec}$$

The value of g_J quoted above is consistent with Ritter's value[30]; $g_J(^2D_{5/2}) = -1.20040 \pm .00016$. Moreover the values of $a(^2D_{5/2})$ and $b(^2D_{5/2})$, when combined with the corresponding quantities quoted for the $^2D_{3/2}$ state, lead to

$$\frac{a(^2D_{3/2})}{a(^2D_{5/2})} \quad \text{and} \quad \frac{b(^2D_{3/2})}{b(^2D_{5/2})}$$

ratios which agree, to within experimental error, with the corresponding Lu^{175} and Lu^{177} ratios.

G. Calculation of the Nuclear Moments

Nuclear Magnetic Dipole Moment:

When Eq. (26) is used in conjunction with the measured value of $a(^2D_{3/2})$ for Lu^{176m} (given above) and the known data for Lu^{175} (given in Appendix A), the value

$$\mu_I(Lu^{176m}) = 0.3160\ (14) \text{ nm} \quad \text{(uncorrected)}$$

is obtained for the uncorrected nuclear magnetic dipole moment of Lu^{176m}. This is consistent with the result $\mu_I(Lu^{176m}) = 0.33(2)$ nm obtained

Table 4 . Lu^{176m}, J = 5/2 Resonance Data and Final Hyperfine Output

a = 77.6 ± 2.4 mc/sec

b = -782.3 ± 4.8 mc/sec $\quad \chi^2 = 2.2$

$g_I > 0$

Run No.	ν_K mc/sec	H gauss	ΔH gauss	ν_{Lu} mc/sec	$\Delta\nu_{Lu}$ mc/sec	Residual mc/sec	F_1	M_1	F_2	M_2	Weight factor
1	6.0	8.25	.04	9.90	.03	.001	7/2	1/2	7/2	-1/2	315.1
2	40.0	46.08	.06	55.40	.07	-.001	7/2	1/2	7/2	-1/2	96.0
3	100.0	93.04	.14	112.50	.10	.015	7/2	1/2	7/2	-1/2	25.5
4	200.0	149.71	.15	182.90	.13	.044	7/2	1/2	7/2	-1/2	19.0
5	500.0	278.80	.28	352.80	.50	.291	7/2	1/2	7/2	-1/2	2.5
6	1100.0	504.33	.29	694.50	.70	.011	7/2	1/2	7/2	-1/2	1.4
7	6.0	8.24	.04	12.30	.07	-.024	5/2	-1/2	5/2	-3/2	118.3
8	12.0	15.92	.06	23.90	.07	.024	5/2	-1/2	5/2	-3/2	73.5
9	24.0	29.84	.07	45.00	.10	-.037	5/2	-1/2	5/2	-3/2	46.0
10	40.0	46.08	.06	70.00	.07	-.053	5/2	-1/2	5/2	-3/2	71.4
11	100.0	93.04	.14	143.90	.10	-.109	5/2	-1/2	5/2	-3/2	16.8
12	200.0	149.71	.14	235.00	.22	-.317	5/2	-1/2	5/2	-3/2	10.0
13	500.0	278.80	.28	446.40	.60	.425	5/2	-1/2	5/2	-3/2	1.8

using the rough result given above for $a(^2D_{5/2})$ and also with the value $\mu_I(Lu^{176m}) = .31(6)$ nm determined directly by "Hyperfine" if g_I is allowed to vary freely during the resonance data fitting process. Application of the appropriate diamagnetic shielding correction factor (given in Appendix B) yields for the best corrected value

$$\mu_I(Lu^{176m}) = .3186\ (14)\ \text{nm} \qquad \text{(corrected)} \ .$$

In the case of Lu, Eqs. (23) and (24) lead to the following interaction constant ratios

$$a(^2D_{5/2}) \ / \ a(^2D_{3/2}) = 0.415 \qquad b(^2D_{5/2})/b(^2D_{3/2}) = 1.2538 \ ,$$

while the data given in Appendix A indicates that actually for Lu^{175} and Lu^{177}

$$a(^2D_{5/2})/\ a(^2D_{3/2}) = .7553 \qquad b(^2D_{5/2})/b(^2D_{3/2}) = 1.2311 \ .$$

Although the disagreement between the theoretical and actual ratio of the b's in the $^2D_{5/2}$ and $^2D_{3/2}$ states is not too serious, the large discrepancy in the case of the a's raises considerable doubt about the validity of applying Eq. (28) to perform an alternative calculation of $\mu_I(Lu^{176m})$.

The criteria for applicability of Eqs. (23) - (28), for the most part, seem to be quite well satisfied by Lu. Since the lowest lying electronic configuration for Lu is $5d6s^2$ it clearly has a single d electron outside closed shells. Furthermore the g_J's determined above for the $^2D_{3/2}$ and $^2D_{5/2}$ states both lie quite close to the pure Russel-Sander's predictions of $g_J(^2D_{3/2}) = -0.799549$ and $g_J(^2D_{5/2}) = -1.200458$. Thus a case of almost pure L-S coupling is indicated. The only remaining criterion for the validity of these Equations is that the energy levels must be derived from a single electronic configuration. Consequently it must be assumed that this criterion is violated.

To determine the nature of the perturbing configuration we note, first of all, that it must lie close in energy to the ground state configuration. Second, since the term in the Hamiltonian which is responsible for configuration mixing can only connect eigenstates corresponding to the same J, L, and S, this configuration must contain a ^2D term. Third, since $g_J(^2D_{3/2})$ and $g_J(^2D_{5/2})$ for Lu lie so close to the pure L-S coupling values, the g_J's arising from this ^2D term must be nearly equal

to those arising from the ^2D term of the ground state configuration. Finally, since the theoretical ratio of the b's is much closer to the actual experimental value than is the case with the ratio of the a's, the admixed configuration must be such as to affect the "a" interaction constants much more than the "b". The 5d 6s 7s configuration satisfies all these requirements and if this is assumed to be responsible for the perturbation the method proposed by Schwartz[7] (which is discussed in Section I B) can be used to deal with the configuration mixing.

Assuming $Z_1^{50} = 51.5$ and using Eqs. (33), (34), (35) and the accurate ratio of $a(^2D_{5/2})$ to $a(^2D_{3/2})$ given above for Lu^{175}, leads to a value of

$$\delta'' = -23.375 \text{ mc/sec}$$

for the contribution of the 5d 6s 7s configuration's unpaired s electrons to the $a(^2D_{3/2})$ interaction constant for Lu^{176m}. Subtracting this value from the measured $a(^2D_{3/2})$ yields, for the contribution from the d electron alone

$$a_o(^2D_{3/2}) = 120.570(8) \text{ mc/sec} .$$

This, when entered into Eq. (28) along with $Z_1 = 51.5$, gives for the uncorrected magnetic dipole moment

$$\mu\,(Lu^{176m})_{\text{calc.}} = 0.287 \text{ nm} \quad \text{(uncorrected)}$$

which is in fair agreement with the true value calculated, at the beginning of this Section, using Eq. (26).

Using the correct $\mu(Lu^{176m})$, inversion of Eq. (28) indicates that $Z_1 = 57.2$ is the proper value for Lu. This value is used to determine the $a_o(^2D_{3/2})$ and Relativistic Correction Factors necessary for the evaluation of Q below.

Nuclear Electric Quadrupole Moment:

When $a_o(^2D_{3/2})$ is calculated, in the way described above, assuming that $Z_1 = 57.2$ a value

$$a_o(^2D_{3/2}) = 128.848 \text{ mc/sec}$$

is obtained. Using this result, the experimentally determined $b(^2D_{3/2})$, and the uncorrected $\mu(Lu^{176m})$, Eq. (25) gives

$$Q(Lu^{176m}) = 2.40\ (5) \text{ barns} \quad \text{(uncorrected)}.$$

This result is obtained under the assumption that $b(^2D_{3/2})$ is

completely unaffected by any configuration interaction present. In view of the obvious falaciousness of this assumption (see the theoretical and experimental b ratios given above) and the uncertainties inherent in this type calculation, a reasonable error of about 2% is assigned to the above final value.

H. Discussion of Lu^{176m} Nuclear Spin and Moment Results

Application of the Shell Model:

The Individual Particle Shell Model cannot account for the spins of either Lu^{176} or Lu^{176m} in any straightforward way. This apparent failure is not surprising in view of the fact that the 71st proton assignment is near the middle of the shell ending at 82 nucleons while the 105th neutron is near the middle of the shell ending at 126 nucleons. Furthermore the Lu and Hf isotopes are known to exhibit the largest quadrupole moments of any of the nuclides for which this quantity has been measured. Hence these isotopes would be expected to exhibit strong collective nuclear properties and be described better in terms of the Collective Model.

Application of the Collective Model:

Determining the deformation parameter

Before the Collective Model can be used to predict the properties of any nuclide the deformation parameter δ must be estimated. Mottelson and Nilsson[23] have calculated δ for many even-odd and odd-even isotopes by finding that value of δ which, using the assumed Collective Model Hamiltonian, minimizes the total energy (i.e. maximizes the binding energy) of a given nuclide. Their results for nuclides related to Lu^{176} are shown in column four of Table 5 without parenthesis.

TABLE 5

Name	No. of Protons	No. of Neutrons	δ Calculated by Mottelson and Nilsson	Q (barns)	Q_o (barns)	δ Calculated from Q	Experimental Reference
Lu^{175}	71	104	.28	5.68	12.1	.40	30
Lu^{175*}	71	104	.28	--	--	--	
Lu^{176}	71	105	(.275)	8.0	11.9	.40	33
Lu^{176m}	71	105	(.275)	2.40	24.0	.68	
Lu^{177}	71	106	.26	5.0	10.7	.39	32
Hf^{177}	72	105	.270	--	--	--	
Hf^{179}	72	107	.260	--	--	--	

In the Table, Lu^{175*} signifies the first excited state of Lu^{175}, which lies 340 kev above the ground state.

If one assumes that the deformation of Lu^{175} (Hf^{177}) is not radically altered by the addition of one neutron (removal of one proton), which seems likely in view of the total range of δ in the Table, a logical deformation for Lu^{176} seems to be $\delta = .275$. Furthermore considering the equality of the δ's of Lu^{175} and Lu^{175*} it seems a plausible assumption that the deformation parameter of Lu^{176m} is about the same as that of Lu^{176}.

Another way to estimate δ is by using the measured value of the quadrupole moment, Q, to determine the intrinsic quadrupole moment Q_o and δ from Eqs. (63), (64), and (65) (assuming $Q_c >> Q_p$). The values of δ resulting from this procedure are shown, for the Lu isotopes for which Q has been measured, in column 7 of Table 5. Two features stand out. First, the values of δ calculated from the measured Q's are consistantly larger than the values calculated by Mottelson and Nilsson. Secondly, that the δ's of Lu^{175}, Lu^{176}, and Lu^{177} are about the same while that of Lu^{176m} is considerably higher than any of the others. This seems to indicate that the addition (or removal) of one neutron to Lu^{176} has a much smaller effect on the nuclear shape than does the excitation of the intrinsic particle states of Lu^{176}, which produces Lu^{176m}. Therefore, since adding a neutron to Lu^{176} (which must necessarily enter the next available neutron energy state) would be expected to have an effect on the nuclear shape comparable to that of exciting a neutron in Lu^{176} to the same state, it is likely that an excited proton state constitutes the difference between the configuration of Lu^{176m} and the ground state of Lu^{176}.

Prediction of the Spin and Magnetic Moment of Lu^{176m}

Assuming that δ is greater than or equal to the value extrapolated from the Mottelson and Nilsson calculations ($\delta = .275$) several feasible assignments can be made, using the Nilsson Diagram,[22] for the odd neutron and proton configurations in Lu^{176m}. All these assignments lead to the proper value of I = 1 using the Gallagher and Moszkowski coupling rule GM 2 so that their validity must be judged in other ways. One other criterion of validity is the accuracy with which a calculation based on a given configuration can predict the measured magnetic dipole moment. Table 6 gives the feasible Nilsson asymptotic wave function assignments for Lu^{176m} together with the magnetic moments calculated on the basis of Eq. (67).

Table 6

Parity	Proton configuration	Neutron configuration	μ Calculated (n.m.)	μ exp.
A +	|514 + >	| 514 - >	2.65	.32
B -	|402 + >	| 514 - >	-1.25	
C -	|404 - >	| 512 + >	1.75	
D +	|404 - >	| 624 + >	-1.35	

From this Table, even though none of the assumed configurations seem to predict the moment very well, configuration C gives the right sign and is much closer in absolute value to the measured value than A. Hence on the basis of its ability to predict the magnetic moment C seems to be the most plausible configuration.

On the other hand, Gallagher and Moszkowski[24] have assigned configuration B because the neutron configuration is the same as that assigned to Hf^{177} while the proton configuration corresponds to that of Lu^{175*}. Furthermore assuming for the Lu^{176} ground state the configuration $p \rightarrow |404 - >$, $n \rightarrow |514 - >$ they predicted Lu^{176} to have a spin of 7 and a magnetic moment of 3.06 n.m. which agrees well with Spalding and Smith's[33] published values of I = 7, μ = 3.07 n.m. Moreover, if this assignment for Lu^{176} is assumed correct, then configuration C for Lu^{176m} indicates that a neutron state is excited which, as mentioned above, does not seem likely while configuration B implies an excited proton state, as expected. This lends further support to the Gallagher-Moszkowski assignment.

Summing up then, it seems that the spin of Lu^{176m} (as well as Lu^{176}) can be accounted for quite easily using the Collective Model but that the exact configuration leading to this spin remains vague. It is interesting to note that the measured magnetic moment is almost equal to the sum of those predicted by configurations B and C. This might imply that the actual asymptotic Nilsson state is a mixture of these two states.

VI. THE Br^{80} AND Br^{80m} EXPERIMENT

A. Introduction

The spins of Br^{80} and Br^{80m} have been measured by the atomic-beam method and the values $I(Br^{80}) = 1$ and $I(Br^{80m}) = 5$ have been reported. These measurements were made by Green at the L.R.L. atomic-beam laboratory using what has been referred to in Section IV A as machine no. 1. Both Green[34] and Lipworth[35] have given detailed descriptions of the experimental technique and equipment used for the carrying out of these spin measurements. Even though Green's methods have for the most part been carried over and used for the hyperfine structure measurements described below, for the sake of completeness a description is given in Sections B, C, and D of the entire experimental procedure utilized in these measurements. Special emphasis is given, however, to the discussion of apparatus and techniques which differ from those used by Green.

B. Isotope Production and Handling

Br^{80} and Br^{80m} used for these experiments were produced by bombarding 3-4 gm lots of KBr crystals with thermal neutrons. The KBr, which was incapsulated in pyrex before being sent to the pile, was irradiated in most cases in the Livermore Pool Type Reactor at Livermore, California, but for some of the later runs the General Electric Test Reactor at Vallacitos was used. The neutron flux in the Livermore reactor was about 5.1×10^{12} neutrons/cm^2 sec and the capsules were left in the pile for 3-4 hours, while the neutron flux in the Vallecitos reactor was 9×10^{13} neutrons/cm^2 sec and the capsules were left in this pile for only 20 minutes. After irradiation the samples were returned to L.R.L. by car (about a 1 hour trip from either pile) and a chemical separation of the Br undertaken.

Naturally occurring Br is 50.6% Br^{79} and 49.4% Br^{81} so that neutron irradiation produces Br^{80}, Br^{80m} and Br^{82} in accordance with the reactions:

$$Br^{79} + n \rightarrow Br^{80} + \gamma \text{ or } Br^{80m} + \gamma,$$

$$Br^{81} + n \rightarrow Br^{82} + \gamma .$$

Although Br^{79} and Br^{81} have almost equal total neutron capture cross sections, due to its relatively long half life, very little Br^{82} activity was actually produced during a 4 hr. neutron bombardment and practically

none was produced during a 20 minute bombardment. It was estimated, on the basis of full-beam decay data, that less than 10% of the Br activity after a four hour bombardment was attributable to Br^{82}. Upon arrival at L.R.L. the activity of the KBr capsules ranged anywhere from 2R./hr. at a distance of 1 ft., for 3-hour irradiations at Livermore, to 20 R./hr. at a distance of 1 ft., for 20-minute irradiations at Vallecitos.

The chemical procedure used to liberate the radioactive Br from its KBr compound, which was the same as that used by Green, was done remotely, using manipulators, inside of a lead shielded cave. The glassware used is shown schematically in Fig. 30 while Fig. 31 shows a photograph of the collection vial into which the Br passed during the course of the chemistry. This vial was ultimately attached to the discharge tube assembly of Fig. 32.

After a KBr capsule was introduced into the "chemistry cave" and removed from the protective aluminum capsule holder within which it was irradiated, it was broken and both the broken glass and the KBr crystals dropped into the reaction vessel shown in Fig. 30. Then the top assembly of the reaction vessel was inserted, its stopcock closed, the stopcock of the Br collection vial opened, and a small He flow initiated through the system by way of the He inlet shown in the figure. After the He had been allowed to flow for a while to drive any moisture that might be present out of the system, the collection vial was immersed in a liquid nitrogen bath and enough H_2SO_4 introduced into the reaction vile to cover, by about 1/2", all its solid contents. At this point small amounts of HBr, Br_2, and SO_2 gases were liberated, driven through the drying tube by the He flow, and finally condensed in the cold collection vial. After these gases ceased to be evolved a little H_2O_2 was introduced and molecular Br_2 was liberated by the reaction

$$2Br^- + H_2O_2 + 2H^+ \rightarrow Br^2 + 2H_2O \quad .$$

The Br_2 gas thus generated was driven down the drying tube and condensed in the collection vial. H_2O_2 continued to be added, slowly enough to avoid a violent reaction, until no more Br_2 was generated. The collection vial was then detached from the rest of the glassware and placed into an ice water bath to allow the volatile SO_2 and other contaminants to evaporate off, leaving almost pure liquid Br_2. Finally after closing its stopcock and inserting a glass plug in its side

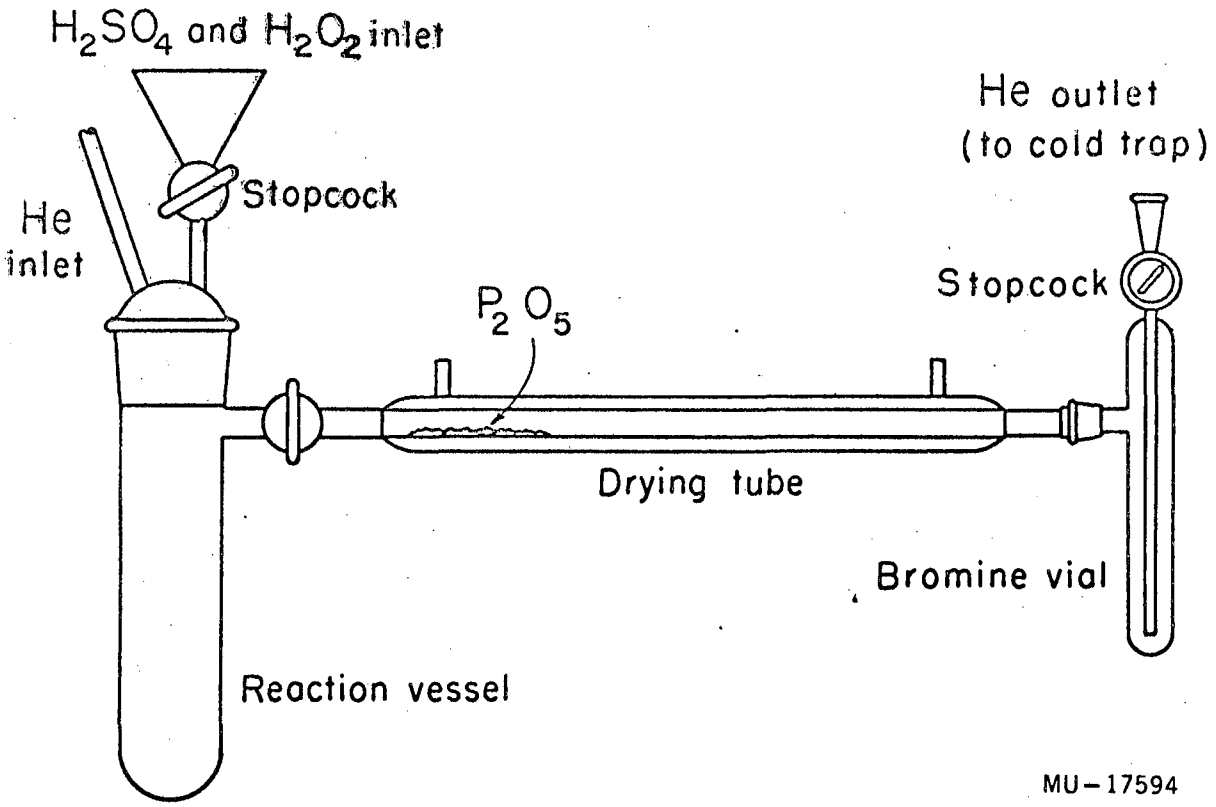

Fig. 27. Glassware used for Br chemistry.

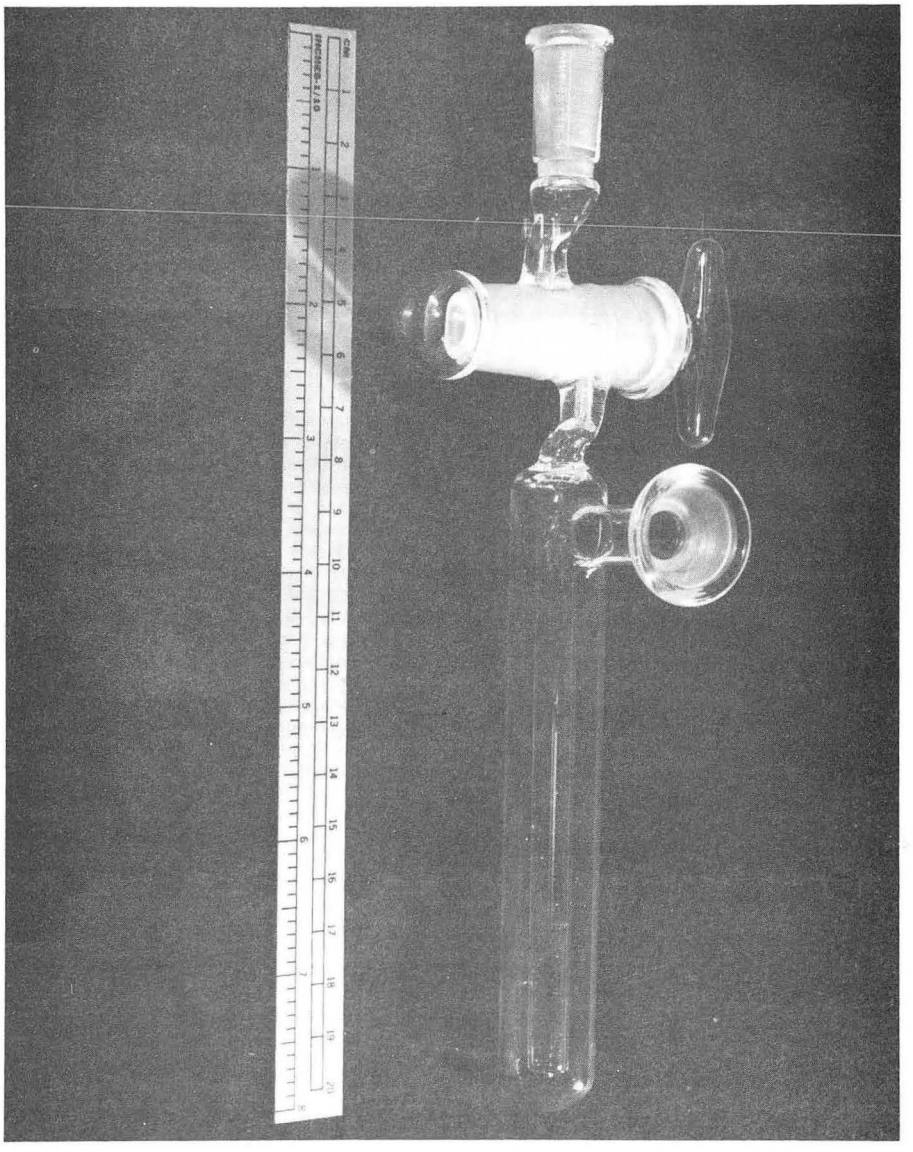

ZN-3402

Fig. 28. Photograph of Br collection vial.

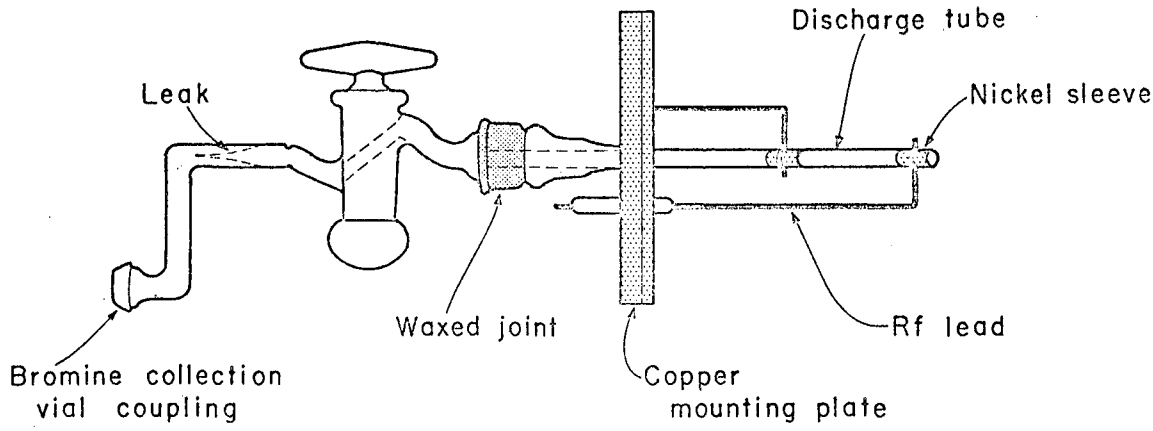

Fig. 29. R.F. dissociator tube assembly used for Br^{80} and Br^{80m}.

opening, the collection vile was put back into the liquid nitrogen bath.

After the Br_2 was completely frozen the collection vial was removed from the liquid nitrogen and quickly carried to the atomic-beam machine using an air-tight carrying case which was specially designed to avoid atmospheric contamination in case some of the Br_2 should re-evaporate in transit. Within the glove-box of the beam-machine the ground glass female coupling on the side of the collection vial was carefully joined to the matching male coupling on the pre-mounted discharge tube assembly of Fig. 32. Then, while in contact with dry ice, the interior of the vial was pumped down to less than 1 micron pressure by a small mechanical pump operating through its stopcock. Finally this stopcock was closed, an ice water bath substituted for the dry ice, and the stopcock on the discharge tube assembly opened to allow the Br_2 to effuse into the atomic-beam machine.

C. Beam Production and Characteristic

The discharge tube assembly served two purposes. First it helped control the Br effusion rate by means of a capillary leak, and second it provided a means of dissociating the Br_2 molecules into Br atoms as they entered the machine. It consists of two separable parts which are joined together during use. One part, which is used again and again, is just a brass plate with a hole through its middle over which has been placed a 19/38 female ground glass coupling. This plate, which is mounted on the atomic-beam machine during operation, also has attached to it two stainless steel wires, with only one of which it makes electrical contact. The other wire passes through the plate but is electrically insulated from it by means of a vacuum tight ceramic kovar. The other part of the assembly constitutes almost all the glassware shown in Fig. 32 and consists essentially of a ground glass coupling to accommodate the collection a leak, a stopcock, a 19/38 male ground glass fitting, and a quartz tube which has a slit in its end and is fitted with two aquadag painted, 3 mil nickel sleeves. Many identical copies of this part of the assembly were made and a new one was used for every run. The leaks which are mounted as shown in Fig. 32, are copies of the one used by Green[34] and discussed by Gordon.[36] They have effusion rates of about 0.3 cc. per hr. of liquid bromine when used as described here and were found to be very easily reproducible. The complete assembly of Fig. 32 is obtained by sealing together with black wax the female 19/38 ground glass coupling of one of its parts with the corresponding male ground glass coupling of the other. When this is done the stainless steel wires make a spring

electrical contact with the nickel sleeves and hence serve as input leads for the R.F. current.

The necessary dissociation of Br_2 molecules into Br atoms was accomplished by exciting an R.F. discharge in the Br vapor as it passed into the machine. This was done, in conjunction with the discharge tube assembly, by means of a 450 kc/sec resonant circuit operating through a Steinmetz Regulator. This Regulator, the circuit diagram of which is shown in Fig. 33, has the property that if its resonant frequency is made to equal the driving frequency (in this case 450 kc/sec) the current through the discharge tube is independent of the resistance of the tube. Therefore operated under these conditions it seemed as a very effective discharge stabilizer. With ordinary working pressure in the oven chamber (about 1×10^{-5} mm) 250 ma of R.F. current yielded 80-90% dissociation of Br_2 when the "hot lead" of the r.f. oscillator was capacitively coupled to the front (nearest the slit) end of the quartz discharge tube. If, on the other hand, the ground lead was coupled to the front, very poor ($\approx$ 40%) dissociation resulted.

By keeping the liquid Br within the collection tube at ice water temperature and allowing it to effuse into the discharge tube through a leak, as described above, usable beams of Br atoms were obtained for periods ranging from 5 to 8 hrs., depending on the size slit used in the end of the discharge tube. Slit widths ranging from 5 mils to 10 mils were tried and a width of 7 mils seemed to yield the most satisfactory compromise between beam intensity and beam lifetime. Using 7 mil discharge tube slits two minute full-beam exposure counting rates of from 700 c/m to 1500 c/m were obtained depending on the activity level of particular source used.

For earlier runs the Br beam was collected on freshly silver plated stainless steel "buttons" of the type shown in Fig. 16. Although these buttons were kept under vacuum when not in use and much care was taken to avoid contaminating them with radioactivity before exposure to the beam, during their use considerable inconsistency was apparent in the experimental data. This inconsistency was attributed to variations in Br collection efficiency among the various buttons due possibly to differences in the quantity and quality of the silver plate and to the presence of foreign substances, such as oil, upon the silver surface. For later runs, therefore, the Br beam was collected on fired platinum foils, just as in the case of Lu. Even though the Br collection efficiency of these foils was only about 80% that of the best silver surfaces used,

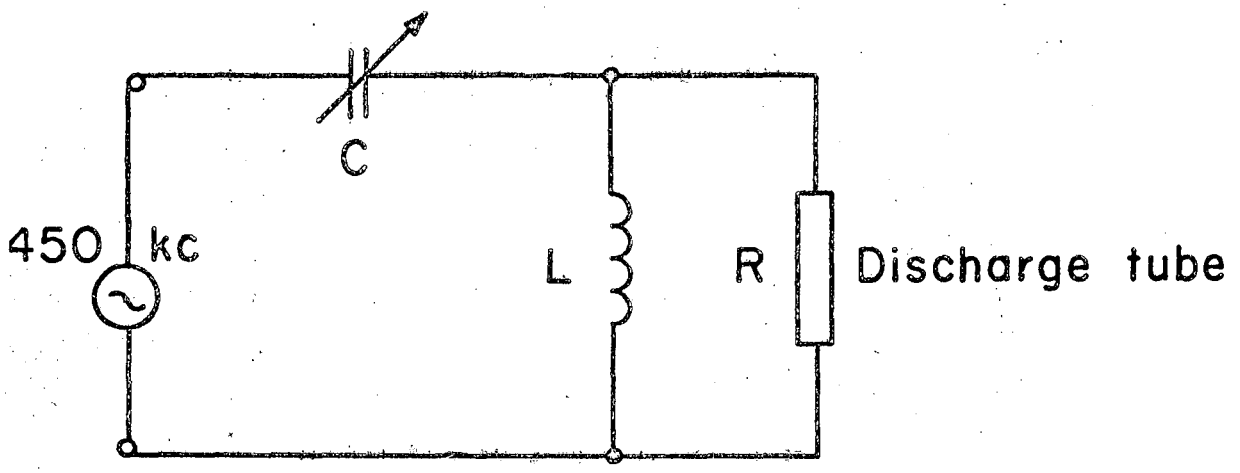

Fig. 30. Steinmetz regulator circuit diagram.

this difference was more than made up by the resulting gain in collection consistency.

D. Operating Procedure

After a usable Br atomic beam had been obtained, little attention was paid to its maintenance. Usually about a 15 minute wait was necessary, immediately after opening the bromine collection vial to the oven chamber, to allow a few tenth of a m.m. pressure to be established in the discharge tube. It was found that at least this low a pressure was necessary to obtain a stable discharge. After a pressure of about 1×10^{-5} mm was registered on the oven ion gauge (indicating that the proper pressure in the discharge tube had been attained) the 450 kc/sec dissociation oscillator was turned on and the discharge tube lined up by sighting with a telescope on its slit using the light given off by the R.F. discharge for illumination. Then a direct beam exposure was taken to make sure that the Br_2 molecules entering the machine were being satisfactorily dissociated and if the dissociation efficiency was normal the throw-out was usually about .80 when A and B magnet currents indicated by the expressions of Section IV D were used. Finally, if all went well, resonance searches were undertaken. The necessary resonance exposure time was determined by insisting that the resonance peak counting rate, which always was equal to about 1/2% of the full-beam counting rate, be greater than 10 counts/minute. Exposure times were usually for 5 minutes although occassionally 7 1/2 minute or even 10 minute exposure times were necessary.

Figure 34 gives the radioactive decay schemes[28] of Br^{80} and Br^{80m}. It is seen that 4.5 hr. Br^{80m} decays by γ emission to Br^{80} which in turn decays, with an 18 minute half life, by β emission to Kr^{80} and Se^{80}. Since the proportional β particle counters used to detect the presence of Br^{80} and Br^{80m} are quite insensitive to γ radiation, Br^{80m} was actually detected by noting the β activity from the Br^{80} produced by its decay. For this reason Br^{80m} resonance buttons were expected to exhibit low counting rates when first removed from the beam machine (that is, when there is no Br^{80} present), to increase in counting rate with the formation of Br^{80} until secular equilibrium is established between the quantities of Br^{80} and Br^{80m} present, and finally to decay with a characteristic 4.5 hr. half life. On the other hand, Br^{80} resonance buttons were expected to exhibit their largest counting rates immediately upon removal from the beam machine and to decay rapidly with a characteristic 18 minute half life. Because of the above considerations care had to be taken to insure that the time which elapsed between the

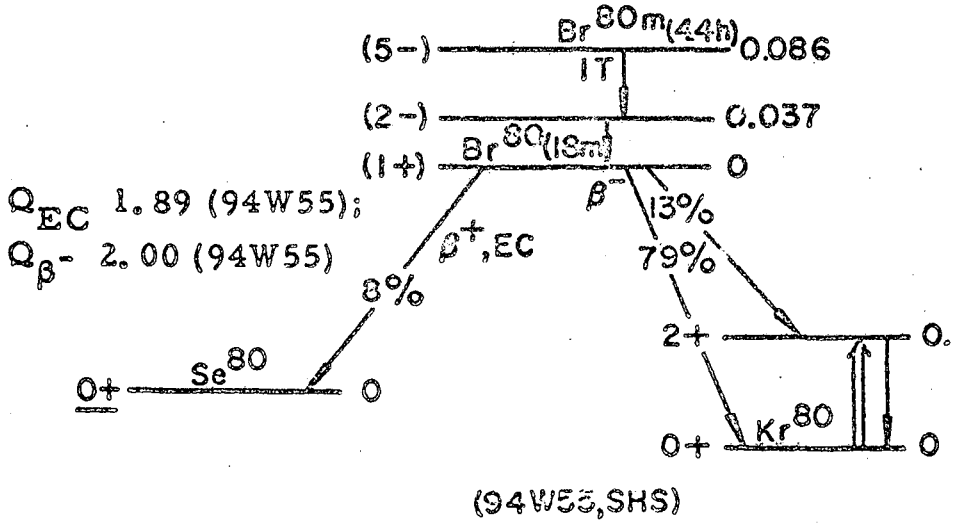

MU-17590

Fig. 31. Radioactive decay schemes of Br^{80} and Br^{80m}.

removal of exposed buttons from the atomic-beam and their insertion into the β counters as well as their total time counted were held constant for all buttons during any given resonance search.

E. Hyperfine Structure Determination; Data and Results

Prior to the redesigning of machine no. 1, ten $\Delta F = 0$ resonances were observed for both Br^{80} and Br^{80m} at fields ranging from 0-93 gauss. Using shifts from linear Zeeman predictions estimates of "a" and "b" were made for both isotopes and using "Hyperfine"[7] a fit of the experimental data was obtained in both cases assuming normal ordering of the hyperfine levels. It was thus established that the observable α and β, $\Delta F = 0$ transitions envolve the levels

for Br^{80}		for Br^{80m}
$\alpha = (5/2, -1/2) \leftrightarrow (5/2, -3/2)$	and	$\alpha = (13/2, -9/2) \leftrightarrow (13/2, -11/2)$
$\beta = (3/2, 1/2) \leftrightarrow (3/2, -1/2)$		$\beta = (11/2, -7/2) \leftrightarrow (11/2, -9/2)$

where $g_I > 0$ for both Br^{80} and Br^{80m} has been assumed. These observable transitions are indicated in the schematic energy level diagrams of Figs. 21(b) and 35 for Br^{80} ($I = 1$, $J = 3/2$) and Br^{80m} ($I = 5$, $J = 3/2$).

After these twenty resonances had been observed, machine no. 1 broke down and all subsequent work was done using machine no. 2.

When machine no. 2 became operative and the method of coping with the R.F. powering problem discussed in Section IV F found, the first task undertaken was to retrace some of the highest field resonances previously observed using machine no. 1. Four lines were retraced for both Br^{80} and Br^{80m} and "Hyperfine" was then used, in conjunction with "JO-9", to predict the frequencies of higher field resonances. In Fig. 36 and Fig. 37 one of the resonance lines obtained using machine no. 1 is compared with the corresponding line obtained using machine no. 2 for the cases of Br^{80} and Br^{80m} respectively. After this preliminary work was completed, resonances and resonance frequency predictions were obtained at higher and higher fields until a total of 15, $\Delta F = 0$ resonances had been observed in both Br^{80} and Br^{80m} at fields ranging from 0 - 504.3 gauss. Examples of some higher field resonance curves are given in Figs. 38 and 39 for Br^{80} and Br^{80m} respectively. In Tables 7 and 8 all the resonance data obtained for Br^{80} and Br^{80m} are collected. In cases where a single line was traced out on both machines only the data collected on machine no. 2 are included. Also given in the tables

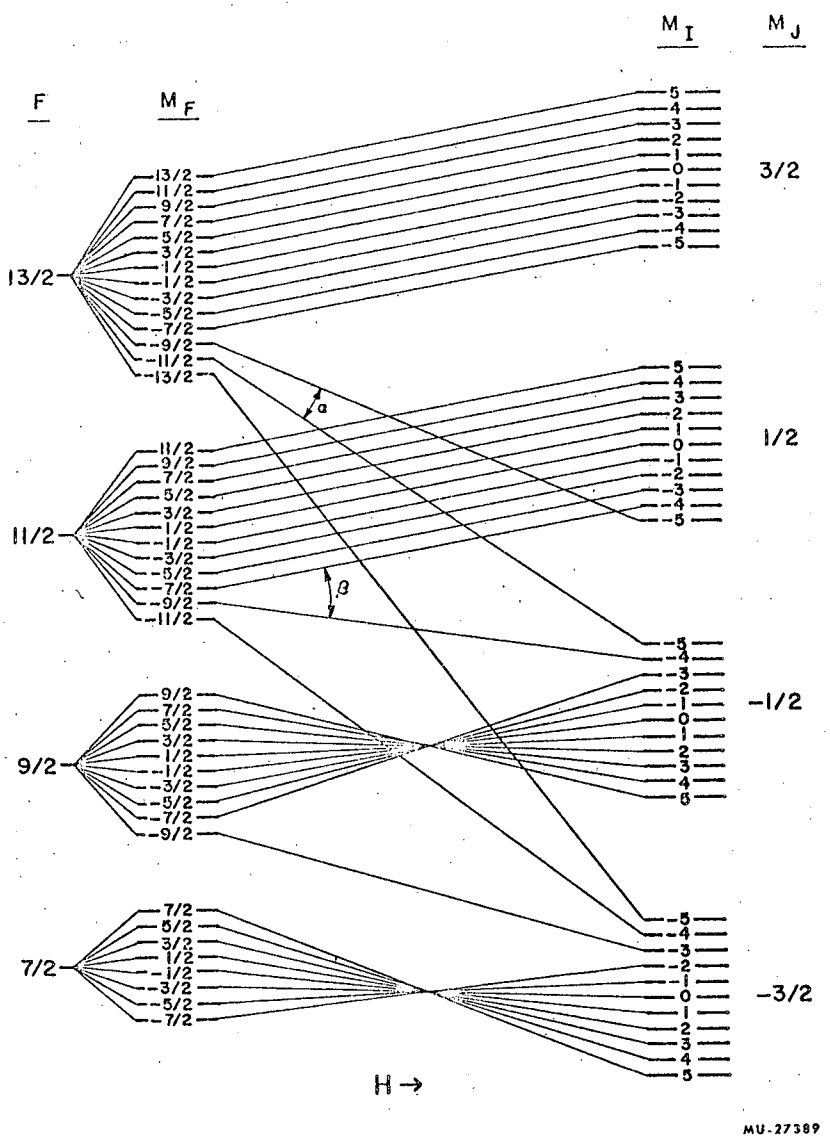

Fig. 32. Schematic energy level diagram for J = 3/2, I = 5 (normal ordering).

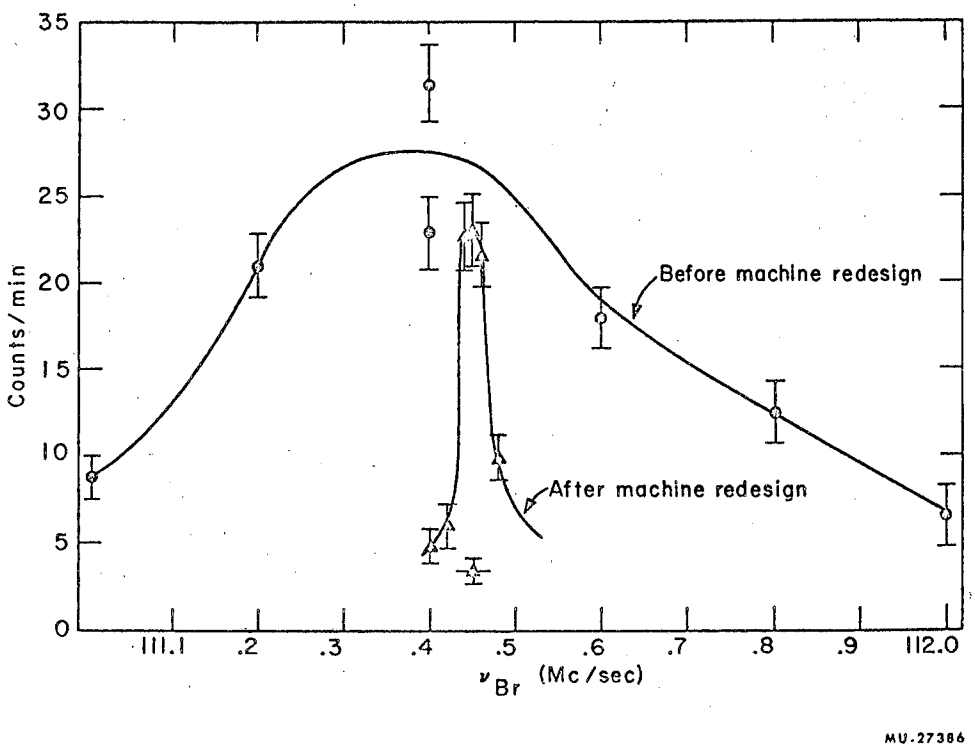

Fig. 33. Br^{80} α resonance curve as it appeared before and after the redesigning of machine no. 1 (ν_K = 100.0 Mc/sec).

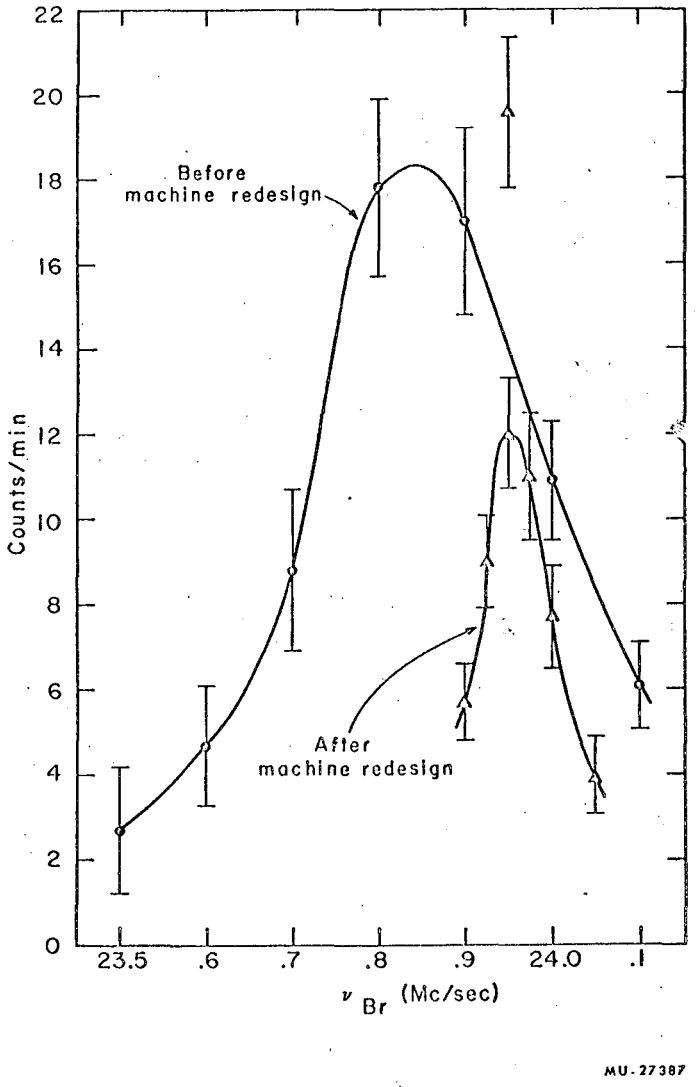

Fig. 34. Br^{80m} β resonance curve as it appeared before and after the redesigning of machine no. 1 (ν_K = 100.0 Mc/sec).

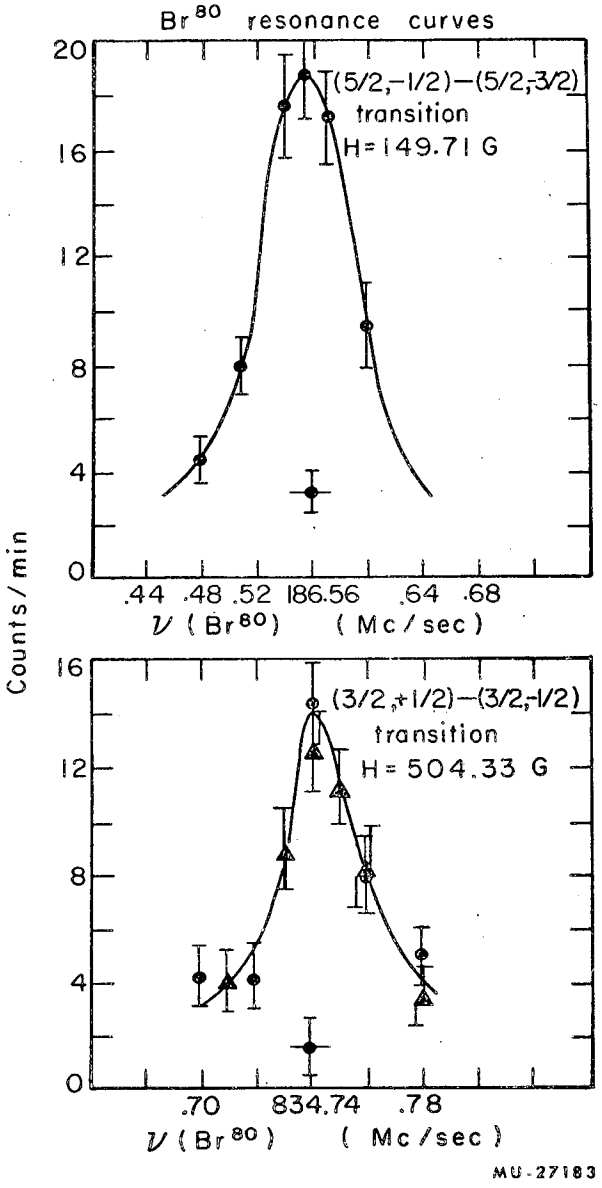
Br 80 resonance curves
(5/2,-1/2)—(5/2,-3/2)
transition
H=149.71 G
Counts / min
20
16
12
8
4
0
.44 .48 .52 186.56 .64 .68
ν (Br 80) (Mc / sec)
(3/2,+1/2)—(3/2,-1/2)
transition
H = 504.33 G
16
12
8
4
0
.70 834.74 .78
ν (Br 80) (Mc / sec)
MU-27183

Fig. 35.

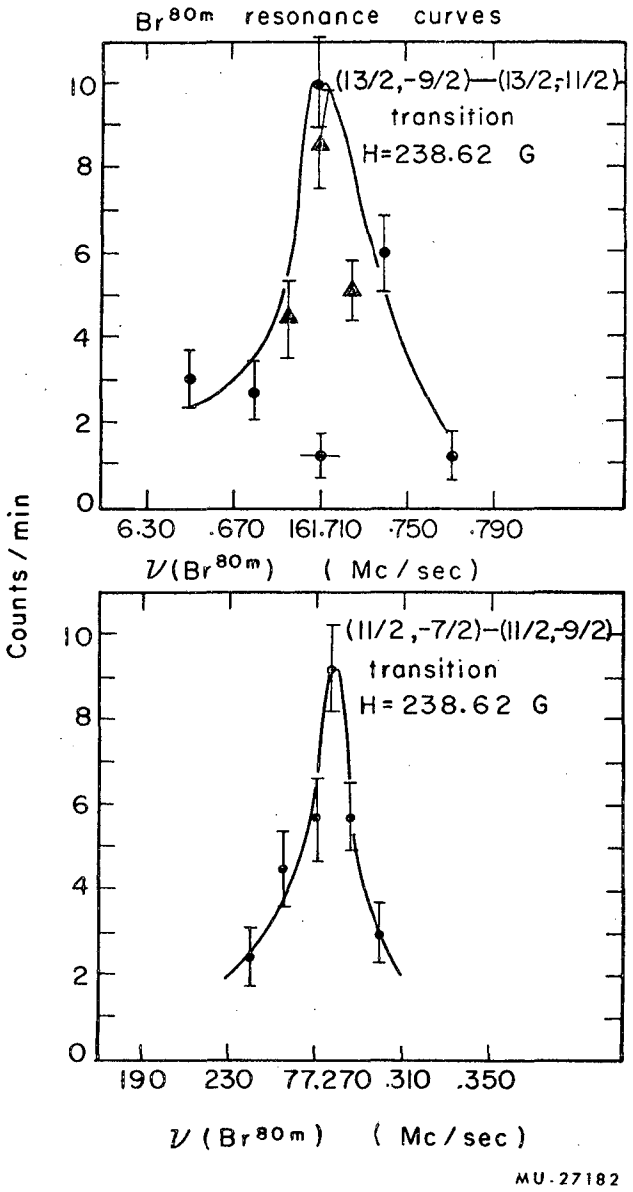
Br80m resonance curves
(13/2,-9/2)—(13/2,-11/2)
transition
H=238.62 G
Counts / min
10
8
6
4
2
0
6.30
.670
161.710
.750
.790
ν(Br80m) (Mc / sec)
(11/2,-7/2)—(11/2,-9/2)
transition
H=238.62 G
190
230
77.270
.310
.350
ν (Br80m) (Mc/sec)
MU-27182

Fig. 36.

Table 7 . Br^{80} Resonance Data and Final Hyperfine Output

A.		B.	
$g_I > 0$		$g_I < 0$	
a = 323.77 ± .08 mc/sec	$\chi^2 = 2.2$	a = -324.01 ± .08 mc/sec	$\chi^2 = 2.1$
b = 227.63 ± .03 mc/sec		b = 227.60 ± .03 mc/sec	

Average of A and B

Sign of g_I is not determined.

$|a| = 323.9 \pm .2$ mc/sec b/a < 0

$|b| = 227.62 \pm .05$ mc/sec

Run No.	ν_K mc/sec	H gauss	ΔH gauss	ν_{Br} mc/sec	$\Delta\nu_{Br}$ mc/sec	Residual mc/sec A	Residual mc/sec B	F_1	M_1	F_2	M_2	Weight factor
1	4.0	5.567	.005	6.275	.060	.015	.014	5/2	-1/2	5/2	-3/2	274.9
2	16.0	20.75	.01	23.650	.067	.057	.051	5/2	-1/2	5/2	-3/2	217.0
3	25.0	30.92	.01	35.400	.067	-.010	-.018	5/2	-1/2	5/2	-3/2	215.1
4	50.0	55.19	.01	64.338	.015	.013	.001	5/2	-1/2	5/2	-3/2	2084.3
5	100.0	93.04	.01	111.450	.015	.004	-.011	5/2	-1/2	5/2	-3/2	2584.7
6	4.0	5.567	.005	7.620	067	-.001	-.002	3/2	1/2	3/2	-1/2	220.1
7	16.0	20.75	.01	28.400	.083	-.032	-.037	3/2	1/2	3/2	-1/2	141.7
8	25.0	30.92	.01	42.400	.033	.033	-.004	3/2	1/2	3/2	-1/2	763.6
9	50.0	55.19	.01	75.938	.015	.007	-.005	3/2	1/2	3/2	-1/2	1786.7
10	100.0	93.04	.01	129.145	.015	.005	-.013	3/2	1/2	3/2	-1/2	2345.0
11	200.0	149.71	.01	186.555	.015	.008	-.002	5/2	-1/2	5/2	-3/2	1926.8
12	400.0	238.621	.008	314.238	.020	-.005	.003	5/2	-1/2	5/2	-3/2	1816.0
13	200.0	149.71	.01	212.010	.020	.010	-.014	3/2	1/2	3/2	-1/2	1327.3
14	400.0	238.621	.008	352.270	.020	.015	-.009	3/2	1/2	3/2	-1/2	1712.1
15	1100.0	504.329	.007	834.740	.015	-.004	.003	3/2	1/2	3/2	-1/2	2372.2

Table 8 . Br^{80m} Resonance Data and Final Hyperfine Output

$a = 166.047 \pm .009$ mc/sec

$b = -874.9 \pm .1$ mc/sec $\quad \chi^2 = 4.7$

$g_I > 0$

Run No.	ν_K mc/sec	H gauss	ΔH gauss	ν_{Br} mc/sec	$\Delta\nu_{Br}$ mc/sec	Residual mc/sec	F_1	M_1	F_2	M_2	Weight factor
1	4.0	5.57	.03	2.400	.025	-.029	13/2	-9/2	13/2	-11/2	1300.4
2	8.0	10.87	.03	4.800	.020	.000	13/2	-9/2	13/2	-11/2	1860.9
3	16.0	20.75	.05	9.400	.025	.016	13/2	-9/2	13/2	-11/2	886.5
4	32.0	38.24	.03	18.000	.020	-.007	13/2	-9/2	13/2	-11/2	1556.1
5	70.0	71.63	.01	36.375	.015	.006	13/2	-9/2	13/2	-11/2	3685.8
6	8.0	10.87	.03	2.700	.020	.003	11/2	-7/2	11/2	-9/2	2265.4
7	16.0	20.75	.05	5.200	.025	.039	11/2	-7/2	11/2	-9/2	1307.8
8	32.0	38.23	.02	9.500	.015	-.001	11/2	-7/2	11/2	-9/2	4170.8
9	70.0	71.63	.01	18.150	.015	-.006	11/2	-7/2	11/2	-9/2	4266.5
10	100.0	93.044	.009	23.950	.012	-.005	11/2	-7/2	11/2	-9/2	6677.3
11	200.0	149.714	.008	88.838	.023	.013	13/2	-9/2	13/2	-11/2	1783.7
12	400.0	238.62	.01	161.710	.010	-.002	13/2	-9/2	13/2	-11/2	4574.2
13	200.0	149.71	.01	41.235	.015	-.001	11/2	-7/2	11/2	-9/2	4229.6
14	399.988	238.62	.02	77.277	.010	.009	11/2	-7/2	11/2	-9/2	6178.9
15	1100.0	504.329	.007	284.610	.015	-.002	11/2	-7/2	11/2	-9/2	3306.6

are the values of "a" and "b" determined by "Hyperfine" as the ones which best fit the experimental data as well as the errors assigned to these parameters. Since g_I and g_J are known with such great accuracy[37,38] for Br^{79} and Br^{81} only the a's and b's were allowed to vary freely by "Hyperfine," the g_I's being determined by Eq. (26).

Final Results for Br^{80m}:

In view of the small residuals and the small value of $\chi^2 = 4.7$ (compared to an acceptable $\chi^2 = 12$) given in Table 8, the experimental errors in the best values of "a" and "b", given there, are probably pessimistic. However to be very sure that the actual values lie within the quoted errors, twice these error assignments are used and the final values given are

$$a = 166.05 \pm .02 \text{ mc/sec}$$

$$b = -874.9 \pm .2 \text{ mc/sec} \quad .$$

Also using the equations of Appendix C the hyperfine structure separations are

$$\nu_{13/2,\ 11/2} = 13/2\ a + 13/20\ b = (510.62 \pm .25) \text{ mc/sec}$$

$$\nu_{11/2,9/2} = 11/2\ a - 5/12\ b = (1277.80 \pm .18) \text{ mc/sec} \quad .$$

The algebraic signs of a and b given above hold on the assumption that g_I' (Br^{80m}) is positive. That this is the case was established (as for Lu^{176m}) both by trying to fit the data using a negative g_I' in conjunction with the Fermi-Segre Formula and by starting g_I' with a negative value and then allowing it to vary freely while trying to fit the experimental data. In the first case a value of $\chi^2 = 50.9$ was obtained as compared to $\chi^2 = 4.7$ assuming g_I' positive. In the second case a positive value of g_I' consistent with the Fermi-Segre Formula was converged upon by "Hyperfine."

Final Results for Br^{80}:

As in the case of Br^{80m} the small residuals and χ^2 value shown in Table 7 indicate that the frequency error assignments quoted there are pessimistic and that the errors given for a and b by "Hyperfine" are probably too large. However in the case of Br^{80} we have an interesting case where two different "a" values, one associated with a positive g_I and the other associated with a negative g_I, lead to equally good fits of the experimental data. It is seen from the table that the "a" and "b" values associated

with positive g_I (grouped under heading A) and the corresponding parameters associated with negative g_I (grouped under heading B) lead to frequency residuals of about the same magnitude and have associated with them χ^2 values of 2.2 and 2.1 respectively. Therefore the sign of g_I cannot be decided upon, using the data presently available. However, as indicated in Section G below, this sign is very likely positive.

Taking the average values of a and b given in the table and doubling the assigned errors we have for Br^{80}

$$|a(Br^{80})| = 323.9 \pm .4 \text{ mc/sec}$$
$$|b(Br^{80})| = 227.62 \pm .10 \text{ mc/sec}$$
$$a/b < 0$$

and again using the equations of Appendix C

$$|\Delta \nu_{5/2,3/2}| = 5/2\ a + 5/4\ b = 525.2 \pm 1.2 \text{ Mc/sec}$$

$$|\Delta \nu_{3/2,1/2}| = 3/2\ a - 9/4\ b = 998.0 \pm 1.0 \text{ Mc/sec}$$

F. Calculation of the Nuclear Moments

Nuclear Magnetic Dipole Moment:

Using the bromine data collected in Appendix A and the magnetic dipole interaction constants given above, Eq. (26) yields for the uncorrected magnetic dipole moments of Br^{80} and Br^{80m}

$$\mu(Br^{80}) = \pm 0.4905\ (6) \text{ nm} \quad \text{(uncorrected)}$$
$$\mu(Br^{80m}) = 1.2573\ (6) \text{ nm} \quad \text{(uncorrected)} .$$

Multiplying by the appropriate diamagnetic shielding factor of Appendix B gives for the final corrected values

$$\mu(Br^{80}) = \pm 0.5138\ (6) \text{ nm (corrected)}$$
$$\mu(Br^{80m}) = 1.3170\ (6) \text{ nm (corrected)} .$$

Furthermore, in the case of Br^{80m}, allowing g_I to vary freely during fitting of the experimental resonance data by "Hyperfine" led directly to

$$\mu(Br^{80m}) = 1.2(2) \text{ nm} \quad \text{(uncorrected)}$$

which is consistent with the above result.

Though almost pure L-S coupling is indicated for Br by the known g_J value[37], no measurements have been made of the hyperfine interaction

constants in the excited $^2P_{1/2}$ state for any of the Br isotopes. Hence the presence of configuration mixing cannot be established (or ruled out) by the method employed for Lu in Section V and therefore a good test for the applicability of Eq. (28) to the case of bromine is not available. As indicated in Section VII, configuration mixing of the type discussed by Koster[39] seems to be definitely present in the case of iodine (Z = 53). However, since the effect of such mixing seems to increase with increasing Z, it is possible, as suggested by King and Jaccarino[37], that this effect is negligible in the case of bromine (Z = 35). If this is assumed to be the case and the experimentally determined "a" values given above are used in conjunction with $Z_1 = 31$ (recommended by Barnes and Smith[40]) Eq. (28) yields

$$\mu\,(Br^{80})_{calc.} = \pm .471 \text{ nm} \quad \text{(uncorrected)}$$

$$\mu\,(Br^{80m})_{calc.} = 1.21 \text{ nm} \quad \text{(uncorrected)} .$$

The fact that these results agree quite well with those obtained above using Eq. (26) implies that ignoring configuration interaction in the case of bromine is fairly well justified. Inverting Eq. (28), after inserting the correct μ values, leads to $Z_1 = 32.3$ for both Br^{80} and Br^{80m}. This value is employed for determination of the Relativistic Correction Factors used in the calculation of Q below.

Nuclear Electric Quadrupole Moment:

When the measured "a" and "b" values for Br^{80} and Br^{80m} are inserted into Eq. (25) along with the magnetic moments of these isotopes (as calculated using Eq. (26)), the following electric quadrupole moments are obtained

$$Q(Br^{80}) = \pm 0.182\ (8) \text{ barns} \quad \text{(uncorrected)}$$

$$Q(Br^{80m}) = 0.70\ (3) \text{ barns} \quad \text{(uncorrected)} .$$

A 4% error is assigned in both cases. This assignment seems logical when the uncertainties in the a's and b's and in Z_1 are compounded with the probable maximum error introduced by ignoring the possibility of configuration interaction and other perturbations.

The absolute algebraic signs of the Br^{80} nuclear moments are not known since the algebraic signs of "a" and "b" were not determined by the experiment described above. However, it was established that

$a(Br^{80})/b(Br^{80}) < 0$ which, on the basis of Eqs. (23) and (24) implies that $\mu(Br^{80})/Q(Br^{80}) > 0$. Furthermore, the discussion of Section G indicates that both these moments are probably positive.

G. Discussion of Br^{80} and Br^{80m} Nuclear Moment Results

Application of the Shell Model:

Mayer and Jensen[15] have predicted, using the Single Particle Shell Model, a $[(f_{5/2})^4 (2p_{3/2})^3]_{3/2}$ configuration for the last odd proton in odd-even bromine isotopes. This prediction is well born out by the measured 3/2 spins and positive quadrupole moments of Br^{79} and Br^{81} as[37] well as by the 3/2 spin measured[34] for Br^{77}. On the basis of the Shell Model this same proton configuration would also be expected to hold for the odd-odd isotopes of Br.

The neutron configurations for odd-odd Br isotopes are not as clearly indicated. Straight forward application of the Single Particle Shell Model would, for example, assign the last odd neutron of Br^{76}, Br^{80}, Br^{80m}, and Br^{82} to a $(1g_{9/2})$ orbital and would predict the same spin for all these isotopes. Actually the measured spins are 1, 1, 5 and 5 respectively. Furthermore other nuclear properties, such as values of nuclear moments and parities of nuclear states, also do not seem compatable with the straightforward single particle approach.

Table 9 gives the spins[28] and expected configurations[15] of some even-odd isotopes with neutron numbers, N, lying between 40 and 50. These nuclides have their outermost neutrons lying in the $(1g_{9/2})$ subshell and would thus be expected to exhibit neutron configurations accessible to the odd-odd Br isotopes. In the table each configuration is assigned a number for the sake of discussion. In the case of Se^{175}, which according to Aamodt and Fletcher[41] exhibits several equally plausible configurations compatible with its spin and nuclear moment values, all the plausible configurations are given in the table. It seems logical to assume that only those configurations which have been observed in even-odd isotopes having neutrons in the $(1g_{9/2})$ subshell (i.e. the configurations of Table 9) are likely to occur in Br^{80} or Br^{80m}.

Table 9

Number	Name	N	Neutron Configuration	Spin
1	Ge^{73}	41	$(g_{9/2})^1_{9/2}$	9/2
2	Se^{75}	41	$[(p_{1/2})(g_{9/2})^2]_{5/2}$	5/2
3	Se^{75}	41	$[(g_{9/2})^3]_{5/2}$	5/2
4	Se^{75}	41	$[(f_{5/2})^5]_{5/2}$	5/2
5	Se^{77}	43	$[(p_{1/2})^1(g_{9/2})^4]_{1/2}$	1/2
6	Se^{79}	45	$[(p_{1/2})^0(g_{9/2})^7]_{7/2}$	7/2
7	Kr^{83}	47	$[(g_{9/2})^7]_{9/2}$	9/2
8	Kr^{85}	49	$[(g_{9/2})^{-1}]_{9/2}$	9/2
9	Sr^{87}	49	$[(g_{9/2})^{-1}]_{9/2}$	9/2

Configuration Assignment for Br^{80}:

Assuming a $[(f_{5/2})^4(p_{3/2})^3]_{3/2}$ configuration for the 35th proton, the proton angular momentum, J_p, should equal 3/2. Therefore, since the measured spin of Br^{80} is 1, the total neutron angular momentum must be 1/2, 3/2, or 5/2. However, since none of the configurations of Table 9 lead to $J_n = 3/2$ we eliminate this as a possibility and only consider configurations leading to $J_n = 5/2$ and 1/2.

Aamodt and Fletcher[41] calculated the expected magnetic dipole moment, μ, for Se^{75} (which is the only isotope of Table 9 having I = 5/2) by basing their calculations on each of the configurations nos. 2-4. Taking the results of any of these calculations as the expected neutron contribution to the magnetic moment of Br^{80} and calculating the electric quadrupole moment of Br^{80} based on the corresponding configuration, one always arrives at the conclusion that the μ and Q of Br^{80} have opposite signs. This result is contrary to experiment and hence makes any of these configurations seem unlikely.

On the other hand, calculations based on configuration no. 5 lead to the values

$$\mu\ (Br^{80}) = 2.84 \text{ nm}$$

$$Q(Br^{80}) = +\ .03 \text{ barns}$$

if a proton contribution to the magnetic moment given by Eq. (53) is used in conjunction with a neutron contribution based on the μ of Se^{77}. If a proton contribution based on the average μ of Br^{79} and Br^{81} is used the values

$$\mu(Br^{80}) = 1.84 \text{ nm}$$

$$Q(Br^{80}) = .03 \text{ barns}$$

are obtained.

Hence although not predicting their absolute values very well, configuration no. 5 at least leads to the correct relative signs of $\mu(Br^{80})$ and $Q(Br^{80})$. In addition this configuration, in conjunction with the proton configuration given above, leads to the known[28] (positive) parity of Br^{80} and correctly predicts its spin upon application of Nordheim's Strong Rule. Therefore the neutron configuration $\left[(p_{1/2})^1(g_{9/2})^4\right]_{1/2}$ seems most likely for Br^{80}.

Configuration Assignment for Br^{80m}:

Again assuming that $J_p = 3/2$ we must now have $J_n = 7/2$, $9/2$, $11/2$, or $13/2$, since the spin of Br^{80m} is 5. None of the configurations of Table 9 lead to a spin of $11/2$ or $13/2$ so we restrict our consideration to $J_n = 7/2$ and $9/2$. On the basis of the Single Particle Shell Model (and on the basis of Table 9) $J_n = 9/2$ would seem most likely. However, a calculation of $Q(Br^{80m})$ assuming $J_n = 9/2$, always leads to a negative value. This makes $J_n = 9/2$ seem unlikely, since the Shell Model is usually quite successful in predicting the signs of quadrupole moments. Calculating $Q(Br^{80m})$ and $\mu(Br^{80m})$ assuming configurations no. 6, however, leads to the values

$$\mu(Br^{80m}) = 1.2 \text{ n.m.}$$

$$Q(Br^{80m}) = .20 \text{ barns} \quad ,$$

using effective nucleon gyromagnetic ratios.

Hence the calculated $\mu(Br^{80m})$ agrees quite well with the measured value while $Q(Br^{80m})$, although too low is in absolute value, has the right sign. For this reason, together with the fact that this configuration leads to the known (negative) parity of Br^{80m} and to the correct spin (using the Brennan and Bernstein coupling rule no. BB1), we assign the configuration $\left[(p_{1/2})^0(g_{9/2})^7\right]_{7/2}$ to the neutrons in Br^{80m}.

General Discussion:

Some known data pertaining to the odd-odd isotopes of Br as well as data pertaining to related even-odd isotopes of Se are[28] given in Table 10.

Table 10

Neutron Configuration	Even-odd Nuclide	I	μ (n.m.)	Q (barns)	Odd-odd Nuclide	I	μ (n.m.)	Q (barns)
4	Se^{75}	5/2	(0)	+1.1	Br^{76}	1	(-.55)	(+.27)
5	Se^{77}	1/2	+.53	<.002	Br^{80}	1	(+.51)	(+.20)
6	Se^{79}	7/2	-1.02	+0.9	Br^{80m}	5	+1.3	+.75
6	Se^{79}	7/2	-1.02	+0.9	Br^{82}	5	(+1.63)	(+.76)

The results for Br^{76} and Br^{82} were obtained by Green, Lipworth, Garwin and Nierenberg[42,43] and the neutron configurations for these isotopes were also assigned by these authors. In the cases of Br^{76}, Br^{82}, and Br^{80} the relative signs of μ and Q have been well established but the actual signs given in the table, although the most likely on the basis of the data collected, are not definitely known. From this table the correspondences between a given Se isotope and the Br isotopes which has the same neutron configuration is quite clear. Two points are particularly noteworthy of mention.

(a) There is apparently a one-to-one correspondence in the order of the neutron level filling in Se and in Br. This indicates, as predicted by the Shell Model[15], that the presence of the odd proton configuration (even if this has associated with it a non-zero net angular momentum) has little effect on the neutron configuration.

(b) The difference in the sign of the magnetic moment (or at least relative signs of μ and Q) of Br^{76} and Br^{80}, which at first sight seems surprising because of the other similarities of these isotopes (i.e. $I(Br^{76}) = I(Br^{80})$; $\mu(Br^{76}) \cong \mu(Br^{80})$; $Q(Br^{76}) \cong Q(Br^{80})$)is reflected by a similar difference between Se^{77} and Se^{75}, and is apparently due to radically differing neutron configurations.

Also the systematic trends in Table 10 seem to support the configuration assignments and signs of nuclear moments given above for Br^{80} and Br^{80m} as well as those given for the other Br isotopes by other authors. In particular the positive signs of μ and Q for Br^{82} seem very likely in view of the similarity exhibited between this isotope and Br^{80m}.

Application of the Collective Model:

Although, as shown above, the Shell Model description of Br^{80} and Br^{80m} can account quite well for the spins and relative signs of the nuclear moments, this model does not give a satisfactory quantitative result for the nuclear magnetic dipole moment of Br^{80}. Furthermore the fact that the Shell Model estimates of the electric quadrupole moments of both Br^{80} and Br^{80m} are considerably lower than the measured values implies that collective properties might play a significant role in the nature of these nuclides, even though their mass number of A = 80 lies far outside the range $150 < A < 190$ where collective effects are expected to be important.[23] This was, in fact, found to be true in the case[43] of Br^{79} so we should not be surprised to find it also true in the cases of Br^{80} and Br^{80m}.

Determining the Deformation Parameter:

No theoretical calculations have been made to determine the deformation parameter, δ, for nuclides with mass numbers in the neighborhood of A = 80. Therefore we must rely on the measured value of Q to determine this parameter. Using Eqs. (62)-(65) in conjunction with the measured values of Q for Br^{80} and Br^{80m} (and assuming the intrinsic single particle contribution that the Q's to be insignificant compared to the contribution from collective motion) the following values of δ are obtained

$$\delta\ (Br^{80}) = .24$$
$$\delta\ (Br^{80m}) = .12 \ .$$

To these we add the value of δ calculated for Br^{76} by Lipworth et al.[42]

$$\delta\ (Br^{76}) = .31 \ .$$

The apparent inconcistency of these values, as opp sed to the almost constant values of δ found in the mass range $150 < A < 190$, suggests that collective aspects of the nucleus are not well defined in the mass range near A = 80 and that the assumptions underlying the above calculations of δ are perhaps not too well founded.[23]

Prediction of the Spins and Magnetic Dipole Moments of Br^{80} and Br^{80m}:

If we accept any value in the range $.1 < \delta < .3$ as a possible value of δ, the plausible proton and neutron configurations for Br^{80} and Br^{80m} are given in Table 11.

Table 11

	Nilsson Number	Ω n	Ωp	Parity	Asymptotic wave function
Plausible Configurations for 45th neutron	22	5/2	--	+	|422 +>
	15	5/2	--	-	|303 ->
	30	1/2	--	+	|431 ->
	26	1/2	--	-	|301 ->
	21	7/2	--	+	|413 +>
	34	1/2	--	+	|420 +>
	18	9/2	--	+	|404 +>
Plausible Configurations for 35th proton	19	--	3/2	-	|301 +>

In Table 12 are given the various combinations of neutron and proton configurations which satisfy the conditions; (a) They give the correct spin values using the Gallagher and Moszkowski coupling rules. (b) They give the correct parity (i.e. positive for Br^{80} and negative for Br^{80m}).

Table 12

	Proton Configuration			Neutron Configuration			
	Asymptotic Wave Function	Nilsson Number	Parity	Asymptotic Wave Function	Nilsson Number	Parity	Configuration Designation
Probable Br^{80} Configurations	|301 +>	19	-	|301 ->	26	-	A
	|301 +>	19	-	|303 ->	15	-	B
Probable Br^{80m} Configurations	|301 +>	19	-	|413 +>	21	+	C

In view of the fact that all isotopes of Se and Br for which the sign of Q have been measured possess positive quadrupole moments, it seems quite likely that this is the case for Br^{80} as well as for Br^{80m}. Assuming this to be the case a calculation based on configuration "B" for Br^{80} leads to a negative value of μ, while calculations based on configurations "A" for Br^{80} and "C" for Br^{80m} both lead to positive values of μ. This is the case if any value of δ greater than .1 is used in the calculations. Since both $\mu(Br^{80m})$ and $Q(Br^{80m})$ are known to be positive while $\mu(Br^{80})$ and $Q(Br^{80})$ are known to have the same sign, 'assignment of Nilsson asymptotic wave functions; p→|301+>, n→|301 ->

to Br^{80}; and $p \rightarrow |301\rangle$, $n \rightarrow |413\rangle$ to Br^{80m} seem most plausible. These are the same configurations assigned made by Gallagher and Moszkowski[24] without knowledge of the nuclear moments and they are obviously consistent with the Shell Model assignments made above.

If Eq. (66) is used to calculate the magnetic moments assuming various values of δ, it is found that any value in the range $.1 < \delta < .2$ leads to values of μ for Br^{80} and Br^{80m} which agree satisfactorily with the experimentally measured quantities.

Hence, as in the case with many nuclides,[15,24] both the Shell Model and the Collective Model seem capable of describing Br^{80} and Br^{80m} to about comparable degrees of accuracy.

VII. THE I^{132} EXPERIMENT

A. Introduction

The spin measurement as well as the original determination of "a" and "b" were done, for I^{132}, by Garvin.[25] This work was done using the machine referred to above as machine no. 1 and the following results were reported

$$I = 4$$

$$|a| = 566 \pm 5.0 \text{ mc/sec}$$

$$|b| = 67 \pm 36 \text{ mc/sec} \qquad a/b > 0 \ .$$

Though the above value of "a" is sufficiently accurate for testing the applicability of existing nuclear models the value of "b" is quite crude. For this reason an attempt was made to add more resonances to Garvin's hyperfine structure data until a reasonably accurate value of "b" (and hence of the electric quadrupole moment Q) was obtainable using the "Hyperfine" program. The final "a" and "b" which resulted from this attempt, are reported in this paper.

The experimental techniques and equipment used in extending Garvin's work were exactly the same as those used by him, and are described in detail in Reference 25. Therefore, although a brief description of the entire I^{132} experiment is given below, many experimental details are left out which can be found in the above Reference.

B. Isotope Production and Handling

The I^{132} was obtained by "milking" (that is, by flushing out with dilute NH_4OH) an I^{132} generator provided by the Brookhaven National Laboratory. The I^{132}, while inside the generator, was in secular equilibrium with its 77-hr. parent Te^{132}. Hence the whole contents of the generator decayed with a characteristic 77 hr. half life so that not much activity was lost during the approximately 24 hrs. necessary for delivery. Starting with no I^{132} present, it took about 12 hours for the secular equilibrium to be established so that for maximum yield the generator could be milked at 12-hr. intervals. From five to nine I^{132} runs were made using a single generator before the Te^{132} had decayed too much to yield useable I^{132} activities. The glove-box used for chemical separation of the iodine from the NH_4OH solution is shown in Fig. 40. An iodine generator and the arrangement used for "milking" it are shown in this Figure, mounted on top of the glove-box.

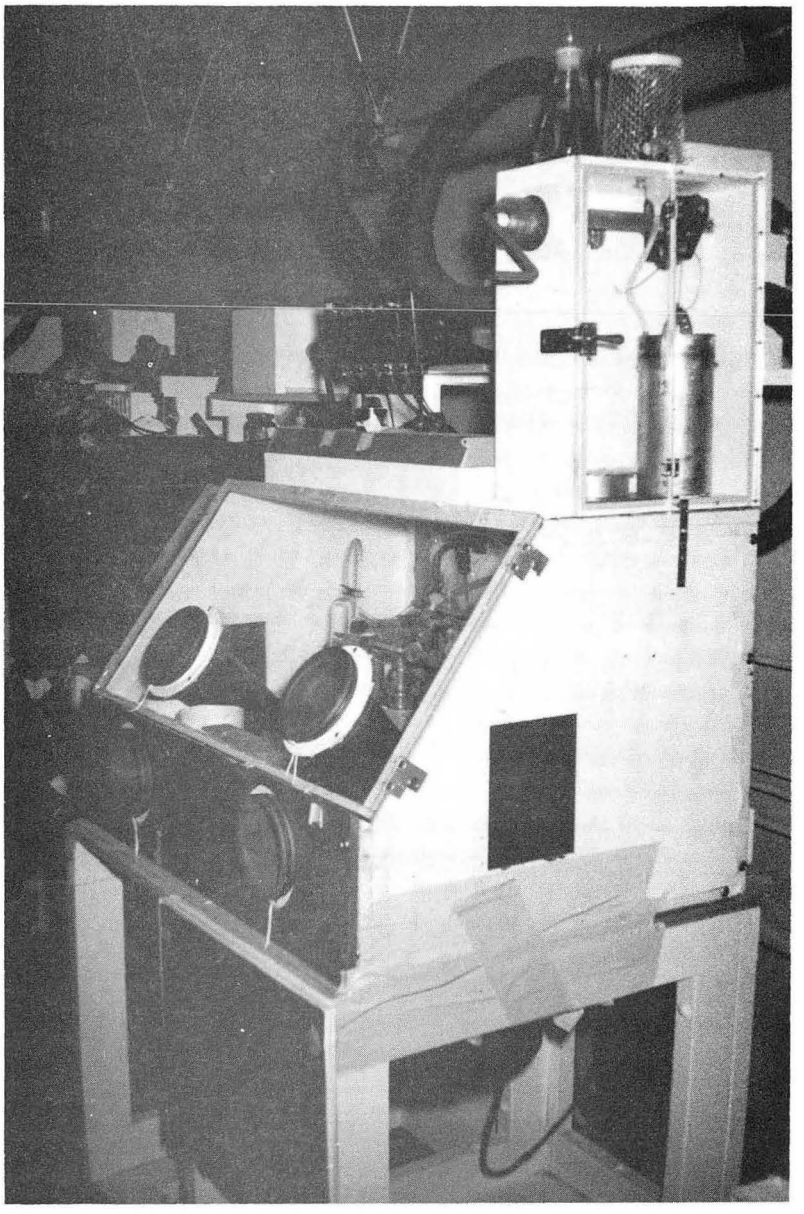

ZN-2211

Fig. 37. Glove box used for I^{132} chemistry.

After the I^{132} had been flushed from the generator with 25 ml. of .01M NH_4OH solution, the resulting liquid was collected within the glove-box of Fig. 40 and made slightly acidic by addition of H_2SO_4. Then $NaNO_2$ solution was added to oxidize the I^- to its elemental form, which was then extracted in CS_2. Next a predetermined quantity (40-100 mg) of stable iodine carrier, which had previously been dissolved in CS_2, was mixed thoroughly with the extracted radioactive iodine and the composit CS_2 solution was evaporated to dryness by pumping upon the surface of the liquid. Finally the small spherical pyrex flask, which at the conclusion of the evaporation process contained dry crystals of I^{132} and stable iodine, was removed from the chemistry glove-box and transported to the atomic-beam machine.

The whole chemical separation procedure was performed as rapidly as possible first because of the short 2.3 hr. half life of I^{132} and second because of radiation level outside the glove-box was usually 200-300 MR./hr. and speed was necessary to avoid excessive radiation exposure. The procedure usually took less than thirty minutes and at its conclusion the activity level at the surface of the sample containing flask ranged from 5-20 R./hr. depending on how many times the I^{132} generator had been used.

C. Beam Production and Characteristics

Inside the atomic-beam machine glove-box the flask containing the iodine sample was attached, by means of a ground glass coupling, to the thermal dissociator assembly that is shown schematically in Fig. 41. This assembly consists essentially of glass fittings necessary to accommodate the iodine flask, a brass mounting plate, and a heat shielded platinum tube. The dissociator was always mounted and lined up optically prior to introduction of the iodine sample.

After it had been connected to the dissociator, the interior of the sample flask was roughed down to a pressure of less than .5 micron by means of a small mechanical vacuum pump operating through the three way high vacuum stopcock shown in Fig. 41. Finally the stopcock was reversed in position and the flask opened directly into the oven chamber of the beam machine.

For each run a useable atomic iodine beam was obtained by allowing the iodine vapor, produced by sublimation at room temperature of the solid iodine contained in the sample flask, to effuse into the beam machine through the platinum tube of the thermal dissociator.

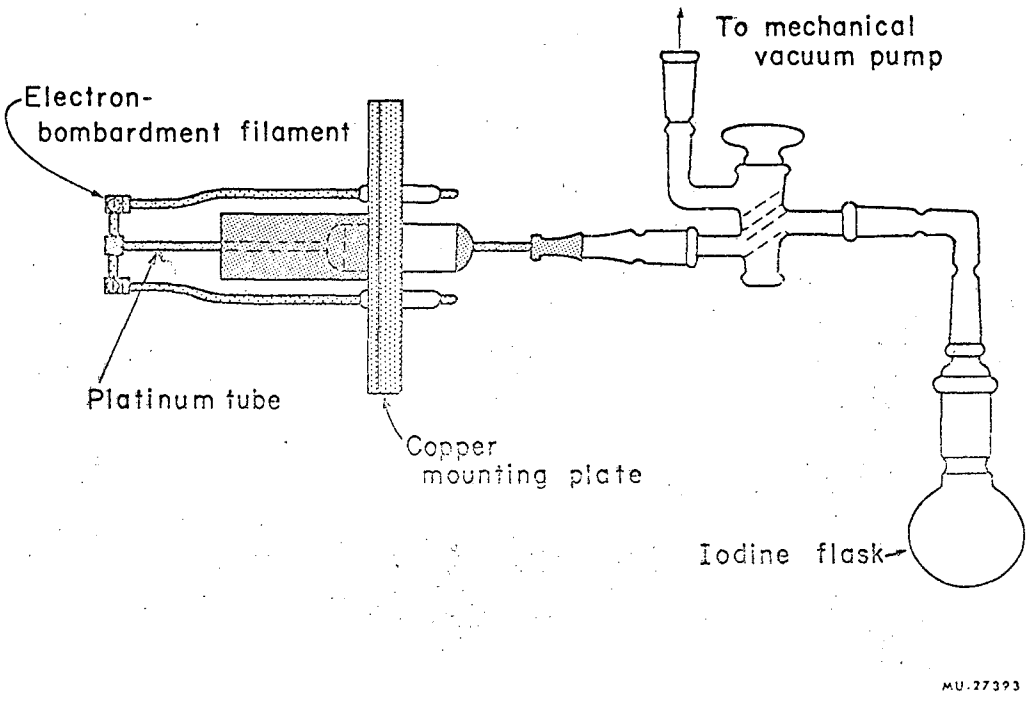

Fig. 38. Thermal dissociator assembly used for I^{132}.

Eighty- Ninety percent dissociation of the I_2 diatomic molecules was effected by heating the tip of this tube, through electron bombardment, to a temperature of about 900°C. The iodine beam was collected on silver plated stainless steel "buttons" such as were used during the early bromine experiments. By the above method full-beam counting rates (after two minutes of beam exposure) ranging from 500-700 counts/minute were obtained while beam life times were from 1 1/2 to 3 hours long, depending on the amount of stable iodine carrier used. Throw-outs of .80-.85 were usual and the normal I^{132} resonance signal to background ratio was about 3/1.

D. Hyperfine Structure Determination; Data and Results

Including Garvin's resonance data, a total of sixteen $\Delta F = 0$, $\Delta m_F = \pm 1$ transitions were observed in I^{132} at magnetic fields ranging from 0 - 347.7 gauss. As indicated in Fig. 42 the observable $\Delta F = 0$ transitions for $I = 4$, $J = 3/2$, and normal ordering of the zero field hyperfine levels correspond to transitions between the following low field quantum states

$$\alpha = (11/2, -7/2) \leftrightarrow (11/2, -9/2)$$

$$\beta = (9/2, -5/2) \leftrightarrow (9/2, -7/2) \quad .$$

The eight α transitions and eight β transitions observed were fit satisfactorily by "Hyperfine" using these level assignments, so that normal ordering of the zero field hyperfine levels in I^{132} can be assumed. Figure 43 shows the two highest field resonance lines traced out for I^{132} while Table 13 contains all the resonance data that was gathered as well as the best values of "a" and "b" determined by "Hyperfine." Doubling, as usual, the errors given in the table, the following final results are obtained

$$|a| = 567.6 \pm 2.6 \text{ mc/sec}$$

$$|b| = 128.2 \pm 20.6 \text{ mc/sec}$$

$$b/a > 0 \quad .$$

Comparing these results with the values obtained by Garvin, it is noticed that the quoted error in "b" has been reduced from 54% to about 16%. The fact that Garvin's "b" value does not agree, to within the given experimental errors, with the "b" quoted in this Section, though somewhat disturbing, is not too serious when it is noted that he used only one standard deviation (that is the value quoted by "Hyperfine")

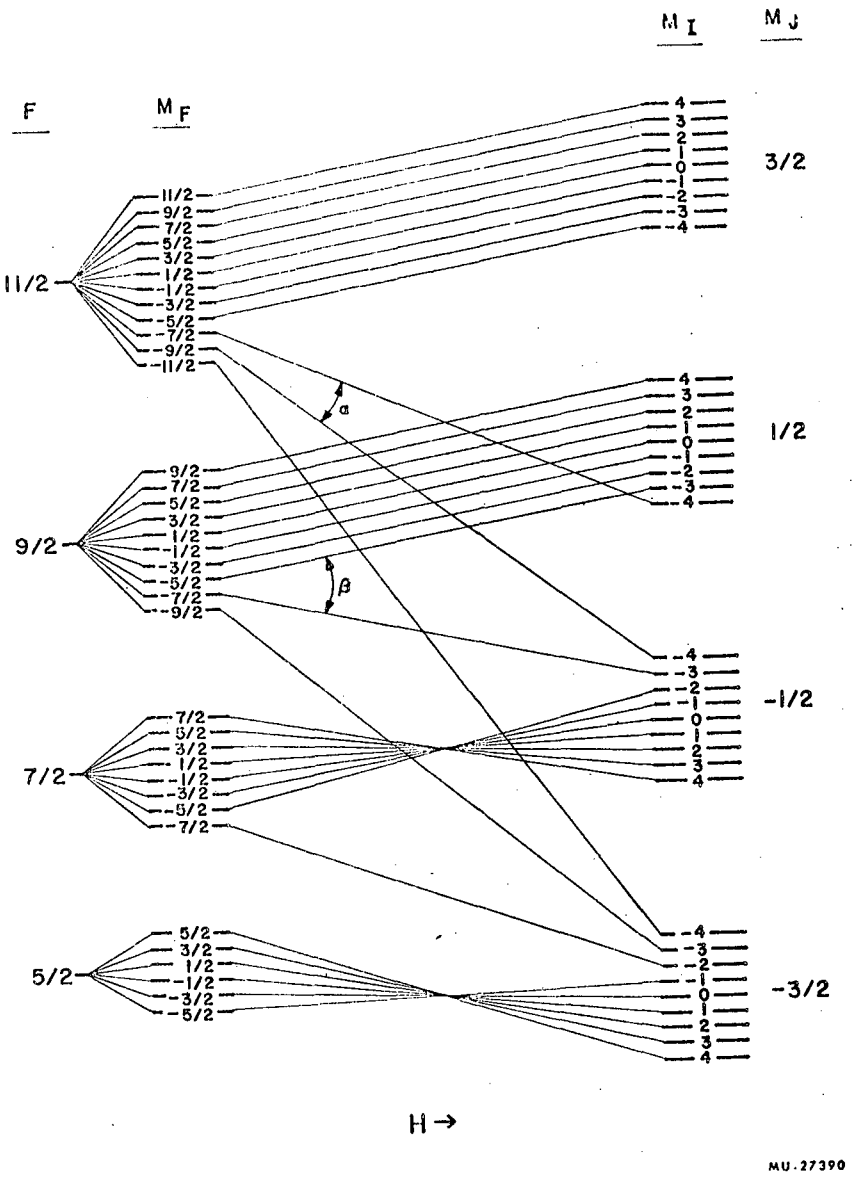

Fig. 39. Schematic energy level diagram for J = 3/2, I = 4 (normal ordering).

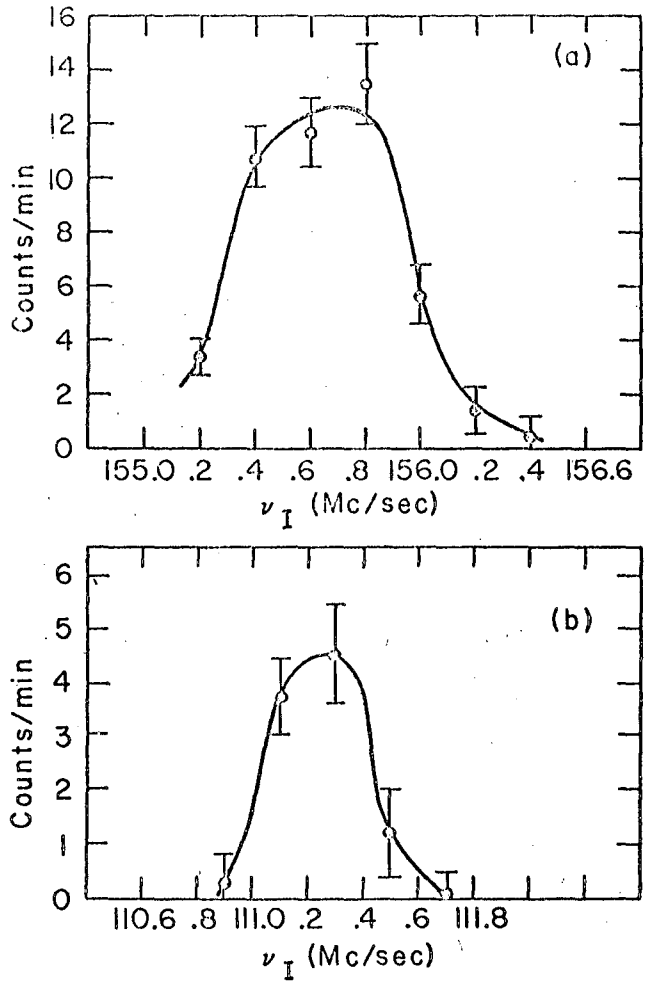

Fig. 40. I^{132} intermediate field, $\Delta F = 0$, resonances

(a) α transition (ν_K = 500.0 mc/sec)

(b) β transition (ν_K = 500.0 mc/sec) .

Table 13. I^{132} Resonance Data and Final Hyperfine Output

Sign of g_I is not determined

$|a| = 567.6 \pm 1.3$ mc/sec $a/b > 0$ $\chi^2 = 13.7$

$|b| = 128.2 \pm 10.3$ mc/sec

Run No.	ν_K mc/sec	H gauss	ΔH gauss	ν_I mc/sec	$\Delta\nu_I$ mc/sec	Residual mc/sec	F_1	M_1	F_2	M_2	Weight factor
1	5.0	6.915	.006	3.570	.028	.043	11/2	-7/2	11/2	-9/2	1256.6
2	10.0	13.421	.006	6.880	.020	.020	11/2	-7/2	11/2	-9/2	2435.8
3	20.0	25.39	.01	13.020	.016	-.008	11/2	-7/2	11/2	-9/2	3441.6
4	40.0	46.08	.02	23.840	.020	.028	11/2	-7/2	11/2	-9/2	2003.8
5	95.0	89.687	.008	47.070	.062	.034	11/2	-7/2	11/2	-9/2	258.8
6	250.0	173.74	.01	93.800	.064	.079	11/2	-7/2	11/2	-9/2	241.8
7	5.0	6.915	.006	2.250	.023	.023	9/2	-5/2	9/2	-7/2	1873.6
8	10.0	13.421	.006	4.350	.018	.005	9/2	-5/2	9/2	-7/2	3046.1
9	20.0	25.39	.01	8.290	.030	- .009	9/2	-5/2	9/2	-7/2	1093.6
10	40.0	46.08	.02	15.320	.050	.000	9/2	-5/2	9/2	-7/2	393.3
11	95.0	89.687	.008	30.800	.062	- .089	9/2	-5/2	9/2	-7/2	259.5
12	250.0	173.74	.01	63.850	.064	-.085	9/2	-5/2	9/2	-7/2	242.8
13	500.0	278.80	.09	111.300	.450	.200	9/2	-5/2	9/2	-7/2	4.9
14	500.0	278.80	.09	155.700	.140	-.036	11/2	-7/2	11/2	-9/2	44.0
15	750.0	374.70	.15	215.800	.200	-.221	11/2	-7/2	11/2	-9/2	20.2
16	750.0	374.70	.15	160.200	.100	+.082	9/2	-5/2	9/2	-7/2	60.0

as the probable maximum experimental error in his results. In this case statistical considerations indicate that there is about a 30% probability that the actual value lies outside of the error limits given.[31] If, on the other hand, two standard deviations are used as the probable maximum experimental error (as has been done throughout this paper) the probability that the actual value lies outside the quoted limits is reduced to only about 5%. To determine, then, whether a serious experimental discrepancy exists between the "b" given in this Section and the previously determined value, the error quoted by Garvin should probably be doubled. When this is done agreement is reached between the two reported values.

E. Calculation of the Nuclear Moments

Nuclear Magnetic Dipole Moment:

When the $a(I^{132})$ quoted above is used in conjunction with the known I^{127} data given in Appendix A, an uncorrected value of

$$\mu\ (I^{132}) = \pm\ 3.06\ (2)\ \text{nm} \quad \text{(uncorrected)}$$

is obtained using Eq. (26). Then, applying the diamagnetic shielding correction factor given in Appendix B one arrives at a corrected magnetic dipole moment of

$$\mu(I^{132}) = \pm\ 3.08\ (2)\ \text{nm} \quad \text{(corrected)}\ .$$

Before Eq. (28) can be used to perform an alternative calculation of $\mu(I^{132})$ some value of Z_1 must be assumed. Barnes and Smith[40] have suggested that $Z_1 = 48$ is reasonable for iodine while Lande[44] and Murakawa[45] have recommended values of $Z_1 = 49$ and $Z_1 = 50$ respectively. Using $Z_1 = 49$ Eq. (28) gives

$$\mu(I^{132}) = \pm\ 2.55\ \text{nm} \quad \text{(uncorrected)}$$

which does not agree very well with the result obtained above. Furthermore if it is assumed that the $\mu(I^{132})$ given by Eq. (26) is correct, inversion of Eq. (28) leads to a value of $Z_1 = 58.8$. This result is clearly physically unreasonable since it would mean that the charge seen by the valance electron (or in this case, hole) while inside the closed electron shells is greater than the total charge on the I^{132} nucleus ($Z = 53$).

The reason for this apparent failure of the simple theory can be explained, as suggested by Murakawa[45], by assuming that the lowest lying $5\ s^2\ 5\ p^5$ configuration of iodine is perturbed by the $5\ s\ 5\ p^5\ 6s$ configuration. This could have the result of lowering the observed

"$a(I^{132})$" to a value quite a bit below that which would result from a pure $5s^2 5p^5$ configuration and might, therefore, explain the discrepancy mentioned above. Koster[39] showed, through a detailed calculation for Ga, that a configuration interaction of this type, while having considerable effect on "a" because of the unpaired s electrons of the excited configuration, would be expected to have little effect on the value of "b". Also, since s electrons do not possess orbital angular momentum, the fine structure separation δ would not be changed.

Nuclear Electric Quadrupole Moment:

If, as suggested above, configuration interaction is present in the case of iodine, using Eq. (25) to determine $Q(I^{132})$ would be expected to give too large a value because of the suppression of $a(I^{132})$ by the admixed configuration. Koster suggested that the most accurate, simple, way to determine Q in this case is to use expression (27) for δ to eliminate the $\langle r^{-3} \rangle$ term from Eq. (24). This equation can then be rearranged to yield an expression for Q in terms of $b(I^{132})$ and δ both of which are quite insensitive to the configuration mixing. This technique gave values of Q for Ga^{69} and Ga^{71} which were within 1% of the values obtained by means of Koster's detailed calculation and was also employed with success by Murakawa[45] in the case of I^{127}. Taking $Z_1 = 49$ and using the $b(I^{132})$ determined above this method gives, when applied to I^{132}

$$Q(I^{132}) = \mp\ 0.075\ (15)\ \text{barns} \quad \text{(uncorrected)}$$

a 4% probable error in Z_1 is compounded with the 16% error in b to give the uncertainty in $Q(Lu^{176m})$ quoted above.

Although (as in the case of Br^{80}) the algebraic signs of μ and Q are not established by the experimental data of Table 13, Eqs. (23) and (24) show that since $a/b > 0$ these moments must have opposite signs. Analysis in terms of the Single Particle Shell Model strongly indicates, however, that μ is positive while Q is negative (see Section F).

F. Discussion of I^{132} Nuclear Moment Results

Application of the Shell Model:

The fact that the nuclear electric quadrupole moment of I^{132} is quite small ($Q = .075$ barns) implies that the deformation of this nucleus is also small and consequently the Single Particle Shell Model should be suitable for discussion of its properties.

Straightforward application of this model[15] assigns the 53rd proton of I^{132} to a $5g_{7/2}$ orbital, while the filling of the neutron levels leaves a single hole in the $5d_{3/2}$ subshell. These configuration

assignments are supported by the measured spins ($I = 7/2$) of I^{131} and I^{133}, which have the same number of protons as I^{132} but one less and one more neutron respectively, and by the measured spin ($I = 3/2$) of Ba^{135}, which has the same number of neutrons as I^{132} but an even number of protons.[25,46]

Assuming the above neutron and proton configurations to be correct, the neutron contribution to the total angular momentum of the I^{132} nucleus ($J_n = 3/2$) and the corresponding proton contribution ($J_p = 7/2$) must vectorially add to give the total measured spin of $I = 4$. This is clearly possible since $J_n + J_p > I > |J_n - J_p|$. Furthermore since $I = 4 = J_n + J_p - 1$ Brennan and Bernstein's Coupling Rule BB3, which applies to the coupling of holes with particles in odd-odd nuclei, holds in the case of I^{132}.

Calculation of the Nuclear Moments:

Using the configuration above, Eq. (55) gives for the Shell Model prediction of the I^{132} nuclear magnetic dipole moment

$$\mu(I^{132})_{calc} = + 2.12 \text{ nm} \quad .$$

Although this does not agree too well with the experimentally determined value of $\mu(I^{132})_{exp} = \pm 3.08$ nm, much better agreement is obtained by assuming, as Schwartz has suggested,[20] that the proton contribution to the magnetic moment of I^{132} is equal to the average magnetic dipole moments of I^{131} and I^{133} while the neutron contribution is equal to the known magnetic dipole moment of Ba^{135}. A Shell Model calculation based on these assumptions leads to the value

$$\mu(I^{132})_{calc} = +3.00 \text{ nm} \quad .$$

A calculation of the nuclear electric quadrupole moment of I^{132} on the basis of Eq.(56) gives

$$Q(I^{132}) = -.05 \text{ barns}$$

for the Shell Model prediction. This is in fair agreement with the experimentally determined value of $Q(I^{132}) = \mp .075$ barns.

Although the experimental data given in Table 13 is not capable of giving the algebraic signs of $\mu(I^{132})$ and $Q(I^{132})$ but can only establish that these signs are opposite, it seems very likely that the sign of μ is positive while that of Q is negative. That such is the case is implied by the following facts:

1. The Shell Model is capable of predicting the absolute values of μ and Q quite well and indicates the μ is positive while Q is negative.
2. All odd-even isotopes with I = 7/2 and mass numbers in the neighborhood of A = 132, for which these moments have been measured, have μ positive and Q negative.[28]
3. All even-odd isotopes with I = 3/2 and mass numbers in the neighborhood of A = 132, for which these moments have been measured, have μ positive and Q negative.[28]
4. Cs^{134}, which has 79 neutrons and 55 protons (differs from I^{132} by a pair of protons only) has I = 4 (as does I^{132}) and $\mu(Cs^{134})$ = +2.973. This magnetic moment is very close in absolute magnitude to that of I^{132} (as it should be on the basis of the Shell Model) and has a positive algebraic sign.[47,48]

VIII. APPENDICES

Appendix A

A list of pertinent known data for all the isotopes used either for nuclear moment calculations or in conjunction with the "Hyperfine" I.B.M. 704 computer program, during the course of the work reported in this paper, are given below. All nuclear moments quoted are uncorrected for diamagnetic shielding and core polarization. The data sources are also indicated.

K^{39} (J= 1/2)	Reference
$I = 3/2$	(49)
$\Delta\nu = 461.719690\ (30)$ mc/sec	(50)
$\mu_I = 0.390873\ (13)$ nm	(51)
$g_J = -2.00228\ (2)$	(1)
Lu^{175} (J = 3/2, 5/2)	
$I = 7/2$	(52)
$a(^2D_{3/2}) = 194.3316\ (4)$ mc/sec	(30)
$b(^2D_{3/2}) = 1511.4015(30)$ mc/sec	(30)
$a(^2D_{5/2}) = 146.7790\ (8)$ mc/sec	(30)
$b(^2D_{5/2}) = 1860.6480(80)$ mc/sec	(30)
$\mu_I = 2.211\ (10)$ nm	(53)
$Q = 5.68\ (6)$ barns	(30)
$g_J(^2D_{3/2}) = -0.79921\ (8)$	(30)
$g_J(^2D_{5/2}) = -1.20040(16)$	(30)
$\delta = 1993.92\ cm^{-1}$	(59)
Br^{79} (J = 3/2)	
$I = 3/2$	(37)
$a = 884.810\ (3)$ mc/sec	(37)
$b = -384.878\ (8)$ mc/sec	(37)
$c \leqslant .0001$ mc/sec	(37)
$\mu_I = 2.00991(10)$ nm	(38)
$Q = 0.32(2)$ barns	(37)
$g_J = -1.3338(3)$	(37)
$\delta = 3685\ cm^{-1}$	(58)

Br^{81} (J = 3/2)	Reference
I = 3/2	(37)
a = 953.770(3) mc/sec	(37)
b = -321.516(8) mc/sec	(37)
μ_I = 2.2596(11) nm	(38)
Q = 0.27(2) barns	(37)
g_J = -1.3338(3)	(37)
δ = 3685 cm^{-1}	(58)
I^{127}(J= 3/2)	
I = 5/2	(55)
a = 827.265(3) mc/sec	(54)
b = 1146.356(10) mc/sec	(54)
μ_I = 2.7937 (4) nm	(55)
Q = -.79(3) barns	(45)
g_J = -1.333977	(56)
δ = 7603.15 cm^{-1}	(57)

Appendix B

Tabulated below are Relativistic Correction Factors, Diamagnetic Correction Factors, and Core Polarization Correction Factors for the elements considered in this paper. The Relativistic and Diamagnetic Correction Factors are all obtained (by interpolation when necessary) from the tables given by Kopfermann in Ref. 5. The Core Polarization Correction Factors are taken from the table given by Sternheimer in Ref. 6.

Element	Atomic State J	L	Effective Change Z_1	Relativistic Correction Factors $F(J,Z_1)$	$H(L,Z_1)$	$R(L,J,Z_1)$	Diamagnetic Correction Factor K	Core Polarization Correction Factor C
Lu	3/2	2	51.5	1.0580	1.0190	1.1625	1.00827	1.107
	3/2	2	57.2	1.0722	1.0236	1.2046		
	5/2	2	51.5	1.0245	1.0190	1.0482		
	5/2	2	57.2	1.0303	1.0236	1.0598		
Br	3/2	1	31.0	1.0204	1.0231	1.0500	1.00309	1.040
	3/2	1	32.3	1.0221	1.0251	1.0453		
I	3/2	1	49.0	1.0522	1.0603	1.1084	1.00548	1.029

Appendix C

Determination of "a" and "b" from 3rd order perturbation theory:

From Eq. (42) we have

$$\mathcal{H} = a\,\vec{I}\cdot\vec{J} + b\,\frac{3(\vec{I}\cdot\vec{J})^2 + 3/2\,\vec{I}\cdot\vec{J} - I(I+1)\,J(J+1)}{2I(2I-1)J(2J-1)} - g_J\frac{\mu_o H}{h}\,J_z$$

(in units of mc/sec) $$-g_I'\frac{\mu_o H}{h}\,I_z \qquad (1A)$$

For small values of H this equation can conveniently be written

$$\mathcal{H} = \mathcal{H}_o + \mathcal{H}' \qquad (2A)$$

where

$$\mathcal{H}_o = a\,\vec{I}\cdot\vec{J} + b\,\frac{3(\vec{I}\cdot\vec{J})^2 + 3/2\,(\vec{I}\cdot\vec{J}) - I(I+1)\,J(J+1)}{2I(2I-1)J(2J-1)} \qquad (3A)$$

$$\mathcal{H}' = -g_J\frac{\mu_o H}{h}\,J_z - g_I'\frac{\mu_o H}{h}\,I_z \approx -g_J\frac{\mu_o H}{h}\,J_z \quad .$$

Using 3rd order perturbation theory the approximate energy of a level specified by I J F m_F (referred to as n below) is given by[8]

$$W(n) = W^o(n) + W^1(n) + W^2(n) + W^3(n) \qquad (4A)$$

where

$$W^o(n) = \langle n|\mathcal{H}_o|n\rangle$$

$$W^1(n) = \langle n|\mathcal{H}'|n\rangle$$

$$W^2(n) = \sum_m \frac{\langle n|\mathcal{H}'|m\rangle\langle m|\mathcal{H}'|n\rangle}{W^o(n) - W^o(m)} \qquad (5A)$$

$$W^3(n) = \sum_k{}'\sum_m{}' \frac{\langle n|\mathcal{H}'|m\rangle\langle m|\mathcal{H}'|k\rangle\langle k|\mathcal{H}'|n\rangle}{[W^o(m) - W^o(n)]\,[W^o(k) - W^o(n)]} - \langle n|\mathcal{H}'|n\rangle \sum_m{}' \frac{|\langle n|\mathcal{H}'|m\rangle|^2}{[W^o(m) - W^o(n)]^2}$$

where the primes on the summations indicate that the m(or k) = n terms are to be skipped.

If we define,

$$W^{o}(n) - W^{o}(m) = \nu^{o}_{nm}$$

$$F_{\alpha} = I + J$$

$$F_{\beta} = I + J - 1$$

$$F_{\gamma} = I + J - 2$$

$$\left.\begin{matrix} m_{\alpha i} \\ m_{\alpha f} \end{matrix}\right\} \text{ initial and final } m_F\text{'s for } \alpha \text{ transition} \qquad (6A)$$

$$\left.\begin{matrix} m_{\beta i} \\ m_{\beta f} \end{matrix}\right\} \text{ initial and final } m_F\text{'s for } \beta \text{ transition}$$

$\Delta\nu_{\alpha}$ = shift of α transition frequency from the linear Zeeman prediction

$\Delta\nu_{\beta}$ = shift of β transition frequency from the linear Zeeman prediction.

Eqs. 2A-5A and the matrix elements evaluated in Ref. 8 give for atoms with observable α and β transitions

$$\Delta\nu_{\alpha} = \left(\frac{g_J \mu_o H}{h}\right)^2 \frac{1}{\nu^{o}_{F_\alpha F_\beta}} \left[E(F_\alpha, m_{\alpha f}) - E(F_\alpha, m_{\alpha i}) \right]$$

$$-\left(\frac{g_J \mu_o H}{h}\right)^3 \frac{\left[D(F_\beta) - D(F_\alpha) \right]}{(\nu^{o}_{F_\alpha F_\beta})^2} \left[m_{\alpha f} E(F_\alpha, m_{\alpha f}) - m_{\alpha i} E(F_\alpha, m_{\alpha i}) \right] \qquad (7A)$$

$$\Delta\nu_{\beta} = \left(\frac{g_J \mu_o H}{h}\right)^2 \left\{ \frac{E(F_\alpha, m_{\beta f}) - E(F_\alpha, m_{\beta i})}{-\nu^{o}_{F_\alpha F_\beta}} + \frac{E(F_\beta, m_{\beta f}) - E(F_\beta m_{\beta i})}{\nu^{o}_{F_\beta F_\gamma}} \right\}$$

$$-\left(\frac{g_J \mu_o H}{h}\right)^3 \frac{\left[D(F_\gamma) - D(F_\beta) \right]}{(\nu^{o}_{F_\beta F_\gamma})^2} \left\{ m_{\beta f} E(F_\beta, m_{\beta f}) - m_{\beta i} E(F_\beta, m_{\beta i}) \right\}$$

$$-\left(\frac{g_J \mu_o H}{h}\right)^3 \frac{\left[D(F_\alpha) - D(F_\beta) \right]}{(\nu^{o}_{F_\alpha F_\beta})^2} \left\{ m_{\beta f} E(F_\alpha, m_{\beta f}) - m_{\beta i} E(F_\alpha, m_{\beta i}) \right\}$$

where

$$D(F) = \frac{J(J+1) - I(I+1) + F(F+1)}{2F(F+1)}$$

$$E(F,m) = \frac{\left[F^2 - m^2 \right] \left[F^2 - (J-I)^2 \right] \left[(J+I+1)^2 - F^2 \right]}{4F^2 (4F^2 - 1)}$$

and also using Eq. (19)

$$W^{o}(IJFm_{F}) = \frac{aK}{2} + b \frac{3/4\ K(K+1)-I(I+1)J(J+1)}{2I(2I-1)J(2J-1)} \qquad (9A)$$

If $\Delta\nu_{\alpha}$ and $\Delta\nu_{\beta}$ are known Eqs. (7A) and (7B) can be solved for $\nu^{o}_{F_{\alpha}F_{\beta}}$ and $\nu^{o}_{F_{\beta}F_{\gamma}}$. These expressions can then be expressed in terms of "a" and "b" using Eqs. (6A) and (9A). Finally the resulting simultaneous equations for "a" and "b" can be solved to yield initial values for use in "Hyperfine".

Equation (6A) expressed as

$$\nu^{o}_{F,F'} = W^{o}(IJF) - W^{o}(IJF')$$

serves to define the "hyperfine structure separation" of the levels specified by total angular momenta F and F'.

IX. ACKNOWLEDGMENTS

So many people have been instrumental in enabling the completion of the work reported in this paper that it would be impossible to mention all of them here. In particular, however, I would like to thank;

1. Professor William A. Nierenberg for his support.
2. Professor Edgar Lipworth for suggesting the experiments and for rendering valuable guidance during the initial stages of the research.
3. Dr. Victor Cohen and his group at B.N.L. for their aid and cooperation during the Lu^{176m} experiments.
4. Professor Howard Shugart, Dr. Richard Marrus, and Dr. Douglas McColm for helpful discussions during the checking out of the redesigned atomic-beam machine.
5. Mr. Douglas MacDonald and Mr. Richard Reimers for solving many of the engineering problems that arose during the redesigning process.
6. Mr. Isaac Maleh for joining me in the struggle to get the machine back on the air.
7. Mr. Robert McCracken of Health Chemistry for his aid in securing radioactive materials.
8. Dr. Seymour Alpert, Mr. Walter Doyle, Mr. Walter Edmonds and Mr. John Padilla for helping out during runs.
9. Mr. Kaye Voice for his services both as a Radiation Monitor and as an all-round technician.
10. Mr. H. Powell and Mr. W. Berland of the glass shop for their infinite patience and expert advice during the perfecting of the bromine glassware.

Finally to my wife, Marianne, who typed the manuscripts of this paper and whose constant encouragement and faith throughout the course of my work has been invaluable, Ich nicke der Kopf und sage, "danke schön."

X. REFERENCES

1. Norman F. Ramsey, Molecular Beams (Oxford University Press, London, 1956).
2. A. R. Edmonds, Angular Momentum in Quantum Mechanics (Princeton University Press, 1957).
3. M. Tinkham, Physics 223A Notes (Department of Physics, University of California), 1958.
4. H.B.G. Casimer, On the Interaction Between Atomic Nuclei and Electrons (Tyler's Tweede Genootschap, Haarlem, 1936).
5. Hans Kopfermann, Nuclear Moments, English translation by E. E. Schneider (Academic Press, Inc., New York, 1958).
6. R. Sternheimer, Phys. Rev. 86, 316 (1952).
7. C. Schwartz, Phys. Rev. 97, 380 (1955).
8. E. U. Condon and G. H. Shortley, Theory of Atomic Spectra (Cambridge University Press, Cambridge, England, 1957).
9. Joseph Winocur, Some Nuclear and Electronic Ground-state Properties of Pa^{233}, Am^{241}, and 16-hr Am^{242} (thesis) UCRL-9174 (April 1960).
10. P. Kusch and V. W. Hughes, Atomic and Molecular Beam Spectroscopy, in Handbuch der Physik, Vol. 37 (Springer 1959).
11. H. Salwen, Phys. Rev. 99, 1274 (1955).
12. E. Majorana, Nuovo cimento 9, 43 (1932).
13. G.K. Woodgate and R. W. Hellwarth; Proc. Phys. Soc. London A69, 588 (1956).
14. Lawrence L. Marino, Some Nuclear Properties of Pi^{206}, Tl^{200}, Th^{201}, Th^{202}, In^{109}, In^{110m}, and In^{111} (thesis), UCRL-8721, April, 1959.
15. Maria Goeppert Mayer and J. Hans D. Jensen, Elementary Theory of Nuclear Shell Structure (John Wiley and Sons, Inc., New York, 1955).
16. L. A. Nordheim, Revs. Modern Phys. 23, 322 (1951).
17. M. H. Brennan and A. M. Bernstein, Phys. Rev. 120, 927 (1960).
18. C. Schwartz, Phys. Rev. 94, 95 (1954).
19. R. J. Blin-Stoyle, Theories of Nuclear Moments (Oxford University Press, London, 1957).
20. H. M. Schwartz, Phys. Rev. 89, 1293 (1953).
21. A. Bohr and B. R. Mottelson, Kgl. Danske Videnskab. Selskab, Mat.-fys. Medd. 27, 16 (1953).
22. S. G. Nilsson, Kgl. Danske Videnskab. Selskab, Mat-fys Medd. 29, 16 (1955).

23. B. R. Mottelson and S. G. Nilsson, Kgl. Danske Videnskab. Selskab, Mat.-fys, Skrifter, 1, 8 (1959).
24. C. J. Gallagher, Jr., and S. A. Moszkowski, Phys. Rev. 111, 1282 (1958).
25. Hugh Leslie Garvin; Nuclear-Spin and Hyperfine-structure Measurements on the Radioactive Iodine and Astatine Isotopes (thesis) UCRL 8860 August, 1959.
26. S. Penselin, T. Moran, and V. W. Cohen, Brookhaven National Laboratory (to be published) [Precision Measurements of hfs of Stable Rb Isotopes].
27. Gilbert O. Brink, Nuclear Spins of Th^{197}, Th^{198m}, Th^{199}, and Th^{204} (thesis) UCRL-3642, June 1957.
28. D. Strominger, J. M. Hollander, and G. T. Seaborg, Revs. Modern Phys. 30, 585 (1958).
29. P.F.A. Klinkenberg, Physica XXI, 53 (1955).
30. George J. Ritter, Phys. Rev. 126, 240 (1962).
31. R. A. Fisher, Statistical Methods for Research Workers (Hafner, New York, 1958).
32. F. Russell Petersen and Howard A. Shugart, Phys. Rev. 126, 252 (1962).
33. I. T. Spalding and K. F. Smith, Proc. Phys. Soc. 79, pt. 4, p. 787.
34. Thomas Myer Green, III., Spins, Moments, and Hyperfine structures of Some Bromine Isotopes (thesis) UCRL-8730 (June 1959).
35. Edgar Lipworth, A Review of Source Techniques used in Radioactive Atomic-Beam Experiments, UCRL-9400 (Sept. 1960).
36. S. A. Gordon, Rev. Sci. Instr. 29, 501 (1958).
37. J. J. King and V. Jaccarino, Phys. Rev. 94, 1610 (1954).
38. H. E. Walchli, A Table of Nuclear Moment Data, O.N.R.L.-1469 Suppl. II, Feb. 1, 1955.
39. G. F. Koster, Phys. Rev. 86, 148 (1952).
40. R. G. Barns and W. K. Smith, Phys. Rev. 93, 95 (1954).
41. Aamodt and Fletcher, Phys. Rev. 98, 1224 (1955).
42. Lipworth, Green, Garvin, and Nierenberg, Phys. Rev. 119, (1960).
43. Garvin, Green, Lipworth, and Nierenberg, Phys. Rev. 116, 393 (1959).
44. A. Lande, Z. Physik 25, 46 (1924).
45. Kiyashi Murakawa, Phys. Rev. 100, 1369 (1955).
46. J. E. Mack, Revs. Modern Phys. 22, 64 (1950).
47. V. Jaccarino, B. Nederson, and H. H. Stroke, Phys. Rev. 87, 676 (1952).

48. H. H. Stroke, V. Jaccarino, D. S. Edmonds, Jr., and R. Weiss Phys. Rev. 105, 590 (1957).
49. S. Millman, Phys. Rev. 47, 739 (1935).
50. Arnold F. Bloom and John B. Carr, Phys. Rev. 119, 1946 (1960).
51. E. Brun, J. Oerer, H. H. Staub, and C. G. Telscaw, Phys. Rev. 93, 171 (1954).
52. H. Schüler and T. H. Schmidt, Z. Physik 95, 265 (1935).
53. A. H. Reddock and G. J. Ritter (National Research Council, Ottawa) private communication, 1961.
54. Jaccarino, King and Stroke, Phys. Rev. 94, 1798 (1957).
55. Walchli, Livingston, and Hebert, Phys. Rev. 82, 97 (1951).
56. Bower, Kamper and Lustig, Proc. Royal Soc. B. Vol. 70, 445 (1957).
57. Charlotte E. Moore, Atomic Energy Levels, Vol. III, NBS-467 (National Bureau of Standards, Washington, D.C., 1958).
58. Charlotte E. Moore, Atomic Energy Levels, Vol. II, NBS-467 (National Bureau of Standards, Washington, D.C., 1952).
59. P.F.A. Klinkenberg, Physica XXI, 53 (1955).
60. E. R. Cohen, K. M. Crowe, and J.W.M. DuMond, Fundamental Constants of Physics (Interscience Publishers, Inc., New York, 1957).
61. Amado Y. Cabezas, Electronic and Nuclear Properties of some Radioactive Rare-Earth Elements (thesis) UCRL-9346 (Aug. 9, 1960).
62. Richard Marrus, Hyperfine Structure Measurements on Some Transuranic Elements (thesis), UCRL-8547 (Nov. 1958).